

POLITECNICO DI MILANO
Corso di Laurea Specialistica in Ingegneria Informatica
Dipartimento di Elettronica e Informazione



**Mitosis detection in histological images:
Algorithms based on machine learning
and their performance compared to
humans**

Relatore: Prof. Vincenzo Caglioti
Correlatore: Ing. Alessandro Giusti

Tesi di Laurea di:
Claudio G. Caccia, matricola 751302

Anno Accademico 2012-2013

a Elena, Giovanna e Leonardo

Sommario

Acknowledgements

....

Contents

| | |
|---|-------------|
| Sommario | i |
| Acknowledgments | iii |
| List of Figures | x |
| List of Tables | xi |
| Glossary | xiii |
| 1 Introduction | 1 |
| 2 State of the art | 7 |
| 2.1 Background | 7 |
| 2.1.1 Tissue preparation | 9 |
| 2.1.2 Digital Pathology | 9 |
| 2.1.3 Mitosis Counting | 9 |
| 2.1.4 Challenges in Mitosis Detection | 10 |
| 2.2 Mitosis Detection and Computer Vision | 14 |
| 2.2.1 Software Tools | 14 |
| 2.2.2 Features and Detectors | 14 |
| 2.2.3 Texture Algorithms | 15 |
| 2.2.4 Image Segmentation | 18 |
| 2.2.5 Object detection and recognition | 19 |
| 2.3 Machine Learning | 19 |
| 2.3.1 Pattern Recognition | 20 |
| 2.3.2 Classification | 21 |
| 2.3.3 Binary Classification | 21 |
| 2.3.4 Binary Classifiers | 22 |
| 2.3.5 Software Tools | 23 |

| | |
|--|-----------|
| 3 Problem Definition | 25 |
| 3.1 Framework | 26 |
| 3.1.1 Detection | 26 |
| 3.1.2 From Detection to Classification | 26 |
| 3.1.3 Performances | 27 |
| 3.2 Definition of Classification | 28 |
| 3.3 Review of Algorithms solving the mitosis detection problem . | 29 |
| 3.4 Performance and Benchmarking | 31 |
| 3.4.1 Pathologists' Agreement | 32 |
| 3.4.2 Benchmarking | 32 |
| 3.5 Performances on ICPR Contest | 37 |
| 4 Design of a Mitosis Detection algorithm | 39 |
| 4.1 Dataset | 39 |
| 4.1.1 Image Candidates | 40 |
| 4.1.2 Extended Dataset | 41 |
| 4.2 Feature Extraction | 42 |
| 4.2.1 Simple Features | 42 |
| 4.2.2 Color Histograms and Intensities | 43 |
| 4.2.3 Texture Features | 44 |
| 4.3 Classifiers | 46 |
| 4.3.1 Support Vector Machines | 47 |
| 4.3.2 Random Forests | 48 |
| 4.4 Classification Process | 49 |
| 5 Design of a User Study | 51 |
| 5.1 Test Design | 51 |
| 5.1.1 Dataset | 52 |
| 5.1.2 Programming Framework | 52 |
| 5.2 User Interface | 52 |
| 5.2.1 Introduction | 53 |
| 5.2.2 Training | 53 |
| 5.2.3 Evaluation | 54 |
| 5.2.4 Comments | 55 |
| 5.2.5 Performances | 55 |
| 5.3 Data collection | 57 |
| 5.4 Source Code | 59 |

| | | |
|---------------------|---|------------|
| 6 | Experimental Results | 61 |
| 6.1 | Experimental setup | 61 |
| 6.2 | Experiments | 62 |
| 6.2.1 | Normalization | 62 |
| 6.2.2 | Normalization: Experimental Results | 63 |
| 6.2.3 | Extended Dataset | 64 |
| 6.2.4 | Extended Dataset: Experimental Results | 65 |
| 6.2.5 | Best Feature Combinations | 70 |
| 6.2.6 | Best Feature Combinations: Experimental Results | 70 |
| 6.2.7 | Dataset Dimension | 73 |
| 6.2.8 | Dataset Dimension: Experimental Results | 74 |
| 6.2.9 | SVM parameters | 76 |
| 6.2.10 | SVM parameters: Experimental results | 76 |
| 6.2.11 | Principal Component Analysis | 78 |
| 6.2.12 | PCA: Experimental results | 79 |
| 6.2.13 | Size of the Image Patch | 81 |
| 6.2.14 | Image Size: Experimental Results | 83 |
| 6.3 | Accuracy of Humans | 84 |
| 6.3.1 | Humans and ICPR Contest Algorithms | 87 |
| 6.3.2 | Humans and ad hoc Classifiers | 89 |
| 6.4 | Difficulties | 89 |
| 6.4.1 | Humans vs. ICPR Algorithms | 90 |
| 6.4.2 | Humans vs. ad hoc Classifiers | 91 |
| 6.5 | Difficulties among Classifiers | 93 |
| 7 | Conclusions | 95 |
| 7.1 | Context and Results | 95 |
| 7.2 | Future Work | 97 |
| Bibliography | | 99 |
| A | Samples | 109 |
| A.1 | C1 and C0 samples | 109 |
| A.2 | Human Difficulties | 109 |
| A.3 | Classifier Difficulties | 109 |

List of Figures

| | | |
|------|--|----|
| 1.1 | Mitosis of a cell | 3 |
| 1.2 | Histological images with labeled mitoses (Y) and non-mitoses (N) | 3 |
| 2.1 | Aperio ScanScope XT scanner | 10 |
| 2.2 | Examples of digital histological images | 11 |
| 2.3 | Example of image with highlighted mitoses | 12 |
| 2.4 | Detail of Figure 2.3 | 13 |
| 2.5 | Examples LBP neighbors and distances | 17 |
| 3.1 | Flowchart of Detection Algorithm | 28 |
| 3.2 | Example of ROC curves | 36 |
| 3.3 | Performances of best algorithms in ICPR 2012 contest | 37 |
| 4.1 | Extended Dataset | 41 |
| 4.2 | Color Histograms | 43 |
| 4.3 | Example of mean gray-scale intensities feature | 44 |
| 4.4 | Example of VAR(8,1) feature | 45 |
| 4.5 | Representation of a SVM classification | 48 |
| 4.6 | Example of a Decision Tree | 49 |
| 5.1 | Intro page | 53 |
| 5.2 | Training page | 54 |
| 5.3 | Evaluation page | 55 |
| 5.4 | Examples of classification feedback | 56 |
| 5.5 | Current performance | 56 |
| 5.6 | Comment page | 57 |
| 5.7 | user results page | 57 |
| 5.8 | Overall results page | 58 |
| 5.9 | Download buttons | 59 |
| 5.10 | User comments | 59 |

| | | |
|------|---|----|
| 6.1 | ROC curves for MSi feature classification | 64 |
| 6.2 | ROC curves for MSiHLV feature classification | 65 |
| 6.3 | ROC curves for MSiHU features - SVM classification | 67 |
| 6.4 | ROC curves for MSiHU features - RF classification | 68 |
| 6.5 | ROC curves for MSiHR features - RF classification | 69 |
| 6.6 | ROC curves for best feature-set - SVM classification | 71 |
| 6.7 | ROC curves for best feature-set - RF classification | 72 |
| 6.8 | Features MSiVHL - overall performances | 72 |
| 6.9 | Features MSiVHR - overall performances | 73 |
| 6.10 | Features MSiVHU - overall performances | 73 |
| 6.11 | subset size and trials | 74 |
| 6.12 | Features iVHL - sample size | 75 |
| 6.13 | Features MiVHU - sample size | 77 |
| 6.14 | Features MSVHR - sample size | 78 |
| 6.15 | Features MSidHLV - Principal Component Analysis | 80 |
| 6.16 | Features MSidHUV - Principal Component Analysis | 82 |
| 6.17 | Image size and sets with 'H' feature - SVM classifier | 83 |
| 6.18 | Image size and sets with 'LV' features - SVM classifier | 84 |
| 6.19 | Image size and sets with 'HLV' features - RF classifier | 85 |
| 6.20 | Accuracy distribution of humans | 87 |
| 6.21 | best Humans' performance vs. ICPR algorithms | 88 |
| 6.22 | ROC plot humans vs. algorithms | 89 |
| 6.23 | ROC plot humans vs. classifiers | 90 |

List of Tables

| | | |
|------|--|----|
| 3.1 | Confusion Matrix | 33 |
| 6.1 | MSi results | 63 |
| 6.2 | MSiHLV results | 64 |
| 6.3 | MSiHU results (SVM) | 66 |
| 6.4 | MSiHU classified images(SVM) | 66 |
| 6.5 | MSiHU results (RF) | 67 |
| 6.6 | MSiHU classified images (RF) | 67 |
| 6.7 | MSiHR results (RF) | 68 |
| 6.8 | MSiHR classified images (RF) | 69 |
| 6.9 | Best SVM results | 70 |
| 6.10 | Best SVM results - classified images | 70 |
| 6.11 | Best RF results | 71 |
| 6.12 | Best RF results - classified images | 71 |
| 6.13 | Accuracy of human and algorithms on easy, medium and difficult mitosis. | 91 |
| 6.14 | Accuracy of human and Support Vector Machine (SVM) classifiers on sets of mitoses. | 91 |
| 6.15 | Accuracy of human and Random Forest (RF) classifiers on sets of mitoses. | 91 |
| 6.16 | Accuracy of human and average of classifiers on sets of mitoses. | 92 |
| 6.17 | Accuracy of human and SVM classifiers on sets of non-mitoses. | 92 |
| 6.18 | Accuracy of human and RF classifiers on sets of non-mitoses. | 92 |
| 6.19 | Accuracy of human and average of classifiers on sets of non-mitoses. | 93 |
| 6.20 | Frequency of common misclassified mitoses. | 93 |
| 6.21 | Correlation among frequency and human difficulty. | 93 |
| 6.22 | Frequency of common misclassified non-mitoses. | 94 |
| 6.23 | Correlation among frequency and human difficulty. | 94 |

Glossary

AI Artificial Intelligence. 19

BR Bloom and Richardson Grading System. 7, 10, 30

CAD Computer Aided Diagnosis. 12, 94

CNN Convolutional Neural Network. 28, 29, 38, 45

CoC Convention over Configuration. 50

CV Computer Vision. 12, 13, 16, 21, 22, 42

DNN Deep Neural Network. 29

DT Decision Tree. 46–48, 60

FN false negative. 21, 56, 90

FP false positive. 21, 56, 90

GGMM Gamma Gaussian Mixture Model. 28

GLCM Gray-level Co-occurrence Matrix. 14

GLEM Gray-level Entropy Matrix. 14

GLRM Gray-level Run-length Matrix. 14

GT Ground Truth. 30, 45

HE Hematoxylin and Eosin. 9, 30

HPF High Power Fields. 10

HSV Hue Saturation Value. 41

IARC International Agency for Research on Cancer. 2

LBP Local Binary Patterns. 14–16, 42, 43

ML Machine Learning. 19, 20, 24, 26, 28, 76

MRI Magnetic Resonance Imaging. 16

NGS Nottingham Grading System. 7, 8, 93

NN Neural Network. 21

PCA Principal Component Analysis. 76, 77, 79

PR Pattern Recognition. 19, 24

RBF Radial Basis Function. 46, 76

RF Random Forest. xi, 21, 46–48, 59–61, 64, 65, 67, 69–72, 76, 77, 79, 80, 82, 86, 88–90, 116

RGB Red-Green-Blue. 40, 41

ROC Receiver Operating Characteristic. 33, 34, 61, 64–66, 68, 69, 85, 86

ROI Region of Interest. 12, 24, 37

RoR Ruby on Rails. 50

SVD Singular Value Decomposition. 77

SVM Support Vector Machine. xi, 21, 28, 29, 45, 46, 59–61, 64, 67, 68, 70–72, 75–81, 86, 88–90, 116

TN true negative. 21, 56, 64, 66

TP true positive. 21, 56, 64, 66

VAR Rotation Invariant Variance Measure. 15, 16, 43

WT Wavelet Transform. 16

Chapter 1

Introduction

“Λέγειν τὰ προγενόμενα, γνώσκειν τὰ παρεόντα, προλέγειν τὰ ἐσόμενα: μελετᾶν ταῦτα. Άσκειν περὶ τὰ νοσήματα δύο, ὡφελεῖν ἢ μὴ βλάπτειν. Ἡ τέχνη διὰ τριῶν, τὸ νόσημα καὶ ὁ νοσέων καὶ ὁ ἰητρός: ὁ ἰητρός ὑπηρέτης τῆς τέχνης, ὑπεναντιοῦσθαι τῷ νοσήματι τὸν νοσέοντα μετὰ τοῦ ἰητροῦ.

(*The physician must be able to tell the antecedents, know the present, and foretell the future: must mediate these things, and have two special objects in view with regard to disease, to do good or to do no harm. The art consists in three things: the disease, the patient, and the physician. The physician is the servant of the art, and the patient must combat the disease along with the physician.)*”

‘Ιπποκράτης(Hippocrates, Epid. 1.2.11)

Cancer, or in medical terms *malignant neoplasm*, identifies a wide range of diseases, all of which involve unregulated cell growth [76]. While normal cells follow a normal process of growth, division, and death, cancer cells begin to form when this transformation breaks down, as they continue to expand and divide. This leads to a mass of abnormal cells that grows out of control. Healthy tissue can be invaded by cancer cells; it can harm the body when the abnormal cells start to form masses of tissue, known as tumors, which can interfere with the body’s system and function.

There are about 200 known types of cancer¹ and breast cancer is the most frequent type of cancer among women worldwide [80], as also reported by International Agency for Research on Cancer (IARC)², with about 22.9% of incidence and 13.7% of mortality [11].

Prognosis and survival rates for breast cancer vary greatly depending on the cancer type, stage, treatment, and geographical location of the patient.

Early detection of cancer stage plays an important role in selecting the best treatments and reducing cancer mortality. The current procedure for breast cancer grading is manually performed by pathologists, as breast tissue samples of patients are taken and examined under microscopes.

Pathologists grade the tissue samples based on the deviation of the cell structures from normal tissues. A pathologist may have to examine hundreds of slides daily [75], which is a subjective and time consuming process. Histopathological images (images of biopsy samples) are now available in high resolution digital format, which can be further processed to extract useful structural information.

With the growth of computer and image technology, medical imaging has greatly influenced medical field. As the quality of medical imaging affects diagnosis, the medical image processing has become an interesting research topic, not only for the ability to store, retrieve and handling a large amount of data, but rather for automating the analysis process [28].

A cell that divides itself into two daughter cells with the same chromosomes undergoes a process of *mitosis* (see Figure 1.1)³.

The scoring of mitotic figures is an integrated part of the various systems for grading of invasive breast cancer with most rigorous criteria [25]. For this reason, the automatic detection and counting of mitotic figures in breast cancer tissue is an attractive and challenging research topic [98].

An example of histological images for mitosis detection is given in Figure 1.2⁴.

¹<http://www.cancerresearchuk.org/cancer-help/about-cancer/cancer-questions/how-many-different-types-of-cancer-are-there>

²<http://globocan.iarc.fr/factsheets/populations/factsheet.asp?uno=900#WOMEN>

³image taken from <http://en.wikipedia.org/wiki/Mitosis>

⁴image taken from <http://www.breastpathology.info>

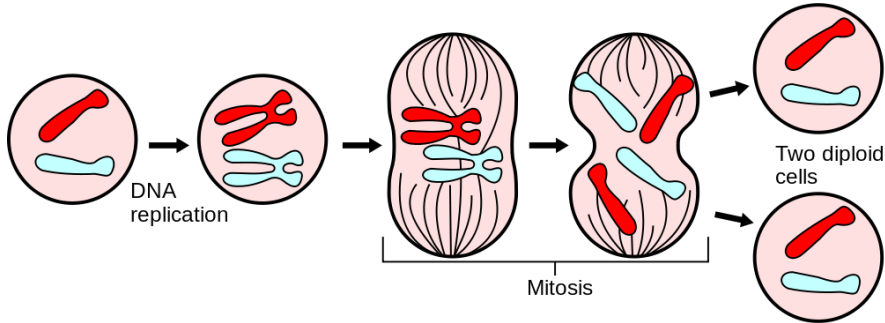


Figure 1.1: Mitosis of a cell

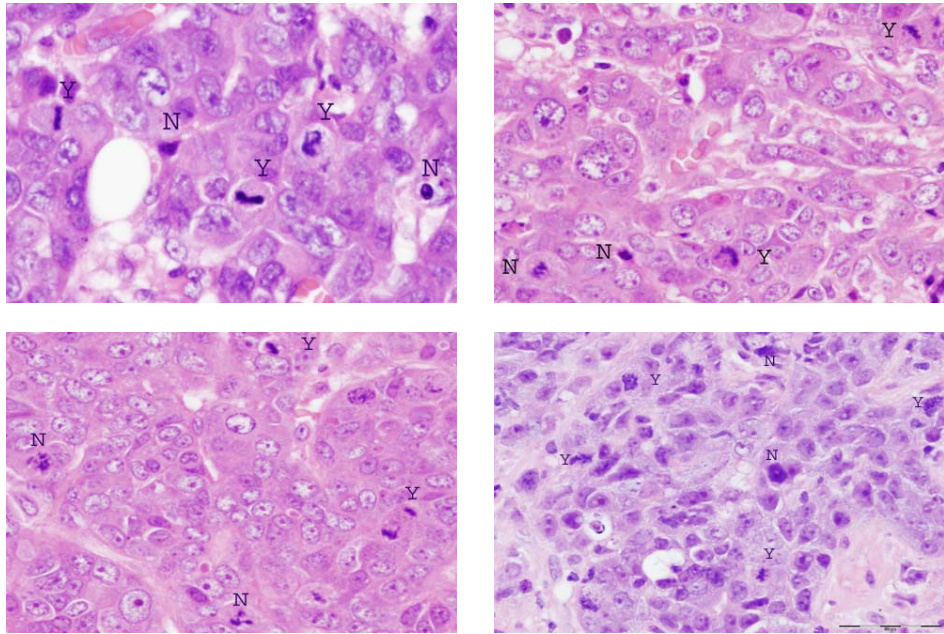


Figure 1.2: Histological images with labeled mitoses (Y) and non-mitoses (N)

The automatic detection process lays its groundwork in the fields of Computer Vision and Machine Learning[94]. Mitotic cells must be found and identified on a histological image. This issue can be faced as a detection problem, to find interesting portions of a histological image, and a supervised learning problem, where a classifier is given a set of labeled samples (mitoses and non-mitoses) from which it must gain some information to classify unseen samples.

Various aspects influence the performances of such automatic processes, which can be summarized into:

- the size and the quality of the dataset,
- the ability of the classifier to gain information and to generalize.

The quality of the dataset is related the idea of data validation form a clinical point of view. Mitosis detection is known to be a difficult problem, and several studies have found that pathologists' agreement on the mitotic grade is fairly modest, with strong biases [59]. This aspect have an impact when using data to train a computerized system for mitosis detection. Conversely, once a dataset and the associated ground truth is accepted, it is the classifier that has to be able to gain information on labeled samples and use this information to perform sufficiently well on new (unseen) data.

From the application point of view, both aspects (dataset and classifier performance) are important to build a reliable automatic mitosis detection system: the most relevant issue is whether such algorithms perform similarly (or better) than experts who routinely solve the same task.

Instead, in this work we put ourselves in the perspective of the machine learning algorithm designer. Within this context, comparing a mitosis detection algorithm with an expert pathologist does not provide much useful information, because they are not competing on a fair basis. In fact, during his formation and previous activity, a pathologist had access to an amount of training information (in form of criteria, guidelines and labeled examples) which is most probably extremely larger than every algorithm's training set. The question that arises is: if the algorithm underperforms, is it because it is not powerful enough, or because it has not enough data to learn? The former case means that the effort should be focused on improving the algorithm ability, the latter implies that effort should be instead focused on gathering larger labeled datasets. We aim to answer this question in the context of mitosis detection in breast cancer histological images using a public dataset.

In our work we focused on the classification problem, extracting labeled samples from images of a public dataset annotated by an expert pathologist. We then built some classifiers based on such images and implemented a testing website to collect classifications by different users. We compared the performances of our classifiers with the ones obtained by algorithms participating to the *ICPR 2012 Mitosis Detection Contest*⁵ (performance measured on the same dataset) and with performances of humans facing the same problem.

⁵<http://ipal.cnrs.fr/ICPR2012/?q=node/1>

Our test subjects were given no guidelines, and were required to learn a classification function solely from the provided training set. This kind of setting can not be recreated when benchmarking humans for other famous instances of visual pattern recognition problems (such as face detection, object recognition, and handwriting understanding). One of such benchmarks [88] focused on the task of classifying traffic sign images, which is a significantly easier problem than mitosis classification; algorithms were given a very large training set (25000 images) and the best algorithm outperformed the best individual (among 8) with an accuracy of 99.46% vs 99.22%. These results are consistent with the ones that we report in this work, based on 7 algorithms and 45 test subjects, compared to 2 different classifiers developed ad hoc.

The dissertation presents the following structure:

- In Chapter 2 we review the state of the art in the main fields of research in which our work is included, such as: mitosis detection for breast cancer grading, applications of computer vision techniques in biomedical imaging, and machine learning methods for biomedical classification.
- In Chapter 3 we define the problem of mitosis counting, in terms of detection and classification. We also describe some implementations of mitosis detection algorithm and define the most important measures of performance for classification task.
- In Chapter 4 we describe the dataset on which all our work is based and define the framework for the classification algorithms that we implemented. We outline the main components needed to carry out a classification task: dataset manipulation, features selection and extraction, classification and analysis of the performances.
- In Chapter 5 we describe the testing website developed to collect users' classifications and performance.
- In Chapter 6 we describe all the experimental results deriving from automatic classification, human classification and we compare the results.
- Chapter 7 is dedicated to conclusions and evaluations on possible future research directions.

One appendix is included in this work: Appendix A shows some of the image samples used for our classification tasks.

Chapter 2

State of the art

“Rem tene, verba sequentur”

(Know the subject, the words will follow)

Marcius Porcius Cato Censorius

2.1 Background

Breast cancer classification divides breast cancer into categories according to different schemes¹, each serving a different purpose. The purpose of classification is to select the best treatment [29].

Within the last decade, histological grading has become widely accepted as a powerful indicator of prognosis in breast cancer. The grading depends on the microscopic similarity of breast cancer cells to normal breast tissue, and classifies the cancer as well differentiated (low grade), moderately differentiated (intermediate grade), and poorly differentiated (high grade), reflecting progressively less normal appearing cells that have a worsening prognosis. Although grading is fundamentally based on how biopsied, cultured cells behave, in practice the grading of a given cancer is derived by assessing the cellular appearance of the tumor.

The Nottingham Grading System (NGS) (also called Elston-Ellis) is a modification [25] of the Bloom and Richardson Grading System (BR) [9, 30]. NGS is judged more reproducible and is the recommended grading method [1].

¹<http://www.breastpathology.info/>

NGS grades breast carcinomas by adding up scores for:

- tubule formation,
- nuclear pleomorphism,
- mitotic count,

each of which is given 1 to 3 points. The scores for each of these three criteria is then added together to give an overall final score and corresponding grade as follows [20]:

3-5 **Grade 1 tumor** (well-differentiated). Best prognosis.

6-7 **Grade 2 tumor** (moderately-differentiated). Medium prognosis.

8-9 **Grade 3 tumor** (poorly-differentiated). Worst prognosis.

Lower grade tumors, with a more favorable prognosis, can be treated less aggressively, and have a better survival rate.

Mitosis is a form of nuclear division of the mother cell into two daughter cells, genetically identical to each other and to their parent cell. By this process, a cell, which has previously replicated each of its chromosomes, separates the chromosomes into two identical sets of chromosomes, each set in its own new nucleus (see [4, 74] for some details).

Mitotic activity is one of the strongest prognosticators for invasive breast carcinoma. It is expressed as the number of mitotic figures per tissue area. Early detection plays an important role in reducing cancer mortality. The current procedure for breast cancer grading is manually performed by pathologists, for both nuclear pleomorphism [23] and mitotic count. Breast tissue samples of patients are taken and examined under microscopes. Pathologists grade the tissue samples based on the deviation of the cell structures from normal tissues. A pathologist may have to examine a great amount of slides [75]. This process can be time consuming and subjective (see 3.4.1).

In the following subsection we give a short overview of the mitosis count procedure [3].

2.1.1 Tissue preparation

After tumor excision is performed, the excised material is sent for analysis in a pathology lab. The tissue preparation process starts with making smaller cuts of the material that are then fixed in formalin and (after processing) embedded in paraffin.

Using a high precision cutting instrument (microtome), thin sections are cut from the paraffin block, which are then put on glass slides. The final stage of the tissue preparation process is the staining of the sections with stains that highlight specific structures of the tissue so they are better visible under a microscope. The standard staining protocol uses the Hematoxylin and Eosin (HE) stains. The hematoxylin dyes the nuclei a dark purple color and the eosin dyes other structures (cytoplasm, stroma, etc.) a pink color.

2.1.2 Digital Pathology

Recent years have brought the trend of digitization of histological slides. Digital slide scanners (see Figure 2.1), in combination with digital slide viewers, aim to provide the experience of viewing a digital slide on a computer monitor in a manner analogous to viewing it under a microscope, but with all the added benefits of the digital format (ease of annotation, image analysis, collaborative viewing etc.). The output of the digital slide scanners are multi-layered images, stored in a format that enables fast zooming and panning. Depending on the area of the tissue that is present on the slide and the magnification and resolution at which the slide is scanned, the lowest layer of the digital slide can be up to several tens of thousands of pixels in width or height. Currently, digital slides are mainly used for research, education and remote consultation purposes. Their use for routine diagnosis and prognosis is not yet common [44]. Availability of automatic image analysis algorithms that can aid pathologists in their work can be a major incentive for acceptance of digital slides in the routine pathology lab workflow.

2.1.3 Mitosis Counting

As previously stated, mitotic activity is one of the strongest prognosticators for invasive breast carcinoma and it is expressed as the number of mitotic figures per tissue area. As part of the BR grading system, mitotic activity is routinely assessed in pathology labs across the world. In addition, the



Figure 2.1: *Aperio ScanScope XT scanner*

mitotic activity can be used as a prognosticator independently of the BR grading system. Typically, the pathologist receives a panel of slides for each case that is to be graded. He or she then proceeds to select one slide where the histological grading will be performed. The mitosis counting is performed in 8-10 consecutive microscope High Power Fields (HPF) [43]. A HPF has a size of $512 \times 512\mu m^2$ (i.e. an area of $0.262 mm^2$), which is the equivalent of a microscope field diameter of $0.58mm$. The standard guidelines are to select an area that encompasses the most invasive part of the tumor, at the periphery and with highest cellularity. Depending on the number of figures counted, a mitotic activity score is assigned. Cases with 7 or fewer mitotic figures present are assigned score 1 (best prognosis). Cases with more than 12 mitotic figures are assigned score 3 (worst prognosis). The intermediate cases are assigned score 2.

2.1.4 Challenges in Mitosis Detection

Because of the aberrant chromosomal makeup of many tumors (aneusomy, polysomy, translocations, amplifications, deletions), the appearance of mitotic figures in the images can significantly differ from the textbook examples of a splitting nucleus [51]. In addition, imperfections of the tissue preparation process result in tissue appearance variability, which can present a challenge also for an automated mitosis detection system.

Most commonly, mitotic figures are exhibited as hyperchromatic objects. In addition, they have absence of a clear nuclear membrane, “hairy”protrusions

around the edges and basophilia instead of eosinophilia of the surrounding cytoplasm. However, these are more guidelines than hard rules, and the bulk of the training of pathologists is done by looking at specific examples of mitotic figures. One of the main challenges in spotting mitotic figures is that other objects such as apoptotic nuclei can have similar appearance, making it difficult even for trained experts to make a distinction [87]. Lymphocytes, compressed nuclei, “junk” particles and other artifact form the tissue preparation process, can also have hyperchromatic appearance. The images in Figures 2.2, 2.3 and 2.4 try to give an idea of the difficulty of the task.

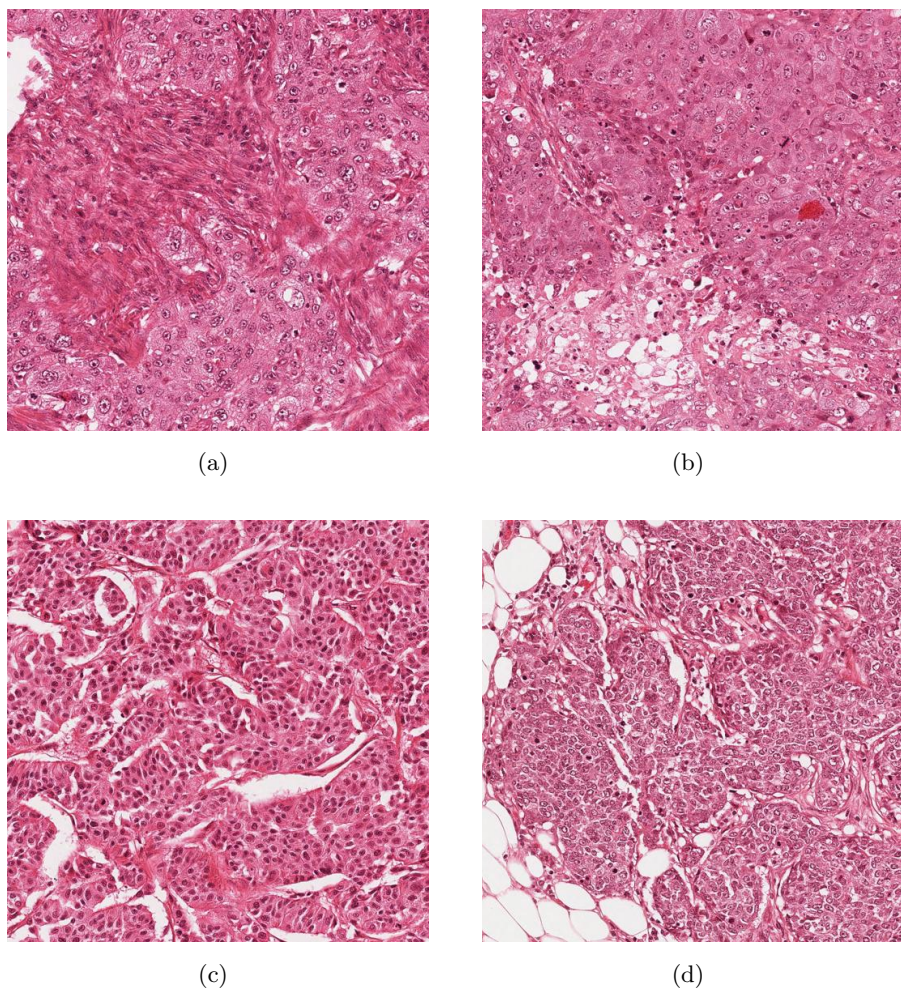
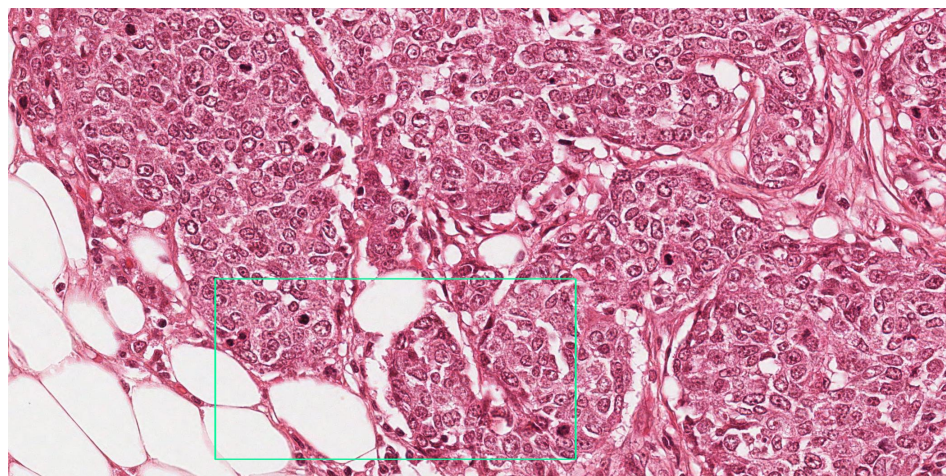
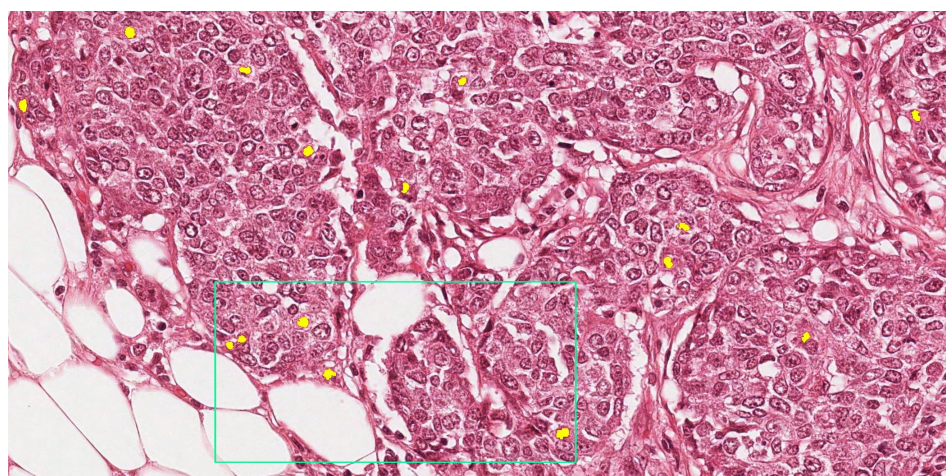


Figure 2.2: Examples of digital histological images

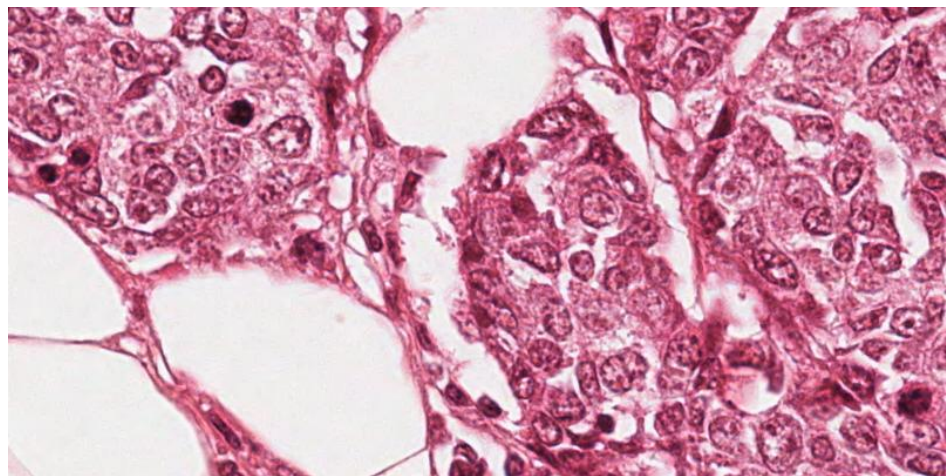


(a) source image

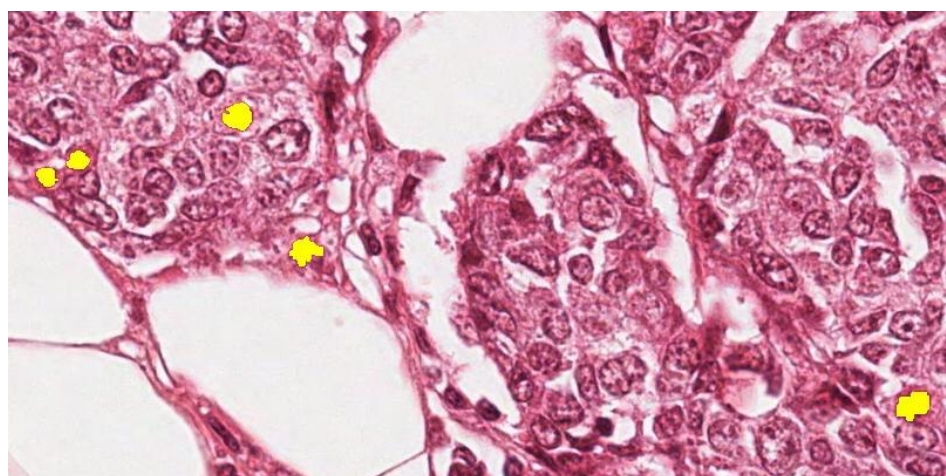


(b) mitoses

Figure 2.3: Example of image with highlighted mitoses (yellow)



(a) source image (detail)



(b) image and mitoses (detail)

Figure 2.4: Example of image with highlighted mitoses (yellow) detail of Figure 2.3

2.2 Mitosis Detection and Computer Vision

The task of automatic mitosis detection involves topics in various fields of research, in particular: Image Analysis and Machine Learning.

We consider a framework in which, in the whole image, some candidates are detected and the classified as mitosis or non-mitosis.

In this chapter we give an overview of the main aspects concerning *image analysis* and in the following one (Section 2.3) we analyze the *machine learning* elements.

Over the past decade, dramatic increases in computational power and improvement in image analysis algorithms have allowed the development of powerful computer-assisted analytical approaches to radiological and histopathological data [32]. Digitized tissue histopathology has now become amenable to the application of computerized image analysis and machine learning techniques. Analogous to the role of Computer Aided Diagnosis (CAD) algorithms in medical imaging to complement the opinion of a radiologist, CAD algorithms have begun to be developed for disease detection, diagnosis, and prognosis prediction to complement the opinion of the pathologist [84].

2.2.1 Software Tools

The imaging modalities rely heavily on computational approaches. In fact, in many cases the computational technology is just as important as the optics, not just for the digital capture that all systems now use but in many cases also for visualizing and properly interpreting the data. An interesting article [24] reviews each computational step that biologists encounter when dealing with digital images and the overall status of available software for bioimage informatics. It is worth highlighting the existence of open-source software tools like *Fiji* [81] and *ImageJ* [82], which supply some basic features for *object detection* and *feature extraction* [78].

2.2.2 Features and Detectors

When dealing with digital image analysis and automatic identification of properties of an image, the idea of *feature* and the functionality of a *detector* are the main topics to be considered.

The concept of feature is used to denote a piece of information which is relevant for solving a computational task [67]. A feature is defined as an

“interesting” part of an image, and features are used as a starting point for many Computer Vision (CV) algorithms. They can be the result of a general *neighborhood operation* [47] applied to the image, or specific structures in the image itself. Types of image features include:

- Edges,
- Corners,
- Blobs or Regions of Interest (ROIs),
- Ridges or elongated objects (i.e. blood vessels in medical images).

Other examples of features are related to motion in image sequences, to shapes defined in terms of curves or boundaries between different image regions, or to properties of such a region [37].

The feature concept is very general and the choice of features in a particular CV system may be highly dependent on the specific problem to be considered.

Many algorithms have been developed to detect specific features, and a complete overview of them is beyond the scope of this work. Some of the most famous ones, like *Canny edge detector* [15], *Harris edge and corner detector*, or SUSAN [86] are available in most widely used commercial and open-source Computer Vision software packages (i.e. MATLAB Image Processing Toolbox² or OpenCV³).

Features are sometimes extracted over several scalings. One of these methods is *Scale-invariant feature transform*; in this algorithm, various scales of the image are analyzed to extract features [57] (the underlying theory can be found in [54]).

2.2.3 Texture Algorithms

An important set of features that can be computed on an image involve the concept of *texture*.

An image texture is a set of metrics designed to quantify the perceived structure of an image. Image texture gives information about the spatial

²<http://www.mathworks.com/products/image/index.html>

³<http://opencv.org/>

arrangement of color or intensities in an image or in selected region of it [26]. Image textures are used in *segmentation* (see 2.2.4), or *classification* of images (see 2.3). To address the issue of texture analysis, the so called “statistical approach” is more widely used as it is easier to compute. This approach sees an image texture as a quantitative measure of the arrangement of intensities in a region. Here we briefly describe the main statistical feature algorithms.

Co-occurrence Matrix

Co-occurrence matrix captures numerical features of a texture using spatial relations of similar gray tones. Numerical features computed from the co-occurrence matrix can be used to represent, compare, and classify textures [40, 101]. The following are a subset of standard features derivable from a normalized co-occurrence matrix, as described in [36]:

$$\text{Contrast} = \sum_{n=0}^{N_g-1} n^2 \left\{ \sum_{i=1}^{N_g} \sum_{j=1}^{N_g} p[i, j] \right\}, \text{ where } |i - j| = n \quad (2.1)$$

$$\text{Correlation} = \frac{\sum_{i=1}^{N_g} \sum_{j=1}^{N_g} (i, j) \cdot p[i, j] - \mu_x \mu_y}{\sigma_x \sigma_y} \quad (2.2)$$

$$\text{Entropy} = - \sum_i \sum_j p[i, j] \cdot \log(p[i, j]) \quad (2.3)$$

Where:

- N_g is the number of gray levels in the quantized image,
- $p[i, j]$ is the (i, j) th entry in a normalized gray-tone spatial dependence matrix,
- $\mu_x, \sigma_x, \mu_y, \sigma_y$ are the mean and the standard deviation of respectively $p_x = \sum_{j=1}^{N_g} p(i, j)$ and $p_y = \sum_{i=1}^{N_g} p(i, j)$.

Various algorithms use texture feature like Gray-level Co-occurrence Matrix (GLCM) [71], Gray-level Run-length Matrix (GLRM) [60] or Gray-level Entropy Matrix (GLEM) for image classification, also in medical [13] and biological imaging [105].

Local Binary Patterns

Local Binary Patterns (LBP) is another type of feature used for classification in Computer Vision. LBP is a simple yet very efficient texture operator which labels the pixels of an image by thresholding the neighborhood of each pixel with the value of the center pixel and considers the result as a binary number. The distance and the number of neighbors can be selected, as shown in Figure 2.5 [69]. The notation (P, R) is used for pixel neighborhoods which means P sampling points on a circle of radius of R .

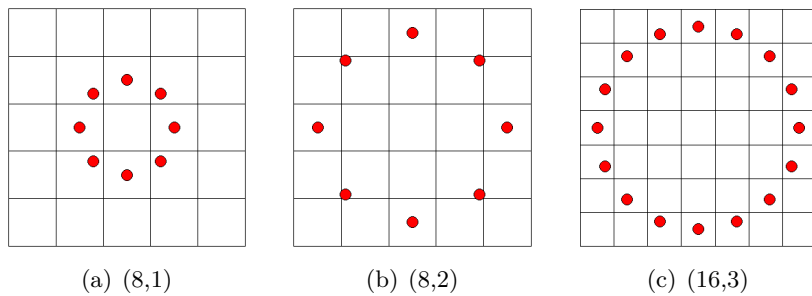


Figure 2.5: Examples LBP neighbors and distances

The computation of the LBP code of a pixel of coordinates (x_c, y_c) is given by:

$$\text{LBP}_{P,R} = \sum_{p=0}^{P-1} s(g_p - g_c) \cdot 2^p \quad \text{where } s(x) = \begin{cases} 1, & \text{if } x \geq 0 \\ 0, & \text{otherwise} \end{cases} \quad (2.4)$$

This operator used jointly with a simple local contrast measure provided very good performance in unsupervised texture segmentation. Another extension to the original operator is the definition of so called uniform patterns, which can be used to reduce the length of the feature vector and implement a simple rotation-invariant descriptor. This extension was inspired by the fact that some binary patterns occur more commonly in texture images than others. A LBP is called uniform if the binary pattern contains at most two bitwise transitions from 0 to 1 or vice versa when the bit pattern is traversed circularly.

In the computation of the LBP labels, uniform patterns are used so that there is a separate label for each uniform pattern and all the non-uniform patterns are labeled with a single label. For example, when using $(8, R)$ neighborhood, there are a total of 256 patterns, 58 of which are uniform, which yields in 59 different labels.

The uniform and rotation invariant LBP can be further enhanced by combining it with a Rotation Invariant Variance Measure (VAR) operator, with the same parameters (P, R), that characterizes the contrast of local image texture [68]. Both operators are also computationally attractive, as they can be realized with a few operations in a small neighborhood and a lookup table. The VAR operator is described by the following relations:

$$\text{VAR}_{(P,R)} = \frac{1}{P} \sum_{p=0}^{P-1} (g_p - \mu)^2 \quad \text{where } \mu = \sum_{p=0}^{P-1} g_p^2 \quad (2.5)$$

$\text{LBP}(P, R)$ and $\text{VAR}(P, R)$ are complementary and a feature set made by the combination of the two is expected to be a very powerful rotation invariant measure of local image texture. It is also possible to use joint feature sets composed by operators with different neighborhood.

Wavelets

The Wavelet Transform (WT) is having greater importance medicine and biology. The main uses of the WT concern the analysis of one-dimensional physiological signals obtained by electrocardiography (ECG) and electroencephalography (EEG), including evoked response potentials [97]. A survey of recent wavelet developments in medical imaging can be found in [96]. These include biomedical image processing algorithms (e.g., noise reduction, image enhancement and detection) and image reconstruction and acquisition schemes (tomography, and Magnetic Resonance Imaging (MRI)).

2.2.4 Image Segmentation

Segmentation is the process of partitioning a digital image into multiple segments (sets of pixels) in order to simplify or change the representation of an image into something that is more meaningful and easier to analyze [52]. Image segmentation is typically used to locate objects and boundaries (i.e. features) in images. Such a process assigns a label to every pixel in an image so that pixels with the same label share certain visual characteristics [87].

2.2.5 Object detection and recognition

Object detection is a Computer Vision technology that deals with detecting instances of semantic objects of a certain class (such as humans, traffic signs, mitotic cells) in digital images. Humans recognize a multitude of objects in images with little effort, despite the fact that the image of the objects may be in different orientation, or in different size/scale. Objects can even be recognized when they are partially obstructed from view. This task is still a challenge for CV systems and represents the connection between Image Analysis topics and Machine Learning. Viola and Jones proposed a well known object detection framework [100, 99], which involves the sums of image pixels within rectangular areas, using the so-called Haar-like features, a name that resembles the Haar wavelet adopted in other works [72]. The technique generates a large amount of features and uses the boosting algorithm *AdaBoost* to reduce the over-complete set, by selecting the best features and training classifiers that use them. The evaluation of the classifiers generated in the learning phase can be quick, but generally not enough to be run in real-time. For this reason, the classifiers are arranged in a cascade in order of complexity, where each subsequent classifier is trained only on those selected samples which pass through the preceding classifiers. If at any stage in the cascade a classifier rejects a sample, no further processing is performed. The cascade therefore has the form of a degenerate tree.

2.3 Machine Learning

Machine Learning (ML), a branch of Artificial Intelligence (AI), deals with the ability to define and to build systems that can learn from data. The core of ML deals with the representation of data and their generalization. Representation deals with the way the system describes the data. Generalization deals with the ability of the system to perform on unseen data samples. In Machine Learning, the observations are often known as *instances*, the explanatory variables are termed *features* (grouped into a *feature vector*), and the possible categories to be predicted are *classes*.

ML algorithms can be divided into different types:

- **Supervised Learning** generates a function that maps inputs to desired outputs usually called *labels*, because they are often provided by human experts classifying the training examples.
- **Unsupervised learning** models a set of inputs. It can also be re-

ferred to as *data mining* and knowledge discovery. Here, labels are not known during training.

- **Semi-supervised learning** combines both labeled and unlabeled examples to generate an appropriate function or classifier.
- **Reinforcement learning** learns how to act given an observation of the world. Every action has some impact in the environment, and the environment provides feedback in the form of rewards that guides the learning algorithm.

There exists a great variety of ML algorithms, and a detailed review is beyond the scope of this work⁴.

We focus, in our analysis, on *Pattern Recognition* and in particular on *Supervised Learning* methods.

2.3.1 Pattern Recognition

Pattern Recognition (PR) is the assignment of a label to a given input value [8, 95]. In its most general form, PR involves:

- **Classification** is the problem of identifying to which of a set of categories a new observation belongs, on the basis of a training set of data containing instances whose category membership is known,
- **Regression** is a technique for estimating the relationships among variables, assigning a real-valued output to each input,
- **Sequence labeling** refers to the assignment of a categorical label to each member of a sequence of observed values, in particular by making choices which depend on the one made for nearby elements (e.g. speech tagging),
- **Parsing** is the process of analyzing a string of symbols according to the rules of a formal grammar.

⁴A list of ML algorithms can be found in http://en.wikipedia.org/wiki/List_of_machine_learning_algorithms

2.3.2 Classification

Among the different types of learning methods and pattern recognition techniques we focus our attention on *classification* which, in general ML terminology, is an instance of *supervised learning*.

The formal definition of a supervised classification problem can be stated as follows: an unknown function g maps the input instances $x \in X$ to the output labels $y \in Y$:

$$g : X \rightarrow Y \quad (2.6)$$

Equation 2.6 represents the *ground truth(GT)*.

The *training set*

$$T = (x_1, y_1), \dots, (x_n, y_n) \quad (2.7)$$

is assumed to represent the mapping of g in an accurate way. The classifier then tries to build a function $h : X \rightarrow Y$ that approximates as closely as possible the correct mapping. The measure of the performance (see 3.4 for details) is generally done on a separate set of data (the *test set*) whose labels are known but whose data are not used during the learning phase [55].

A common subclass of classification is *probabilistic classification*. Algorithms of this type involve statistical tools to define the best class for a given instance [73]. Probabilistic algorithms output a probability that the instance is a member of each of the possible classes. The best class is normally then selected as the one with the highest probability. Classification can be also divided into two separate problems - *binary classification* and *multi-class classification*. In binary classification, only two classes are involved, whereas multi-class classification considers the problem of assigning an object to one of several classes. Since many classification methods have been developed specifically for binary classification, multi-class classification often requires the combined use of multiple binary classifiers.

2.3.3 Binary Classification

Binary classification is the task of classifying the members of a given set of objects into two groups on the basis of whether they have some properties or not [83]. Medical testing is a typical binary classification task (i.e. to determine if a patient has certain disease or not). In traditional statistical hypothesis testing, the tester starts with a null hypothesis and an alternative hypothesis, performs an experiment, and then decides whether to reject the

null hypothesis in favor of the alternative. Hypothesis testing is therefore a binary classification of the hypothesis under study [64]. A *positive* result is one which rejects the null hypothesis. Rejecting the null hypothesis when it is actually true - a False positive (FP) - is a **type I error**; on the other hand, when the null hypothesis is false results in a True positive (TP). A *negative* result is one which does not reject the null hypothesis. Accepting the null hypothesis when it is actually false - a False negative (FN) - is a **type II error**; on the other hand, when the null hypothesis is true results in a True negative (TN). How the number of TP, FP, TN and FN can be used to assess the performances of a classification algorithm is treated in Section 3.4.

2.3.4 Binary Classifiers

An algorithm that implements a classification is defined a **classifier**. The term also refers to the mathematical function, implemented by a classification algorithm, that maps input data to a category (i.e. *class*). A great amount of algorithms has been developed for classification purposes, in particular for CV tasks [58]. Some methods suitable for learning binary classifiers include [102]:

- Naive Bayes classifiers,
- Bayesian networks [104],
- Decision trees [5],
- RFs [38],
- SVMs [42],
- Hidden Markov models,
- Neural Networks (NNs) [77].

In our work we focused on two types of classifiers: *Support Vector Machines* and *Random Forests* which are widely used in CV classification problems (e.g. [87] and [10]).

2.3.5 Software Tools

Classification tasks can be accomplished by a large amount of software tools. Here we mention the ones that we consider to be the most relevant ones.

Weka [27, 33] is a **FLOSS** general purpose data mining software tool developed by the Waikato University⁵ which allows to implement a great variety of classifiers [102]. It also has an interface with **R**⁶ [41].

MATLAB can perform classification task by means of some of its toolboxes (i.e. Bioinformatics⁷ and Statistics⁸).

⁵<http://www.cs.waikato.ac.nz/ml/weka/>

⁶<http://cran.r-project.org/>

⁷<http://www.mathworks.com/products/bioinfo/>

⁸<http://www.mathworks.com/products/statistics/>

Chapter 3

Problem Definition

“πάντες ἀνθρωποι τοῦ εἰδέναι ὡρέγονται φύσει”

(All men naturally desire knowledge)

Ἀριστοτέλης (Aristotle, Met. 1.980a)

The aim of our work is to analyze the performances of mitosis detection algorithms compared to humans trying to classify the same images. To achieve this goal, we selected a subset of samples taken from the publicly-available *MITOS dataset* made for the *ICPR 2012 Contest on Mitosis Detection in Breast Cancer Histological Images*¹. Then we run the following activities:

- collected the performances of the top-scoring algorithms developed for the ICPR 2012 Mitosis Detection Contest (focusing on the subset of the dataset used in the other experiments),
- applied some classifiers to the dataset,
- implemented a web-based test for humans,
- analyzed the performances of the algorithms compared to the results achieved by humans.

The main definitions for the problem in exam are the subject of this chapter.

¹<http://ipal.cnrs.fr/ICPR2012/>

3.1 Framework

The purpose of automating the mitosis detection problem requires the definition of a framework that involves Computer Vision and Machine Learning aspects. ML is growing in importance for biology-related tasks [93]. In general, PR (see 2.3.1) is the computational approach used to analyze datasets of images [85].

3.1.1 Detection

The analysis of digital images requires identifying ROIs or *candidates* within the images. Once a region is isolated, a digital image allows many types of measurements and statistics to be collected, as well as the number of objects and their distribution. This region selection can be done manually by drawing boxes or free-hand regions using an interactive tool [92], or automatically using computer algorithms known as segmentation algorithms [56]. The input to the algorithm may be an entire image, a sub-image region identified with segmentation algorithms, or simply image samples in the form of rectangular tiles.

3.1.2 From Detection to Classification

PR then requires training a computer to classify groups of images (i.e. a subset of images with manually detected mitoses). The machine can learn on its own what aspects of the images represent natural experimental variation and are therefore irrelevant, and what aspects are important for distinguishing the groups of control images (i.e. the testing set) from each other (see Section 3.2). This ability to select different image measurements allows the use of a great variety of image description algorithms, potentially making the collection of algorithms very general. The benefits of subdividing images into ROIs involve:

- reduce the number of pixels to consider,
- bias the algorithm to process objects of interest rather than background,
- center or align objects.

A further step consists in the extraction of image content descriptors (*image features*), which are values that describe the image content numerically.

These values can reflect various texture parameters of the image, the statistical distribution of pixel intensities, edges, etc. While the dimensionality of the raw pixels can be high, the number of image features ranges between a dozen to a few hundred. Each feature value describes a specific image characteristic. Then, the image features are used to draw conclusions about the data. The feature set is then used to infer rules for combining them in a classifier. These two steps constitute the training stage in PR, where the goal is to correctly classify the training images. The trained classifier is then tested on control images that were excluded from the training stage. This cross-validation is important to establish the classifier's ability to identify new images, ensuring that it is not restricted to recognizing images it was trained with (condition known as *overfitting*).

3.1.3 Performances

If the performance of the algorithm are not satisfying (see Section 3.4 for details), the algorithm can be trained again on a different set of features, until the detection capabilities reach the desired values (if feasible). Finally, the results of image classification need to be interpreted by the researcher in an experimental context to reach a biological conclusion. Figure 3.1 shows the steps described above.

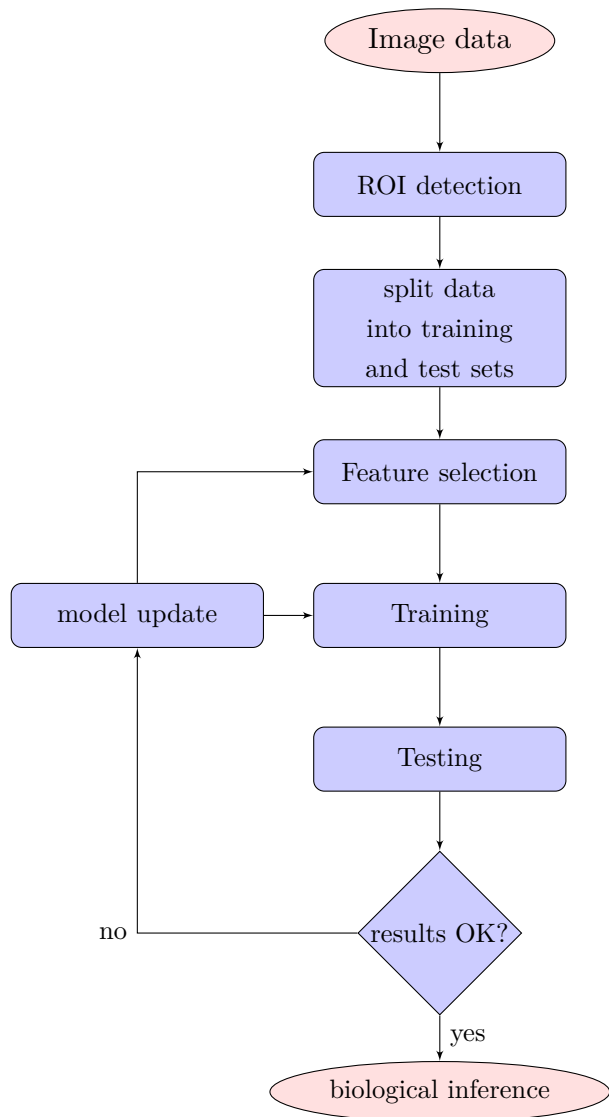


Figure 3.1: Flowchart of Detection Algorithm

3.2 Definition of Classification

In ML, the idea of *classification* refers to the problem of identifying to which of a set of categories (named *classes*) a new observation belongs, on the basis of a training set of data containing instances whose category membership is known. In case of mitosis detection, the elements of a classification are basically the following:

- the *input* to the classification problem is a set of *features* computed on each of the *candidates* selected in a preparatory phase. Each set of features composing a candidate is known as *instance*. Each instance is *labeled* with the *class* which it belongs to.
- the *classes* are simply two: **mitosis** (which we call *class 1* or *positive*) or **non-mitosis** (which we call *class 0* or *negative*) making it a case of binary classification.
- the *output* of the classification can be a *hard* classification: the output of the classifier is simply *0* or *1*, corresponding to mitosis or non-mitosis respectively. On the other hand the classification can be *soft*: the output of the classifier is a real number *c*:

$$0 \leq c \leq 1 \quad (3.1)$$

a subsequent phase of analysis consists in selecting the best threshold so that:

$$\text{class} = \begin{cases} 0, & \text{if } c < \text{threshold}. \\ 1, & \text{otherwise.} \end{cases} \quad (3.2)$$

the selection of the threshold is made in function of the measured performances of the classification algorithm (see Section 3.4).

3.3 Review of Algorithms solving the mitosis detection problem

In a different way with respect to many other pattern recognition tasks, mitotic cells essentially are irregular shape objects. As a result, there is no simple or unique way of extracting the features of mitotic cells candidates and then lots of different classifiers can be made.

Here we briefly review the main algorithms found in literature that solve the mitosis detection task.

- The first method that we considered [98] consists of two main components: candidate extraction and candidate classification. Candidate objects are extracted by image segmentation with the Chan-Vese level

set method [65]. A statistical classifier is trained with a number of features that describe the size, shape, color and texture of the candidate objects.

- Another approach [51] uses, after a phase of automatic segmentation of the image, a Gamma Gaussian Mixture Model (GGMM) to classify the candidates: the GGMM is a parametric technique for estimating probability density function. In this context, it is formulated as a function of pixel intensities.
- A similar work [43] also proposes a two phases approach: the detection candidates points are selected by using an algorithm named eXclusive Independent Component Analysis (XICA), which gives two sets of training patterns: positive and negative patterns (positive and negative basis set). Then a sparse representation method [103] is used to classify the candidates.
- Another approach shows two phases [46]. In the first stage, the detection of candidate mitosis is performed. The input RGB images are transformed into blue-ratio images. A Laplacian of Gaussian (LoG), thresholding and morphological operations on blue-ratio images is then executed to generate candidate mitosis regions. Then, the candidate regions are selected using morphological rules; the center point of each region is used as seed point for mitosis. In the second stage, co-occurrence features, run-length features and SIFT features are computed for each candidate patch. Finally a classification is performed to put the candidate patch either in the mitosis class or in the non-mitosis class. Three different classifiers have been evaluated: decision tree, linear kernel SVM and non-linear kernel SVM.
- An interesting methodology [59] uses a simple rule that extracts blobs representing nuclei of possible mitotic figures to establish a set of candidates. ML is applied in three phases. One phase applies a support vector regression which remaps the color palette of the original image to normalized values. The next phase is a Convolutional Neural Network (CNN), applied at each extracted blob. The CNN contributes a generate a feature vector, which also contains many other measurements regarding the shape, color, mass, and texture of the blob and its neighborhood. In the final phase, a SVM uses the feature vector to classify the area around the blob as a mitotic figure or not.

The last two works that we mention here are particularly interesting

because they work on the same dataset that we used, the *MITOS Dataset* (see Chapter 4 for details).

- The first approach [45] works on z-stack focus planes for detection of mitosis candidates. Then candidates are detected using thresholding and morphological operations on selected band and focus plane. A multi-spectral features vector is computed for detected candidates having intensity and texture features across all bands of multi-spectral images. In addition, using segmented regions of detected candidates, morphological features are also computed. A feature selection algorithm is employed on this features vector in order to save the computation cost, to discard any redundancy in the data, and to improve classification accuracy. Classification is achieved using Bayesian, Decision Tree, Neural Network as well as linear and non-linear SVM classifiers.
- The other work [17] is procedurally simpler than other methods, as no candidate selection is performed. A supervised Deep Neural Network (DNN) is used as a powerful pixel classifier. The DNN is a type of CNN. It directly operates on raw RGB data sampled from a square patch of the source image, centered on the pixel itself. The DNN is trained to differentiate patches with a mitotic nucleus close to the center from all other windows. Mitosis in unseen images are detected by applying the classifier on a sliding window, and post-processing its outputs with simple techniques. Because the DNN operates on raw pixel values, no human input is needed.

In our work, we also used, as a reference, the performances other top-scoring algorithms developed for the *MITOS Dataset*, whose main features will be described in a special issue of the *Journal of Pathology Informatics*² expected for June 2013.

3.4 Performance and Benchmarking

In order to set up a correct and valid comparison among mitosis detection algorithms, a consistent definition of *performance* plays a fundamental role. The general appearance of a mitosis results in the fact that automatically detecting mitoses is very challenging, and in fact even the agreement between pathologists is not perfect.

²<http://www.jpathinformatics.org/>

3.4.1 Pathologists' Agreement

A fundamental work [59] deeply analyzes the agreement among pathologists examining the same HE images. The BR grading system is widely recognized as the one giving the most stable definitions, and its grades are widely used to select treatments. Nevertheless, the level of agreement is shown to be far from perfect.

The level of agreement may be reported in Cohen's Kappa (κ) [18] whose range is $0 \leq \kappa \leq 1$, with **1** corresponding to perfect agreement, and **0** in the case of probabilistically independent decisions.

The value of κ can be divided in ranges:

- **0-0.2** is often considered as *slight* agreement,
- **0.2-0.4** as *fair*,
- **0.4-0.6** as *moderate*,
- **0.6-0.8** as *good*,
- **0.8-1** as almost *perfect*.

Most studies show that value of κ generally varies from *fair* to *moderate* (e.g. the study in [63] reports a value of $\kappa = 0.5$).

The low level of agreement among pathologists is an issue also for algorithms' benchmarking, as it can be difficult to establish a definite Ground Truth (GT) (i.e. the process of gathering the proper objective data for the test). Nonetheless, the images of the *MITOS Dataset* have been annotated by only one pathologist: the algorithms of the *2012 ICPR Contest* and our work based their GT on that.

3.4.2 Benchmarking

Benchmarking of different algorithms and comparison with human performance play a key role in a detection framework, it is so of great importance the definition of *performance*.

Given a GT, the *Confusion Matrix* (or Error Matrix [89]), is so defined: each column of the matrix represents the instances in a predicted class, while each row represents the instances in an actual class. The name originates from the fact that it makes it easy to see if the system is confusing two classes (i.e. mislabeling one as another). The elements of the matrix are:

- **TP**: *True Positive*, a sample labeled as true is predicted as true,
- **TN**: *True Negative*, a sample labeled as false is predicted as false,
- **FP**: *False Positive*, a sample labeled as false is predicted as true (i.e. false alarm, or *Type I error*),
- **FN**: *False Negative*, a sample labeled as true is predicted as false (i.e. miss, or *Type II error*),

| | predicted <i>Positive</i> | predicted <i>Negative</i> |
|---------------------------|------------------------------|------------------------------|
| Actual <i>Positive</i> | True Positive (TP) | False Negative (FN) |
| Actual <i>Negative</i> | False Positive (FP) | True Negative (TN) |

Table 3.1: Confusion Matrix

The data in Table 3.1 represent the minimum required data to assess the performance of a classifier (human or automatic). Starting from this, some other measurements can be done.

The data in the table can be assembled to define some performance indicators.

Accuracy

The accuracy of a test represents the degree of closeness of prediction to the actual value, and it is measured as:

$$\text{Accuracy } ACC = \frac{TP + TN}{P + N} \quad (3.3)$$

$$\text{where } P = TP + FN \text{ and } N = TN + FP \quad (3.4)$$

Precision, Recall, F-Score

A first set of measures that can be done on the data of the confusion matrix are: *precision*, also named Positive Predictive Value (PPV), *recall*, or True Positive Rate (TPR), and *F-Score* [31]. They are defined as follows:

$$\text{Precision } p = \frac{TP}{TP + FP} \quad (3.5)$$

$$\text{Recall } r = \frac{TP}{TP + FN} \quad (3.6)$$

Both precision and recall have a natural interpretation in terms of probability. Precision may be defined as the probability that an instance has class **1**, given that it is classified as **1**, while the recall is the probability that a class **1** object is classified:

$$p = P(\text{label} = \text{true} \mid \text{class} = \text{true}) \quad (3.7)$$

$$r = P(\text{class} = \text{true} \mid \text{label} = \text{true}) \quad (3.8)$$

The weighted (with parameter β) harmonic average of *precision* and *recall* leads to the *F-Score* [62]:

$$\text{F-Score } F_\beta = (1 + \beta^2) \cdot \frac{pr}{r + \beta^2 p} = \frac{(1 + \beta^2)TP}{(1 + \beta^2)TP + \beta^2 FN + FP} \quad (3.9)$$

F_1 -Score is most widely used as a measure of the accuracy of the classifier. It can be interpreted as a weighted average of the precision and recall: an F_1 -Score reaches its best value at **1** and worst score at **0**.

Specificity, Sensitivity

Sensitivity and *Specificity* are often used in clinical tests as a measure of the ability of the test to confirm or refute the presence of a disease [53]. Ideally a test correctly identifies all patients with the disease, and similarly correctly identifies all patients who are disease free. In other words, a perfect test is never positive in a patient who is disease free and is never negative in a patient who is in fact diseased.

The sensitivity of a clinical test refers to the ability of the test to correctly identify those patients with the disease:

$$\text{Sensitivity} = \frac{TP}{TP + FN} \quad (3.10)$$

It can be noted that the definition of sensitivity is the same as the definition of recall. A high sensitivity is clearly important where the test is used to identify a serious but treatable disease.

The specificity, or True Negative Rate (TNR), of a clinical test refers to the ability of the test to correctly identify those patients without the disease:

$$Specificity = \frac{TN}{TN + FP} \quad (3.11)$$

High specificity results in few patients who are disease free being told of the possibility that they have the disease and are then subject to further investigation or treatments. Also the following relation holds:

$$Specificity = 1 - FPR \quad (3.12)$$

$$\text{where } FPR = \frac{FP}{FP + TN} \quad (3.13)$$

Receiver Operating Characteristic (ROC)

As mentioned in Section 3.2, the classifier or diagnosis result can be a real value (continuous output). In this case the boundary between the two classes of the binary classifier must be determined by a threshold value.

A Receiver Operating Characteristic (ROC) space is defined by **FPR** and **TPR** as x and y axes respectively, which depicts relative trade-offs between true positive (benefits) and false positive (costs) [106]. Since TPR is equivalent to sensitivity and FPR is equal to $1 - \text{specificity}$, the ROC graph is sometimes called the *sensitivity vs $(1 - \text{specificity})$* plot [21]. Each prediction result or instance of a confusion matrix represents one point in the ROC space (see Figure 3.2(a)).

The best possible prediction method would yield a point in the upper left corner or coordinate $(0,1)$ of the ROC space, representing 100% sensitivity (no false negatives) and 100% specificity (no false positives). The $(0,1)$ point is also called a perfect classification. A completely random guess would give a point along a diagonal line from the left bottom to the top right corners. The diagonal divides the ROC space. Points above the diagonal represent good classification results (better than random), points below the line poor results (worse than random).

The ROC is used to generate summary statistics. One of the often used is the area under the ROC curve, or *AUC* (Area Under Curve) [14, 34] (see Figure 3.2(b)): AUC is equal to the probability that a classifier will rank a randomly chosen positive instance higher than a randomly chosen negative one. The AUC can be related to other summary statistics like the *Gini coefficient* [22] and the *Mann-Withney U* [61].

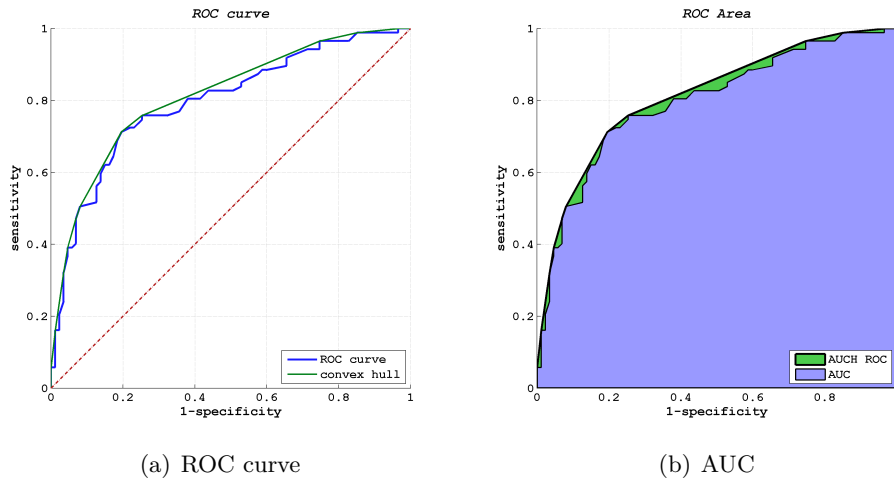


Figure 3.2: Example of ROC curves

Another common measure related to the ROC curve is known as the Area Under the ROC Convex Hull (*AUCH ROC*, in Figure 3.2(b)), which computes the area under the convex hull of the ROC curve, as it can be shown that any point on the line segment between two prediction results can be achieved by randomly using one or other system with probabilities proportional to the relative length of the opposite component of the segment.

3.5 Performances on ICPR Contest

We report here the performances of the best-scoring algorithms that participated to the ICPR2012 Contest, as shown on the contest website (Figure 3.3). The principal metric adopted to compare algorithms is the F_1 -Score (Figure 3.3(a)), but also precision and recall are shown (Figure 3.3(b)).

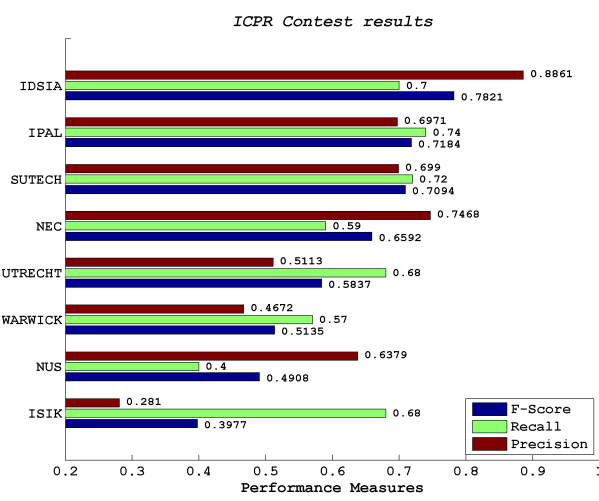
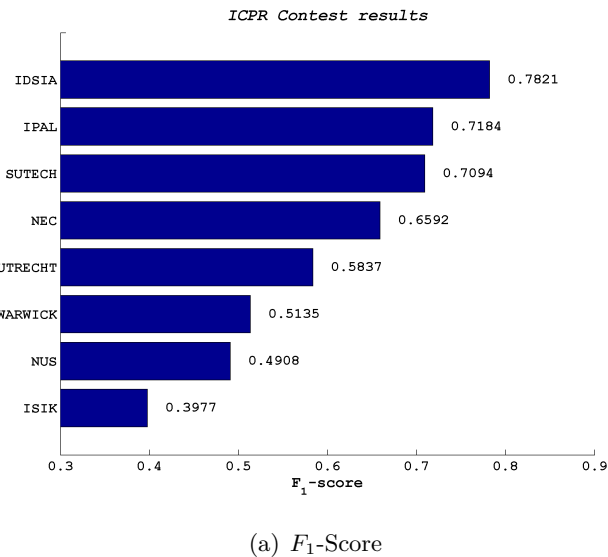


Figure 3.3: Performances of best algorithms in ICPR 2012 contest

Chapter 4

Design of a Mitosis Detection algorithm

*“Ab uno
disces omnis”*
(Learn everything from one)

Publius Vergilius Maro (Aeneis II, 65-66)

We developed an algorithm to perform mitosis-detection as a part of our work, with the aim to compare its results with humans facing the same task.

4.1 Dataset

We used the public MITOS dataset [2]. The dataset is composed by a total of 50 images with size 2084×2084 pixel, covering an area of $512 \times 512 \mu\text{m}$ each, acquired with an APERIO XT scanner (see Figure 2.1). A unique split is defined by the dataset authors, with 35 images used for training and 15 for evaluation. The dataset contains a total of about 300 mitosis, which were annotated by an expert pathologist. The performance of the algorithms participating to the *2012 ICPR mitosis detection contest* are shown in Section 3.5.

With reference to Figure 3.1, we focused on the classification subproblem, with the ROIs given as an input. The input is given in form of an image patch with size 100×100 pixel: such size completely contains the image of the cell.

The task is to map each patch to one of two classes:

C1: the image contains a mitosis at its center,

C0: the image does not contain a mitosis anywhere.

There are no samples in which a mitosis is visible off-center.

4.1.1 Image Candidates

For the ***C1*** class, all the 216 mitosis available in the 35 training images are chosen as training samples, and all 87 mitosis in the evaluation images are chosen as evaluation samples.

We enforced an even distribution of the two classes classes both in training and in evaluation sets, and therefore selected 216 ***C0*** samples for training and 87 ***C0*** samples for evaluation; the resulting training set contained 432 samples.

Millions of different ***C0*** samples may be randomly chosen from the original training and evaluation images: an overwhelming majority of such samples would not contain any nucleus and therefore be non-informative for training and trivial for evaluation. Limiting the choice to non-mitotic nuclei — which greatly outnumber mitotic ones — would not solve the problem, since most of such nuclei look very similar to each other and are trivially identified as non-mitotic. Only a small subset of non-mitotic nuclei — as well as other structures and artifacts — pose an actual challenge, both for humans and for algorithms.

In order to select such objects as ***C0*** samples, we used the output produced by a simple CNN-based mitosis detector, similar to the one outlined in another work on the same dataset [17], for selecting useful training samples. The detector, built at IDSIA, was trained on few images in the training set, then applied on the whole dataset. Because the detector was simple and trained on a small amount of data, it performed poorly and detected a lot of false positives. ***C0*** samples have been randomly chosen among the outputs of such detector which are farther than 50 pixels from the centroid of any mitosis; this ensures that no actual mitosis is visible in the corresponding image patch. The resulting samples do in fact resemble mitosis, are informative in the training set and appear non-trivial in the evaluation set. Finally, 10 ***C0*** samples in the evaluation set are substituted with 5 random false positives obtained from each of the two best performing algorithms (IDSIA and IPAL). These last 10 samples are particularly useful to compare humans to algorithms, in fact allowed us to better observe how test subjects behave

on the algorithms' false positives, which are rare in the evaluation set because algorithms were tuned to solve a problem with very low prevalence of mitotic samples.

4.1.2 Extended Dataset

We extended our dataset by rotating and mirroring each image patch (see Figure 4.1). We used the extended dataset only for the detection algorithm, so that we could analyze the effect of different features, which can be explicitly dependent on orientation or not, on the global performance of the classifier.

In case of extended dataset, the classification of a single image patch becomes the average of the classifications obtained on the 8 samples.

$$c_i = \frac{\sum_{j=1}^8 c_{ij}}{8} \quad (4.1)$$

Where c_i represents the classification of image patch i , and c_{ij} represents the classification of variation j of image patch i .

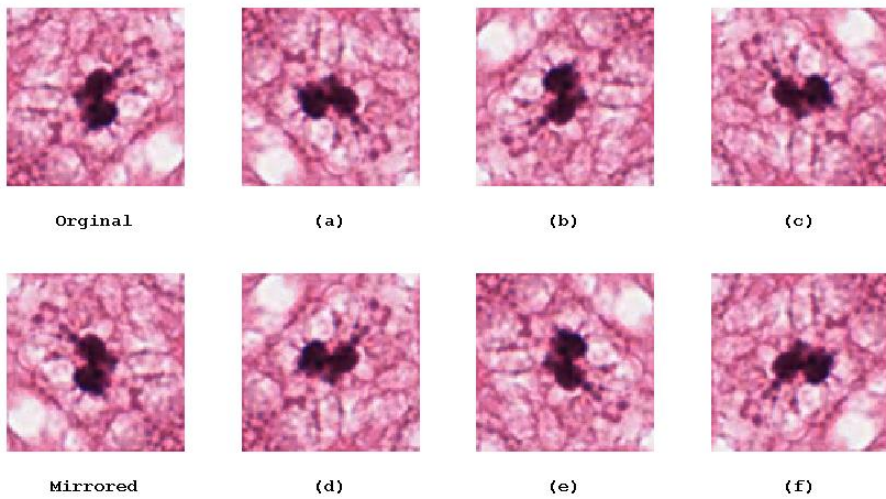


Figure 4.1: Extended dataset

(a),(b),(c): $\pi/2$ clockwise rotations, (d),(e),(f): mirror and $\pi/2$ clockwise rotations.

4.2 Feature Extraction

Each image patch can be represented as a $100 \times 100 \times 3$ matrix, where the $(i, j, :)$ triplet represents the RGB value of point with coordinates (i, j) in the image. Each value is in the range 0 to 255. Starting from these (raw) data we extracted some features by which we trained and tested our classifiers.

4.2.1 Simple Features

The simplest features that can be computed involve the average and the standard deviation of the Red-Green-Blue (RGB) values of the image patch. They can be computed on all the data or can be maintained separated for each RGB component. In the first case, average and standard deviation each give one value every instance:

$$m = \frac{1}{100 \cdot 100 \cdot 3} \left(\sum_{i=1}^{100} \sum_{j=1}^{100} \sum_{k=1}^3 i_{ijk} \right) \quad (4.2)$$

$$\sigma = \sqrt{\frac{1}{100 \cdot 100 \cdot 3} \left(\sum_{i=1}^{100} \sum_{j=1}^{100} \sum_{k=1}^3 (i_{ijk} - m)^2 \right)} \quad (4.3)$$

Otherwise, average and standard deviation produce a vector of three components:

$$\overline{M} = \begin{bmatrix} \frac{1}{100 \cdot 100} \left(\sum_{i=1}^{100} \sum_{j=1}^{100} i_{ij1} \right) \\ \frac{1}{100 \cdot 100} \left(\sum_{i=1}^{100} \sum_{j=1}^{100} i_{ij2} \right) \\ \frac{1}{100 \cdot 100} \left(\sum_{i=1}^{100} \sum_{j=1}^{100} i_{ij3} \right) \end{bmatrix} \quad (4.4)$$

$$\overline{S} = \begin{bmatrix} \sqrt{\frac{1}{100 \cdot 100} \left(\sum_{i=1}^{100} \sum_{j=1}^{100} (i_{ij1} - M(1))^2 \right)} \\ \sqrt{\frac{1}{100 \cdot 100} \left(\sum_{i=1}^{100} \sum_{j=1}^{100} (i_{ij2} - M(2))^2 \right)} \\ \sqrt{\frac{1}{100 \cdot 100} \left(\sum_{i=1}^{100} \sum_{j=1}^{100} (i_{ij3} - M(3))^2 \right)} \end{bmatrix} \quad (4.5)$$

Another simple set of features is represented by the *median* of each RGB value. The median is defined as the numerical value separating the higher half of the data sample, from the lower half and can be found by arranging all the data from lowest value to highest value and picking the middle one, or the mean of the two middle values, in case of even data. Each of the features above are independent of the orientation of the image.

4.2.2 Color Histograms and Intensities

A color histogram is a representation of the distribution of colors in an image, i.e. the number of pixels that have colors in each of a fixed list of color ranges [90], that span the image's color space. The color histogram can be built for any kind of color space, although the term is more often used for three-dimensional spaces like RGB or Hue Saturation Value (HSV). A histogram of an image is produced first by discretization of the colors in the image into a number of bins, and counting the number of image pixels in each bin. We built the RGB color histogram for each image patch, using 16 bins for each channel. The feature vector is so composed of 48 elements. Also this feature is orientation independent.

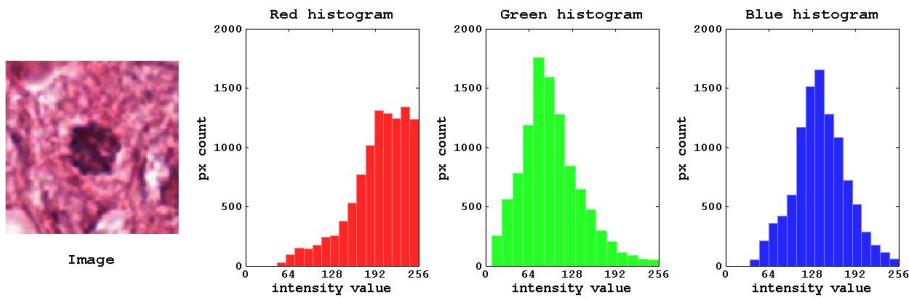


Figure 4.2: Color Histograms of sample image

It is generally possible to transform a color image into a gray-scale one. One typical transformation algorithm, applied pixel by pixel, is the following:

$$pix_{gray} = 0.2989 \cdot pix_{red} + 0.5870 \cdot pix_{green} + 0.1140 \cdot pix_{blue} \quad (4.6)$$

On the resulting monochromatic image, it is possible to compute an *intensity histogram*.

We preferred to compute a slightly different feature: the average intensity in the 25 central regions of the image. We first computed the gray-scale image according to Equation 4.6, then we selected the central part of the image and divided it in a grid of 5×5 elements. We finally computed the mean intensity for each element. Figure 4.3 illustrates the procedure.

The resulting feature vector is composed of 25 values, corresponding to the intensities, ordered columnwise. This type of feature is orientation dependent.

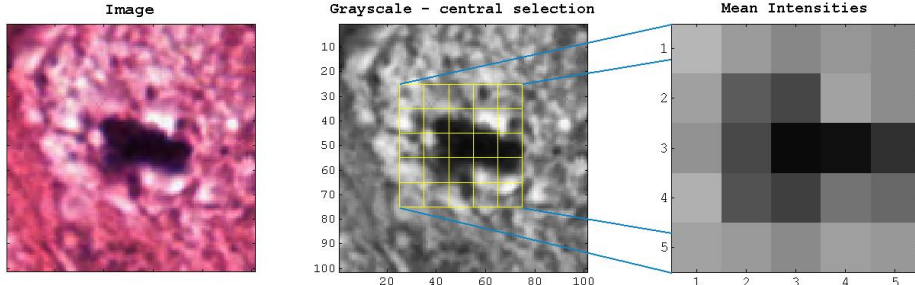


Figure 4.3: Mean gray-scale intensity of central part of image patch

4.2.3 Texture Features

Texture features are widely used in different CV tasks, as pointed out in Section 2.2.3. We focused on the features based on Local Binary Patterns (LBP), described in [69] and [68]. The general idea of LBP is described on page 17. The LBP features considered here are labeled $\text{LBP}_{P,R}$ where P is the number of neighbors considered and R is the distance from the pixel. The two main characteristics of the LBPs considered are:

- *uniformity*: which is a fundamental property of local image texture. It refers to the uniform appearance of the local binary pattern: that is, there is a limited number of transitions or discontinuities in the circular presentation of the pattern. The most frequent uniform binary patterns correspond to primitive “microfeatures”, such as edges, corners, and spots; hence, they can be regarded as feature detectors that are triggered by the best matching pattern.
- *rotation invariance*: which takes into account if a spatial pattern is affected by rotation or not.

Three different types of features can be built, on the basis of the relations described Equation 2.4:

1. $\text{LBP}_{P,R}^{u2}$: uniform feature,
2. $\text{LBP}_{P,R}^{ri}$: rotation invariant feature,
3. $\text{LBP}_{P,R}^{riu2}$: uniform and rotation invariant feature,

In particular we used:

$$\text{LBP}_{8,R}^{\text{type}} \quad \text{where} \begin{cases} \text{type} & \in \{ri, u2, riu2\} \\ R & \in \{1, 2, 3\} \end{cases} \quad (4.7)$$

while building the feature vector, we used the *type* parameter in a mutually exclusive way, i.e. we did not concatenate LBPs of different types. On the other hand, we built feature vectors with various combinations of radii. The following equations show the three different mutually exclusive texture feature sets that we considered.

$$\overline{L} = [LBP_{8,1}^{riu2}, LBP_{8,2}^{riu2}, LBP_{8,3}^{riu2}] \quad (4.8)$$

$$\overline{U} = [LBP_{8,1}^{u2}, LBP_{8,2}^{u2}, LBP_{8,3}^{u2}] \quad (4.9)$$

$$\overline{R} = [LBP_{8,1}^{ri}, LBP_{8,2}^{ri}, LBP_{8,3}^{ri}] \quad (4.10)$$

Finally, we considered the VAR operator, as described in Equation 2.5. As, from early tests, a single VAR value for the entire image patch proved to be non-significant, we decided to follow an approach similar to the one described for the intensity histogram (see Figure 4.3) and evaluated the mean value of a grid of samples in the central region of the image. Figure 4.4 shows a sample of $\text{VAR}(8,1)$ computation. Please note that the gray-scale mapping of the $\text{VAR}(8,1)$ figure has been adjusted to be visible with full gray-scale range.

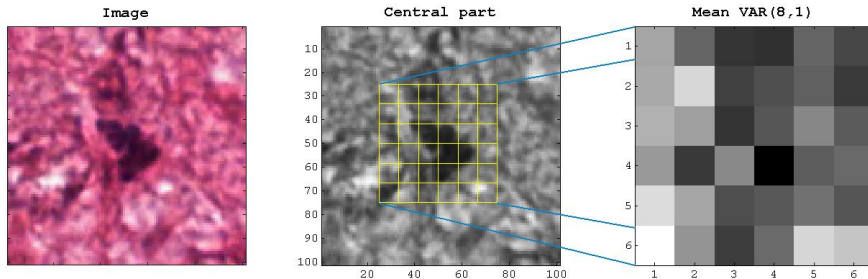


Figure 4.4: Example of $\text{VAR}(8,1)$ feature

The resulting feature vector is composed of 36 values, corresponding to the average $\text{VAR}(8,1)$ in each element of the grid, ordered columnwise. This type of feature is orientation dependent.

The Matlab code implemented to build the feature vectors can be found at <https://github.com/Ccaccia73/mitosis-experiments>, into the subdirectory `common`, function `extractFeatures.m`.

4.3 Classifiers

Once defined the set of feature to be considered, it is possible to build a matrix whose lines represent an *instance* (i.e. an image patch) and whose columns represent a *feature* (or a component of it): Equation 4.11 represents such matrix.

$$M_{feats} = \begin{array}{c|ccccccccc} & & & & & & & & \xrightarrow{\text{features}} \\ \hline & 1 & \cdots & \cdots & \cdots & \cdots & \cdots & \cdots & n_{fc} \\ \begin{matrix} 1 \\ \vdots \\ \vdots \\ \vdots \end{matrix} & \left(\begin{array}{ccccccccc} c_{111} & c_{112} & \cdots & c_{1k1} & \cdots & c_{1kn_k} & \cdots & c_{1n_f 1} \\ \vdots & \vdots & \ddots & \vdots & \ddots & \vdots & \ddots & \vdots \\ c_{n_i 11} & c_{n_i 12} & \cdots & \underbrace{c_{n_i j1} & \cdots & c_{n_i jn_j}}_{feat_j} & \cdots & \underbrace{c_{n_i n_f 1}}_{feat_{n_f}} & \cdots & \end{array} \right) \\ \downarrow n_i & \end{array} \quad (4.11)$$

Where n_f is the total number of features and n_i is the total number of instances. Each feature can be made of more than one component (e.g. $feat_1$ and $feat_j$ in the example). For this reason, the total number of columns in the matrix (n_{fc}) is given by the sum of all the feature components. So, each element of the matrix c_{ijk} is the k^{th} component of the j^{th} feature in the i^{th} instance. The matrix representing the evaluation set is built in the same way.

A vector represents the class which every instance belongs to. Equation 4.12 describes such vector:

$$V_{class} = \begin{array}{c|c} & \xrightarrow{\text{class}} \\ \hline 1 & \left(\begin{array}{c} \widehat{e_1} \\ \vdots \\ e_i \\ \vdots \\ e_{n_i} \end{array} \right) \\ \vdots \\ \downarrow n_i & \end{array} \quad (4.12)$$

where e_i belongs to one of the two classes. In some implementations of binary classifiers it is required that $e_i \in \{-1, 1\} \forall i = 1, \dots, n_i$, otherwise $e_i \in \{0, 1\} \forall i = 1, \dots, n_i$. The vector representing the GT of the evaluation set is built in the same way.

Having a matrix representing the training feature set, a matrix representing the evaluation (i.e. testing) feature set and two vectors including the GT classification of each image patch, it is possible to run a classifier that tries to get insights from the feature set in order to classify the evaluation set.

In our work we focused on two types of classifiers:

- *Support Vector Machines*, which are widely used in computer vision classification problems, in particular in biomedical imaging ([87, 91, 48, 16], see also Section 3.3),
- *Random Forests*, which is a relatively new ensemble approach that can also be thought of as a form of nearest neighbor predictor ([12, 39, 10]).

We also mention CNN, as it played a relevant role in the definition of our dataset (see Section 4.1.1).

4.3.1 Support Vector Machines

We used the Matlab implementation of the *libSVM* described in [42]. SVMs are a popular classification technique. The goal of SVM is to produce a model (based on the training data) which predicts the target values of the test data given only the test data attributes. Given a training set of instance-label pairs (\mathbf{x}_i, y_i) , $i = 1, \dots, l$, where $\mathbf{x}_i \in \mathbb{R}^n$ and $y \in \{-1, 1\}^l$.

The SVM requires the solution of the following optimization problem:

$$\begin{aligned} \min_{\mathbf{w}, b, \xi} \quad & \frac{1}{2} \mathbf{w}^T \mathbf{w} + C \sum_{i=1}^l \xi_i \\ \text{Subject to:} \quad & y_i (\mathbf{w}^T \phi(\mathbf{x}_i) + b) \geq 1 - \xi_i \\ & \xi_i \geq 0 \end{aligned} \tag{4.13}$$

The training vectors \mathbf{x}_i are mapped into a higher dimensional space (maybe infinite), by the function ϕ . SVM finds a linear separating hyperplane with the maximal margin in this higher dimensional space. $C > 0$ is the penalty parameter of the error term. The function

$$K(\mathbf{x}_i, \mathbf{x}_j) = \phi(\mathbf{x}_i)^T \phi(\mathbf{x}_j) \tag{4.14}$$

is called the *kernel function*. Many kernel functions have been defined, the most common are:

- *linear*: $K(\mathbf{x}_i, \mathbf{x}_j) = \mathbf{x}_i^T \mathbf{x}_j$,
- *polynomial*: $K(\mathbf{x}_i, \mathbf{x}_j) = (\gamma \mathbf{x}_i^T \mathbf{x}_j + r)^d$, $\gamma > 0$,

- *Radial Basis Function (RBF)*: $K(\mathbf{x}_i, \mathbf{x}_j) = \exp(-\gamma \|\mathbf{x}_i - \mathbf{x}_j\|^2), \gamma > 0,$
- *sigmoid*: $K(\mathbf{x}_i, \mathbf{x}_j) = \tanh(\mathbf{x}_i^T \mathbf{x}_j + r).$

Where γ , d and r are kernel parameters [66].

In our work we focused on RBFs and sigmoid kernels, which are used in most cases. In SVMs the *support vectors* are the training instances that concur to define the separating hyperplane in the kernel space. The image of Figure 4.5 gives a linear representation of a SVM.

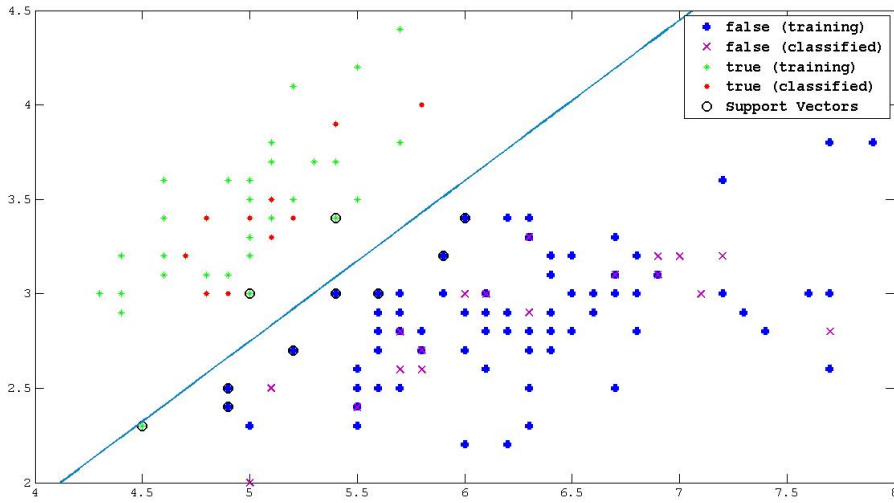


Figure 4.5: Representation of a SVM classification

4.3.2 Random Forests

Decision Trees (DTs) are attractive classifiers due to their high execution speed and simplicity. However, trees often suffer from performance loss, in terms of generalization accuracy on unseen data when the complexity of the problem grows [38].

Random Forests are a combination of tree predictors such that each tree depends on the values of a random vector sampled independently and with the same distribution for all trees in the forest [12]. So, RF can be viewed as an ensemble approach that can also be thought of as a form of nearest neighbor predictor. Ensembles are a divide-and-conquer approach used to improve performance. The main principle behind ensemble methods is that a group of “weak learners” can be combined together to form a “strong learner”.

Each classifier, individually, is a weak learner, while all the classifiers taken together are a strong learner. An example of DT is shown in Figure 4.6.

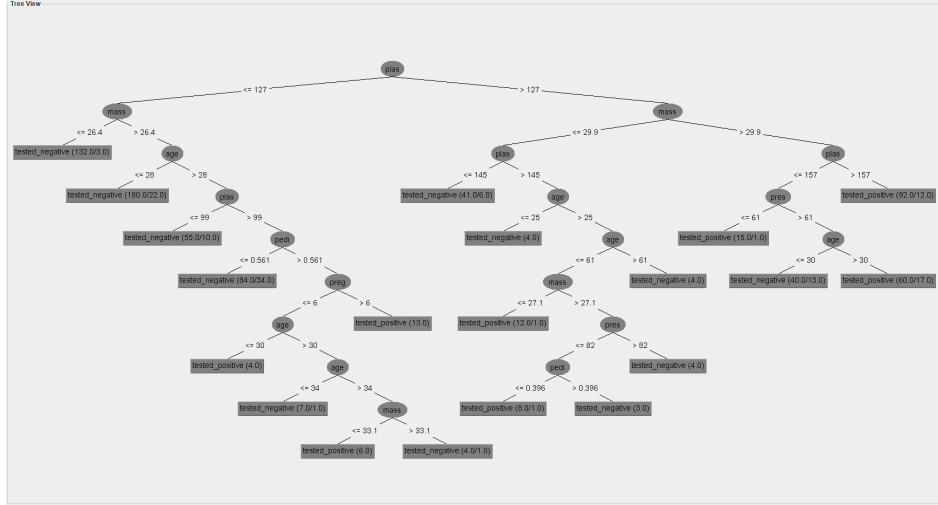


Figure 4.6: Example of a Decision Tree

A RF is composed by a number of trees \mathbf{T} . For some number m , m features are randomly selected from the feature vector. The subset of variables is used to train a DT.

According to Breiman implementation of RFs, m should be that \ll than the number of features.

We adopted the convention (as described in [12]) that $m \leq \log_2 F + 1$ and used an ensemble of 500 trees.

While running a RF, when a new input is entered into the system (a test sample), it is run down all of the trees, each of which classifies it in a *hard* way (see Section 3.2): in a sense, each tree gives a vote for the current sample. The result is the average of all of the terminal nodes that are reached, giving a final *soft* classification. RFs are generally quite fast, robust classifiers, and are also used in image classification [10].

The Matlab code implemented to classify data can be found in function `classifyData.m` in the same repository.

4.4 Classification Process

Once a classifier is trained on the training set, it can be used to classify unseen data (i.e., the evaluation or testing set). The classifier function is applied to each instance of the *evaluation* feature set, which is built as the

matrix described in Equation 4.11.

The output of the classifier is a vector like the one described in Equation 4.12, unless that, generally, the classification process gives a *soft* classification (see Section 3.2), which means that $-1 \leq e_i \leq 1 \forall i = 1, \dots, n_i$, or $0 \leq e_i \leq 1$, depending on the definition of the classes.

The performance parameters are computed as a function of a *classification threshold*, as described in Section 3.4.2.

Chapter 5

Design of a User Study

“πάντων χρημάτων μέτρον, ἄνθρωπον εἶναι, τῶν μὲν ὅντων ὡς ἔστι, τῶν δὲ μὴ ὅντων ὡς οὐκ ἔστιν.”

(man is “the measure of all things, of the existence of the things that are and the non-existence of the things that are not.”)

Πλάτων (Plato, Theaet. 152a)

We built a web interface to collect data originated from mitosis classification performed by humans.

5.1 Test Design

The problem of detecting mitosis can be cast as a problem of classifying image patches. In fact, most detection algorithms are based on classifiers which map an image patch to the probability that a mitosis appears at its center; once such classifier is known, the detection problem is solved by applying it on a sliding window over the input image, or to a set of candidate patches identified in a previous step. The classification task can be presented to an user through a very simple and immediate interaction mechanism: in fact, a single decision is required for each patch. In contrast, detection would require a more complicated interaction with users. For this reason, we focused on the classification subproblem. For a given sample, input is given in form of an image patch with size 100×100 pixel: such size completely contains the image of the cell, and most algorithms generally use

data from a smaller window. The task proposed to the user is the same as the one tackled in automatic classification (see Chapter 4), that is to map each patch to one of two classes:

C1: the image contains a mitosis at its center,

C0: the image does not contain a mitosis anywhere.

with no samples containing a mitosis visible off-center.

5.1.1 Dataset

The dataset is the same as the one described in Section 4.1.

5.1.2 Programming Framework

The user interface has been built in Ruby on Rails (RoR)¹, which is an open source web application framework which runs on the *Ruby* programming language [19], and allows to develop complete, dynamic pages without too much overhead [6]. RoR makes an extensive use of the concept of Convention over Configuration (CoC) which is a software design paradigm that seeks to decrease the number of decisions that developers need to make, gaining simplicity and standardization. In fact the directory structure of a RoR project is auto-generated and standardized, and also class names are conventionally mapped to identically named database tables and the fields to its columns.

The application built for this project has been deployed on the *Heroku application platform*² and its on-line implementation is reachable at the following url: <http://mitosis-detection.herokuapp.com/>.

5.2 User Interface

In this section we describe the user interface built to present samples to the user and to collect the classification data.

¹<http://rubyonrails.org/> [35]

²<https://www.heroku.com/>

5.2.1 Introduction

In the first stage the user receives some information about the purpose of the test and is required to give some simple information (see Figure 5.1), summarized in:

- her/his experience, in particular:
 1. the user doesn't work in biology and new to such a problem,
 2. he is a biologist,
 3. he is an histologist, and so has direct experience in the task.
- her/his color ability, that is:
 1. he has normal color ability,
 2. he is colorblind.
- the user can optionally give a *nickname* that is recorded with the data.

The screenshot shows a web browser window for the 'MITOSIS DETECTION EXPERIMENT' at mitosis-detection.herokuapp.com. The title bar says 'MITOSIS DETECTION EXPERIMENT'. The main content area is titled 'Introduction' and contains the following text:

Image classification experiment on the MITOS dataset

Detecting and counting mitotic nuclei is an important part of the evaluation of breast cancer histological images. However, distinguishing mitotic nuclei from non-mitotic nuclei and other similar structures is hard and time-consuming, therefore researchers are designing automated algorithms for assisting pathologists in this task.

Algorithms learn to detect mitotic nuclei by looking at a large number of examples. In this experiment, we want to compare their accuracy with the accuracy of humans who are new to the problem and are faced with the same task.

The experiment is divided in two phases:

TRAINING: we will show several labeled images including known mitotic nuclei, as well as other structures which look similar but are known NOT to be mitotic nuclei. Just like our algorithms, you should try to find out some criteria to tell the two classes apart.

EVALUATION: then, we will show several unlabeled images, and you will be asked to classify each of them as either **MITOSIS** or **NON-MITOSIS**. During evaluation, you still have access to the full set of training examples to use as a reference, and you can take as much time as you want.

The experiment should take roughly **10 - 15 minutes**: you can classify as few or as many samples you want and exit at any time, and your results will be useful to us.

Below this text, there is a form section with a red bracket labeled 'form' pointing to it. The form contains the following fields:

- Please tell us something about you:
- Your experience? (dropdown menu)
- Your color vision ability? (dropdown menu)
- Nickname
(You can leave it blank) (text input field)

A blue 'Begin the Experiment' button is located at the bottom of the form.

At the very bottom of the page, small text notes:
Names of Authors of this study are currently hidden during NPS blind review period.
The data used in this experiment is part of the public [MITOS dataset](#), built for project MITO by experienced pathologists at the Pitié-Salpêtrière Hospital in Paris, France.

Figure 5.1: Intro page

5.2.2 Training

Once the user decides to participate, a new *detection* entity is created and linked to a unique alphanumeric string that can be used to retrieve the

summary of the performance. The first step of the classification process is the *training* phase, during which the subject is shown 216 labeled **C1** samples, 216 labeled **C0** samples, and instructed to study them and devise some differentiating criteria (see Figure 5.2). The dataset is composed of the same images as the one used for automatic classification (see Section 4.1).

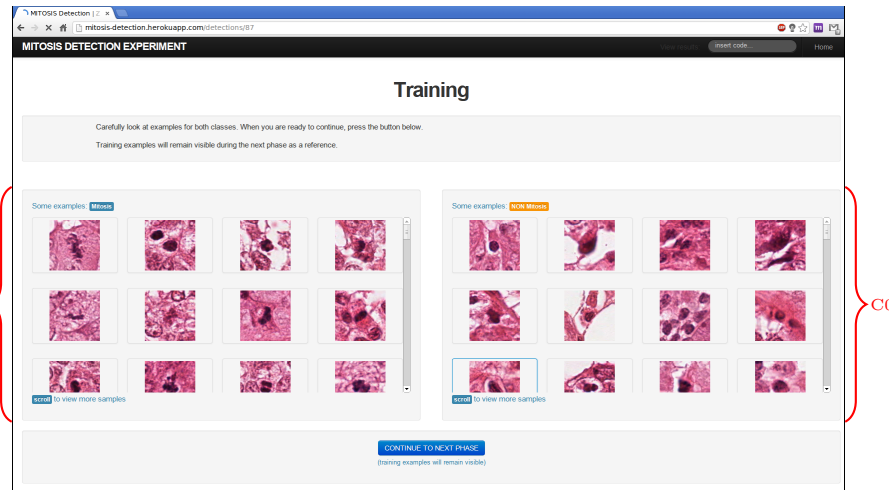


Figure 5.2: Training page

5.2.3 Evaluation

During evaluation, the subject is presented with one evaluation sample at a time (randomly chosen among unseen ones), and asked to provide a classification as one of:

- *definitely mitosis*: $p(C1) = 1.0$,
- *probably mitosis*: $p(C1) = 0.75$,
- *probably non-mitosis*: $p(C1) = 0.25$,
- *definitely non-mitosis*: $p(C1) = 0.0$,

During the evaluation phase, the whole training set remains visible for reference (see Figure 5.3). The number of classification options has been chosen so that the user is led to make a commitment over the type of current image: towards **C0** or towards **C1**.

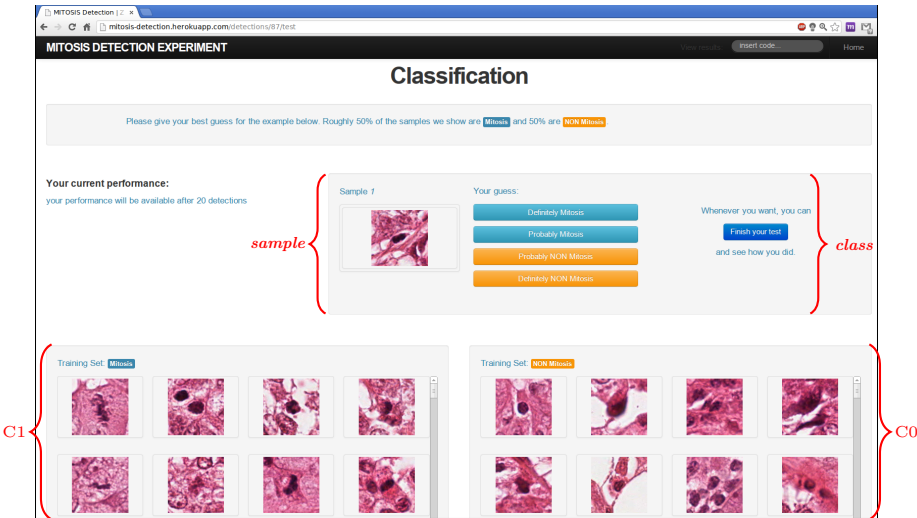


Figure 5.3: Evaluation page

A number of design decisions are taken in order to balance the trade-off between test fairness and subject engagement. Most importantly, the user is given immediate feedback as to whether the last decision was correct or wrong (see Figure 5.4): on one hand, this encourages continuous learning while the evaluation is taken and makes users much more willing to improve and fine-tune their strategies; on the other hand, subjects can count on a growing training set, which gives them an unfair advantage over algorithms.

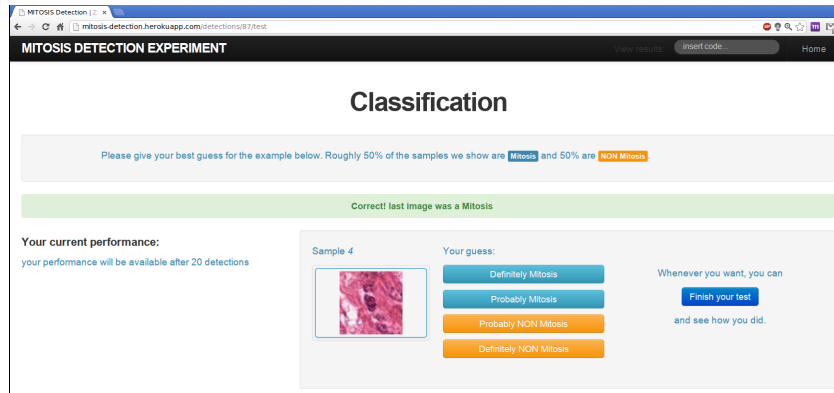
In addition, subjects are allowed to finish the test at any time, the ones who reach a minimum of 20 classifications are shown their current average accuracy, as illustrated in Figure 5.5.

5.2.4 Comments

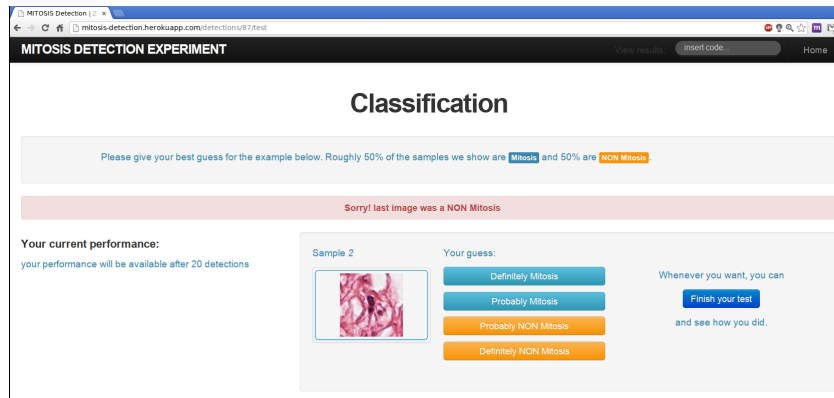
After concluding the classifications, the subject can write his opinions about the classification criteria that he devised during the process (see Figure 5.6).

5.2.5 Performances

Finally, the user can review his overall performance, viewing his *confusion matrix*, his *accuracy*, *sensitivity* and *specificity* (as described in Section 3.4). The results page is shown in Figure 5.7.



(a) positive Feedback



(b) negative Feedback

Figure 5.4: Examples of classification feedback

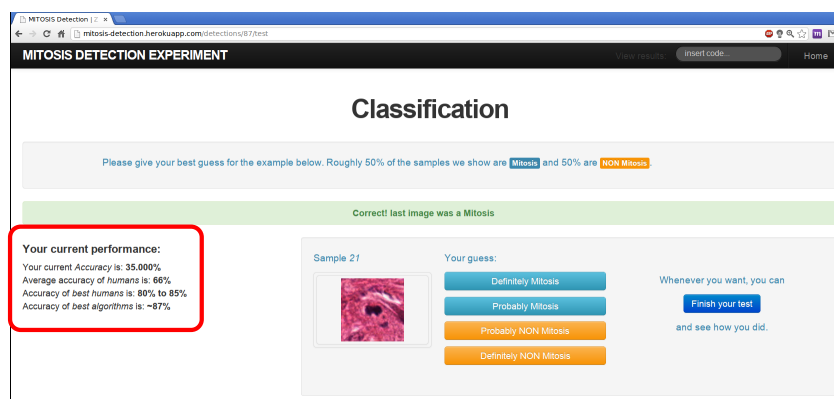


Figure 5.5: Current performance

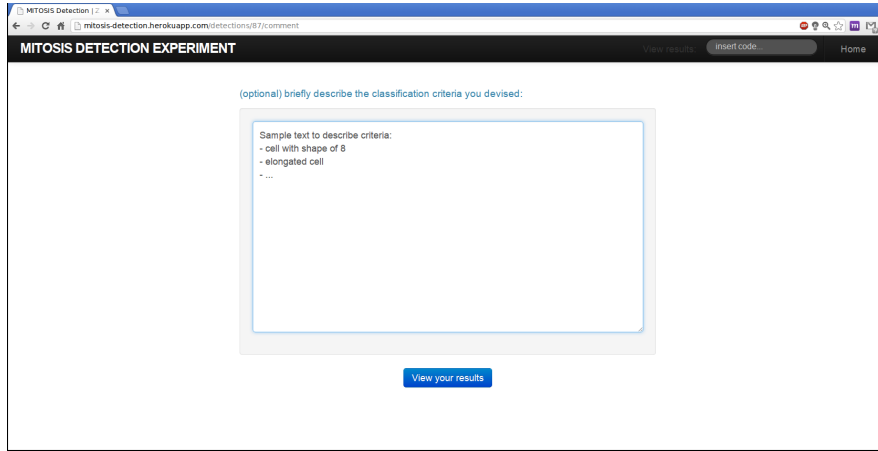


Figure 5.6: Comment page

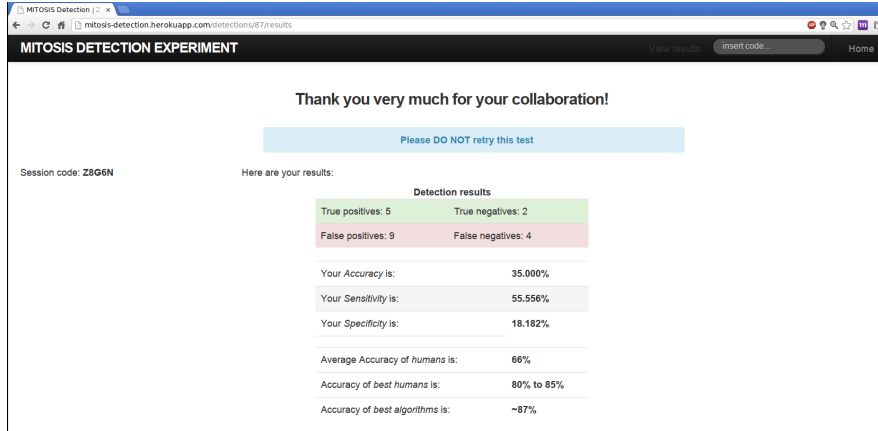


Figure 5.7: user results page

5.3 Data collection

In a not directly reachable web-page, it is possible to view and download all the data collected by the site. A table, shown in Figure 5.8, reports the main information of all the concluded classifications.

It is possible to download (see Figure 5.9) two .csv files. One (**images.csv**) summarizes the dataset, for each image patch it gives:

- *id*: a unique number identifying each image,
- *image*: the name of the image from which the patch has been taken,
- *coordinates*: the (x, y) coordinates of the center in the image,
- *type*: if the image is **C1** or **C0**.

The other file (`users.csv`) summarizes the classifications. Each detection starts with a line beginning with the keyword `USER`. The first line of a detection reports the information concerning user and detection:

- nickname, user type and color ability of the user,
- timestamp of the detection,
- number of detections: TPs, TNs, FPs, FNs,
- *ID* of the detection.

The line concerning the classified images reports:

- *id*: the unique number identifying the patch,
- *image*: the name of the image from which the patch has been taken,
- *coordinates*: the (x, y) coordinates of the center in the image,
- *type*: if the image is **C1** or **C0**.
- *classification*: how the user classified the image: $\{0.0, 0.25, 0.75, 1.0\}$,
- *time*: how many seconds took the user to decide.

Finally it is possible to view all the comments left by the users (see Figure 5.10).

| Code | User | Ability | Nickname | Detections completed: | | | | | | | Date |
|-------|-----------|---------|--------------|-----------------------|----|----|----|----|-----------|-------------------------|------|
| | | | | Total | TP | TN | FP | FN | Avg. time | | |
| R7C9O | newbie | normal | Claudio_test | 2 | 2 | 0 | 0 | 0 | 4.500 | 2013-02-20 15:35:09 UTC | |
| M9Y4L | biologist | normal | | 174 | 81 | 62 | 25 | 6 | 5.914 | 2013-02-20 19:44:00 UTC | |
| X7V3I | newbie | normal | Claudio_test | 10 | 3 | 4 | 2 | 1 | 3.700 | 2013-02-19 21:04:02 UTC | |
| N5E1X | newbie | normal | Lucia | 146 | 35 | 41 | 30 | 40 | 15.281 | 2013-02-23 15:50:47 UTC | |
| N5K9O | newbie | normal | | 0 | 0 | 0 | 0 | 0 | 0.0 | 2013-02-20 08:17:20 UTC | |
| X9N4T | newbie | normal | | 174 | 45 | 78 | 9 | 42 | 4.644 | 2013-02-20 10:31:51 UTC | |
| A8J9N | biologist | normal | | 96 | 23 | 26 | 17 | 30 | 5.042 | 2013-02-20 07:56:07 UTC | |
| M8E8F | biologist | normal | | 37 | 12 | 16 | 4 | 5 | 19.730 | 2013-02-20 21:41:23 UTC | |
| Q4I4J | newbie | normal | | 0 | 0 | 0 | 0 | 0 | 0.0 | 2013-02-21 11:11:58 UTC | |
| J7CTN | newbie | normal | | 54 | 17 | 18 | 10 | 9 | 16.667 | 2013-02-20 08:12:34 UTC | |
| X5D1G | biologist | normal | Wombat | 174 | 70 | 52 | 35 | 17 | 19.902 | 2013-02-25 13:13:08 UTC | |
| CTD8Q | newbie | normal | | 10 | 3 | 2 | 2 | 3 | 5.300 | 2013-02-20 14:56:29 UTC | |
| U2B3R | newbie | normal | Jerome | 4 | 0 | 0 | 3 | 1 | 27.250 | 2013-02-21 18:58:45 UTC | |
| G1V8M | biologist | normal | biotec87 | 150 | 50 | 52 | 29 | 19 | 9.080 | 2013-02-20 08:24:15 UTC | |
| I3G9C | biologist | normal | | 0 | 0 | 0 | 0 | 0 | 0.0 | 2013-02-25 13:11:17 UTC | |

Figure 5.8: Overall results page

The screenshot shows a web browser window titled "MITOSIS Detection | mitosis-detection.herokuapp.com". The main content is a table titled "MITOSIS DETECTION EXPERIMENT" with the following data:

| User | Type | Normal | Dandy1 | 120 | 36 | 33 | 33 | 18 | 11172.608 | Date | |
|-------|-----------|--------|--------|-----|----|----|----|----|-----------|--------|-------------------------|
| K6T9J | biologist | normal | TEST | | 43 | 18 | 20 | 1 | 4 | 98.116 | 2013-03-02 12:20:03 UTC |
| W1T6O | newbie | normal | z | | 21 | 13 | 6 | 2 | 0 | 7.524 | 2013-03-26 07:06:32 UTC |
| G2D6C | newbie | normal | | | 0 | 0 | 0 | 0 | 0 | 0.0 | 2013-04-01 13:21:28 UTC |

Below the table are three buttons: "Download data", "Download image data", and "View Comments". A file download dialog is shown at the bottom left with "images.csv".

Figure 5.9: Download buttons

The screenshot shows a web browser window titled "MITOSIS Detection | mitosis-detection.herokuapp.com/detections/comments". The main content is a list of comments under the heading "All Comments":

- Test of comment after NIPS
— test_NIPS, newbie, normal vision - 2013-05-31 06:35:48 UTC
- this is a sample comment
— claudio_test_comment, newbie, normal vision - 2013-03-06 10:21:37 UTC
- This is another sample comment. Lorem ipsum dolor sit amet, consectetur adipisicing elit, sed do eiusmod tempor incididunt ut labore et dolore magna aliqua.
— Claudio_test, newbie, normal vision - 2013-03-07 09:35:41 UTC
- Sample text to describe criteria: - cell with shape of 8 - elongated cell - ...
— claudio_th, newbie, normal vision - 2013-05-31 17:20:21 UTC

Figure 5.10: User comments

5.4 Source Code

The entire project source code is maintained at the following repository:
<https://github.com/Ccaccia73/tydes>.

Chapter 6

Experimental Results

“Duo enim sunt modi cognoscendi, scilicet per argumentum et experimentum. Argumentum concludit et facit nos concedere conclusionem, sed non certificat neque removet dubitationem ut quiescat animus in intuitu veritatis, nisi eam inveniat via experientiae.”

(There are two modes of acquiring knowledge, reasoning and experience. Reasoning guides us to a sound conclusion, but does not remove doubt from the mind until confirmed by experience.)

Roger Bacon (Opus Majus part VI, ch. I)

In this section we describe the experiments made and the performance obtained from some classifiers built on the feature set described in Section 4.2, furthermore we compare those results with the performances of users who classified the images using the website described in Chapter 5.

6.1 Experimental setup

Here we describe the set of experiments that we run on the dataset. Each experiment has been executed classifying data with a Random Forest (RF) classifier and a Support Vector Machine (SVM).

We adopted some conventions to describe a specific feature-set in a short way. As described in Section 4.3, a feature matrix is composed of features placed side by side, so a complete set can be represented by a string whose characters correspond to a specific feature. We used the following nomenclature:

- M: mean value per color (Section 4.2.1),
- S: standard deviation per color (Section 4.2.1),
- d: median per color (Section 4.2.1),
- H: color histograms (Section 4.2.2),
- i: mean intensities (Section 4.2.2),
- L: LBP^{riu2} with radii 1-2-3, 8 neighbors (Section 4.2.3),
- R: LBP^{ri} with radii 1-2-3, 8 neighbors (Section 4.2.3),
- U: LBP^{u2} with radii 1-2-3, 8 neighbors (Section 4.2.3),
- V: VAR, pixel variance (Section 4.2.3).

Thus a feature set can be described by the string **MSHLV**, meaning that the above corresponding features have been concatenated. We remind here that features L, R and U are used in a mutually exclusive way.

6.2 Experiments

We run different experiments to analyze the performances of the selected classifiers and to determine which feature set is most suitable to classify our data. In this section we describe the experiments made and, for each one of them, we report the most significant results.

6.2.1 Normalization

The first aspect that we took into account regarded *normalization* of data. Each feature in the *feature vector* can range among different values. The procedure that we used as a reference (described in the guide in [42]) claims that the scaling of data is very important in order to obtain a good classification with SVMs [50]. On the other hand, RFs, as composed of DTs, should not be influenced by scaling.

The general idea is to rescale the data so that each new feature z has: $\mu = 0, \sigma = 1$, using the following relations:

$$\mu = \frac{1}{N} \sum_{i=1}^N x_i \quad (6.1)$$

$$\sigma = \sqrt{\frac{1}{N} \cdot \sum_{i=1}^N (x_i - \mu)^2} \quad (6.2)$$

$$z_i = \frac{x_i - \mu}{\sigma} \quad (6.3)$$

We run some test with different sets of features.

We remind here that the Matlab code implemented to run the experiments can be found at <https://github.com/Ccaccia73/mitosis-experiments>, into the sub-directory `classify`.

6.2.2 Normalization: Experimental Results

We tried to classify different feature sets, starting with simple ones.

Features: MSi

With a simple set of features the main results are the following:

| Classifier | AUC | accuracy | precision | F1-Score | sensitivity | specificity |
|------------|------|----------|-----------|----------|-------------|-------------|
| SVM std | 0.79 | 74.14% | 81.82% | 0.71 | 86.21% | 62.07% |
| SVM norm | 0.74 | 71.26% | 70.79% | 0.72 | 70.11% | 72.41% |
| RF std | 0.80 | 75.86% | 77.78% | 0.75 | 79.31% | 72.41% |
| RF norm | 0.80 | 75.86% | 78.48% | 0.75 | 80.46% | 71.26% |

Table 6.1: MSi results

The data in Table 6.1 show that, with normalization, the RF classifier remains almost unchanged, which is to be expected, while, the SVM classifier worsens its performance. With these simple features no advantages have been obtained. The ROC curve of the classifiers is shown in Figure 6.1.

Features: MSiHLV

The results of applying normalization to data are different when much more features are involved. For example, in a MSiHLV feature-set (but same results have been found for example for MSiHUV), the SVM classifier is unable to find a proper classification with standard features; on the other hand, the results

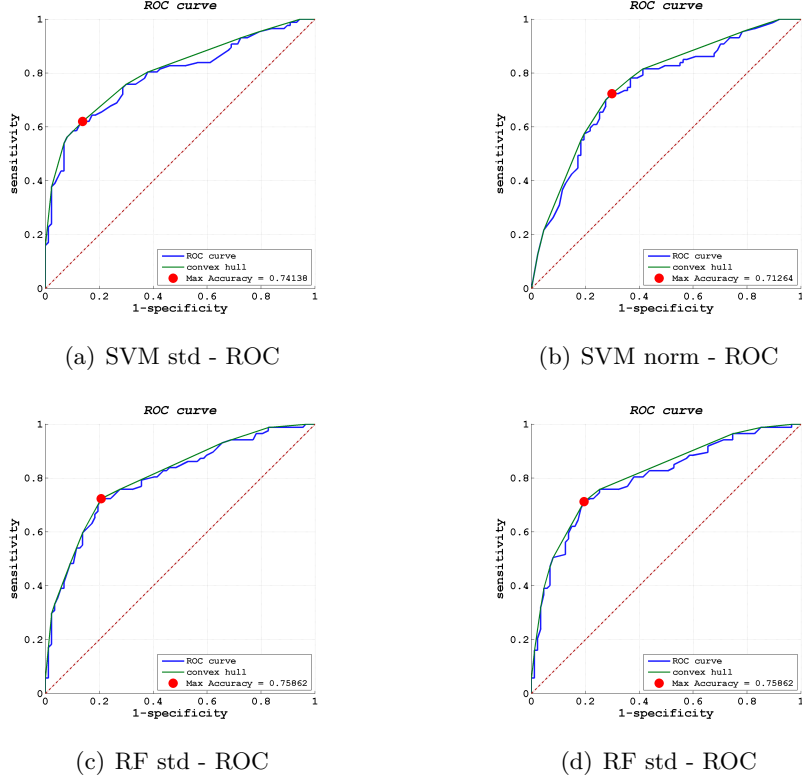


Figure 6.1: ROC curves for MSi feature classification

| Classifier | AUC | accuracy | precision | F ₁ -Score | sensitivity | specificity |
|------------|------|----------|-----------|-----------------------|-------------|-------------|
| SVM norm | 0.87 | 79.89% | 74.07% | 0.82 | 67.82% | 91.95% |
| RF std | 0.89 | 81.03% | 79.35% | 0.82 | 78.16% | 83.91% |
| RF norm | 0.90 | 81.61% | 77.23% | 0.83 | 73.56% | 89.66% |

Table 6.2: MSiHLV results

are interesting when normalization is applied. Similarly to the previous case (Table 6.1), the RF classifier is slightly influenced by normalization.

Table 6.2 shows the results. The ROC curve of the classifiers is shown in Figure 6.2.

As normalization is generally considered a good practice and as we found, with our experiments, advantages when we applied it to our data, we considered only a normalized dataset in all the following experiments.

6.2.3 Extended Dataset

In this experiment we analyzed the effect of considering the extended dataset, as described in Section 4.1.2. Rotated and mirrored images should provide

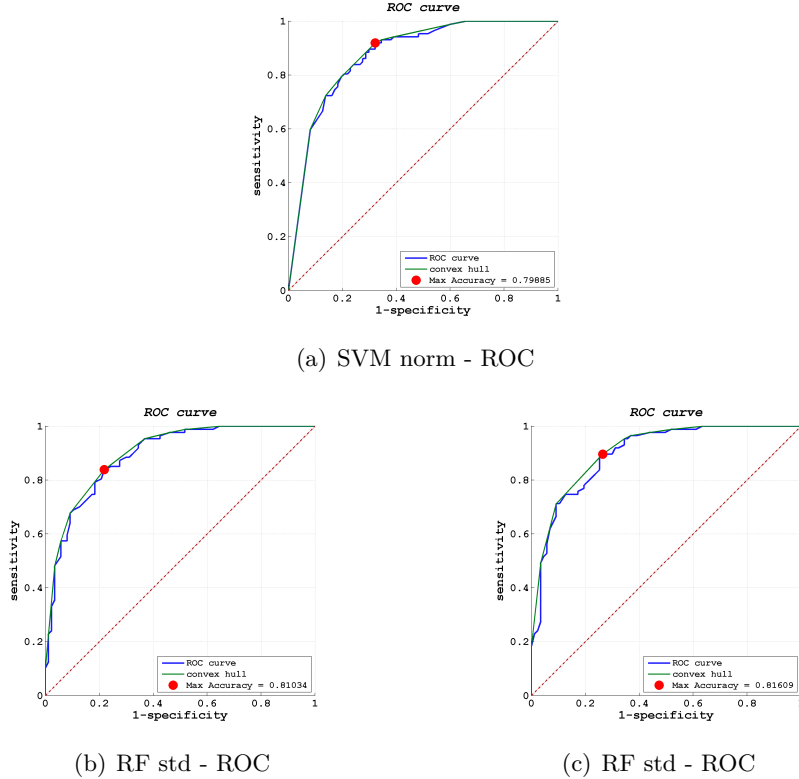


Figure 6.2: ROC curves for MSiHLV feature classification

some information for all the features that are orientation dependent, in all the other cases, the added elements are just replicates of already present instances. Also in this case we run test with different sets of features. The Matlab code implemented to run *experiment 2* is listed in ??

6.2.4 Extended Dataset: Experimental Results

We considered three different ways of extending our dataset, resulting in four different experiments:

- no dataset is extended (abbreviated with *default*),
- the *train* dataset is extended (abbreviated with *ext-T*),
- the *evaluation* dataset is extended (abbreviated with *ext-E*),
- both dataset are extended (abbreviated with *ext-A*).

We expected some advantages in extending the dataset when orientation-dependent features are involved. On the other hand, growing the dataset too much could bring in much more noise than useful information, resulting in a worse performance of the classifier. When the evaluation dataset is extended, the classification value of an image is the average of the classification of the derived images (see Section 4.1.2). We report here the most significant experiments and results.

Features: MSiHU - classifier: SVM

We applied our SVM classifier to the feature-set coded **MSiHU**, please note that feature U is orientation dependent. The results are the following:

| Classifier | AUC | accuracy | precision | F ₁ -Score | sensitivity | specificity |
|------------|------|----------|-----------|-----------------------|-------------|-------------|
| SVM def. | 0.86 | 79.89% | 80.23% | 0.80 | 80.46% | 79.31% |
| SVM ext-T | 0.87 | 81.03% | 80.00% | 0.81 | 79.31% | 82.76% |
| SVM ext-E | 0.87 | 81.61% | 85.71% | 0.80 | 87.36% | 75.86% |
| SVM ext-A | 0.88 | 81.61% | 80.22% | 0.82 | 79.31% | 83.91% |

Table 6.3: *MSiHU results (SVM)*

More in detail, the number of classified images at optimal threshold is the following:

| Classifier | TP | FN | TN | FP |
|------------|----|----|----|----|
| SVM def. | 69 | 18 | 70 | 17 |
| SVM ext-T | 72 | 15 | 69 | 18 |
| SVM ext-E | 66 | 21 | 76 | 11 |
| SVM ext-A | 73 | 14 | 69 | 18 |

Table 6.4: *MSiHU classified images(SVM)*

Looking at Table 6.4, the number of TPs shows an interesting trend. Extending the *train* dataset improves the classification performance of TPs, worsening the number of TNs of just a unit. It appears that an extended dataset brings some more information. When the only *evaluation* dataset is extended, the number of TPs lowers considerably, meaning that the training set lacks some information to classify mitoses. On the other hand, the number of TNs is at top. The overall best performance is found when both datasets are extended. The ROC curves of this classification is shown in Figure 6.3.

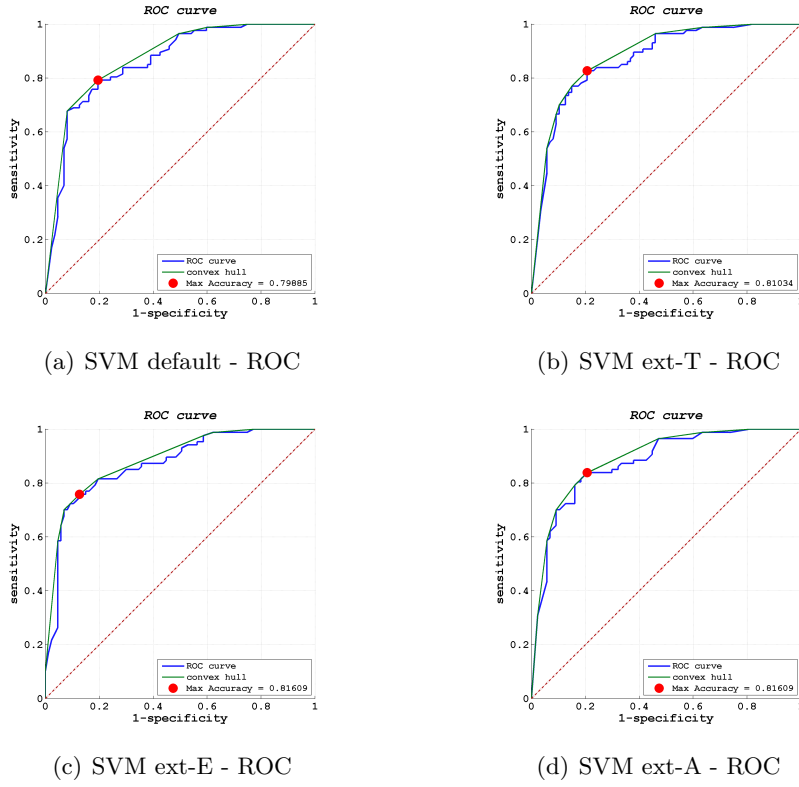


Figure 6.3: ROC curves for MSiHU features - SVM classification

Features: MSiHU - classifier: RF

We applied our RF classifier to the same dataset, with the results shown in Table 6.5.

| Classifier | AUC | accuracy | precision | F ₁ -Score | sensitivity | specificity |
|------------|------|----------|-----------|-----------------------|-------------|-------------|
| RF def. | 0.85 | 78.74% | 81.25% | 0.78 | 82.76% | 74.71% |
| RF ext-T | 0.86 | 79.31% | 76.29% | 0.80 | 73.56% | 85.06% |
| RF ext-E | 0.86 | 78.16% | 74.75% | 0.80 | 71.26% | 85.06% |
| RF ext-A | 0.86 | 77.59% | 74.00% | 0.79 | 70.11% | 85.06% |

Table 6.5: MSiHU results (RF)

More in detail, the number of classified images at optimal threshold is reported in Table 6.6.

| Classifier | TP | FN | TN | FP |
|------------|----|----|----|----|
| RF def. | 65 | 22 | 72 | 15 |
| RF ext-T | 74 | 13 | 64 | 23 |
| RF ext-E | 74 | 13 | 62 | 25 |
| RF ext-A | 74 | 13 | 61 | 26 |

Table 6.6: MSiHU classified images (RF)

In this classification the extended dataset brings an improvement in the detection of mitoses, while worsens the detection of non-mitoses. The ROC curves of this classification is shown in Figure 6.4.

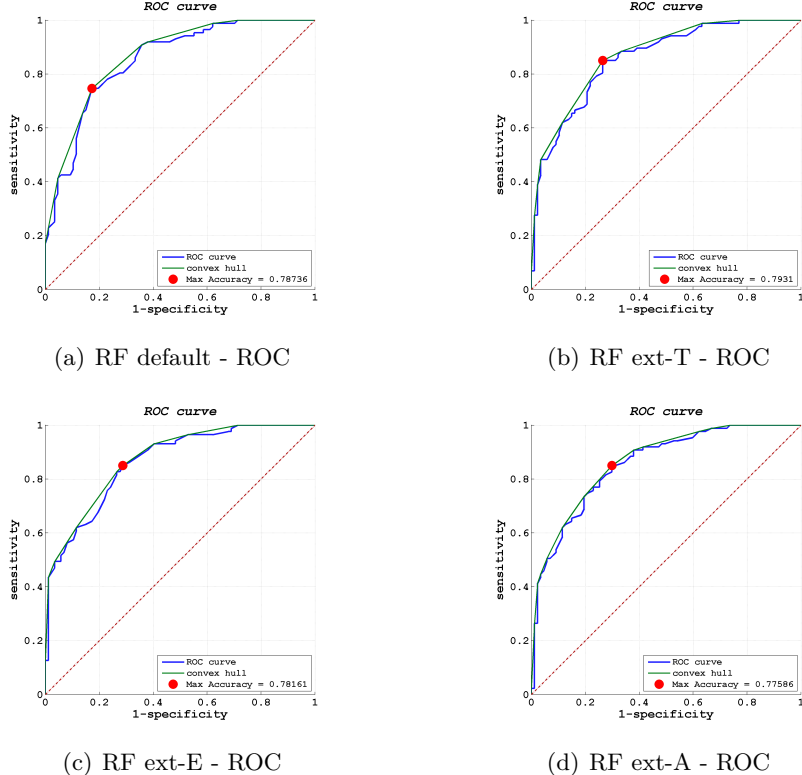


Figure 6.4: ROC curves for MSiHU features - RF classification

Features: MSiHR - classifier: RF

We applied our RF classifier to the feature-set coded **MSiHR**, which is an orientation independent dataset. The results are shown in Table 6.7.

| Classifier | AUC | accuracy | precision | F ₁ -Score | sensitivity | specificity |
|------------|------|----------|-----------|-----------------------|-------------|-------------|
| RF def. | 0.89 | 82.18% | 84.15% | 0.82 | 85.06% | 79.31% |
| RF ext-T | 0.90 | 81.61% | 83.95% | 0.81 | 85.06% | 78.16% |
| RF ext-E | 0.89 | 81.61% | 85.71% | 0.80 | 87.36% | 75.86% |
| RF ext-A | 0.90 | 81.03% | 85.53% | 0.80 | 87.36% | 74.71% |

Table 6.7: MSiHR results (RF)

More in detail, the number of classified images at optimal threshold is reported in Table 6.8.

| Classifier | TP | FN | TN | FP |
|------------|----|----|----|----|
| RF def. | 69 | 18 | 74 | 13 |
| RF ext-T | 68 | 19 | 74 | 13 |
| RF ext-E | 66 | 21 | 76 | 11 |
| RF ext-A | 65 | 22 | 76 | 11 |

Table 6.8: MSiHR classified images (RF)

Looking at Table 6.8, the most interesting trend concerns the number of TPs. In fact, using an extended dataset with no rotation dependent features brings no advantages, instead reduces the number of detected mitoses. In a sense, there is more noise than useful information. On the other hand, it is always visible the fact that TNs are better detected with extended datasets. The ROC curves of this classification is shown in Figure 6.5.

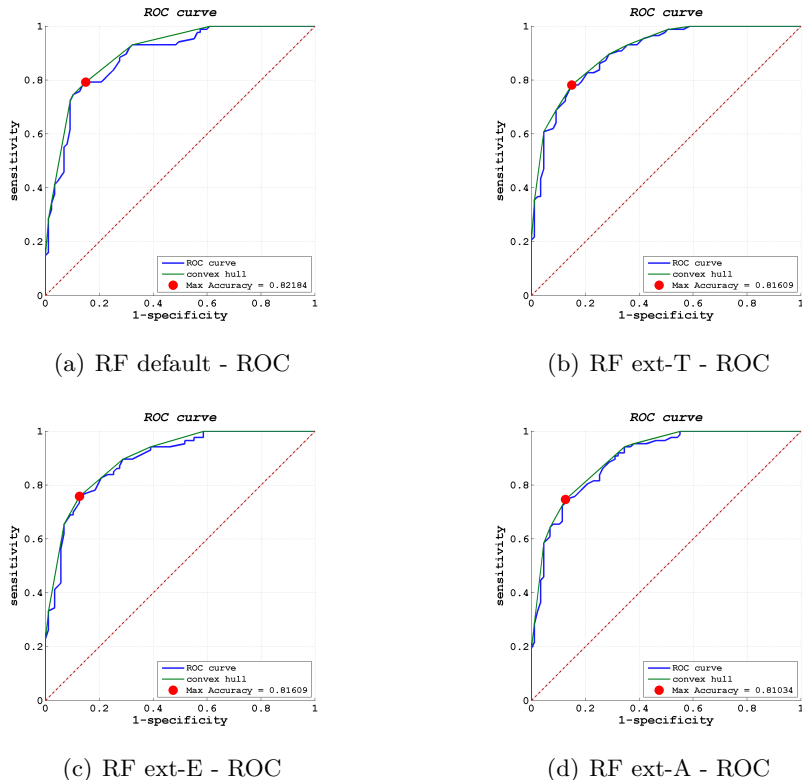


Figure 6.5: ROC curves for MSiHR features - RF classification

In the following examples we considered extended datasets, unless explicitly specified.

6.2.5 Best Feature Combinations

In this experiment we looked for the best combination of features, so we considered all the features described in 4.2. Having n features, maybe multi-component, they can be combined in $2^n - 1$ ways. As the texture features (see Section 4.2.3, in particular Equation 4.8) are mutually exclusive, we run three different experiments, one for each texture feature set.

The Matlab code implemented to run *experiment 3* is listed in ??

6.2.6 Best Feature Combinations: Experimental Results

Having run all possible combinations of features, we report here the best performance found, divided for RF and SVM classifiers.

Best Performances - classifier: SVM

The four feature sets which gave best results, when classified with SVM are described in Table 6.9. The detailed number of classified images, at the optimal classification threshold is shown in Table 6.10.

| Classifier | AUC | accuracy | precision | F ₁ -Score | sensitivity | specificity |
|-------------|------|----------|-----------|-----------------------|-------------|-------------|
| SVM - H | 0.83 | 79.89% | 73.21% | 0.82 | 65.52% | 94.25% |
| SVM - MSiVH | 0.85 | 78.74% | 87.88% | 0.76 | 90.80% | 66.67% |
| SVM - SiU | 0.88 | 84.48% | 81.91% | 0.85 | 80.46% | 88.51% |
| SVM - SiVHU | 0.88 | 80.46% | 77.32% | 0.82 | 74.71% | 86.21% |

Table 6.9: Best SVM results

| Classifier | TP | FN | TN | FP |
|-------------|----|----|----|----|
| SVM - H | 82 | 5 | 57 | 30 |
| SVM - MSiVH | 58 | 29 | 79 | 8 |
| SVM - SiU | 77 | 10 | 70 | 17 |
| SVM - SiVHU | 75 | 12 | 65 | 22 |

Table 6.10: Best SVM results - classified images

The ROC curves of these classifications are shown in Figure 6.6.

Best Performances - classifier: RF

The four feature sets which gave best results, when classified with RF are described in Table 6.11. The detailed number of classified images, at the optimal classification threshold is shown in Table 6.12.

The ROC curves of these classifications are shown in Figure 6.7.

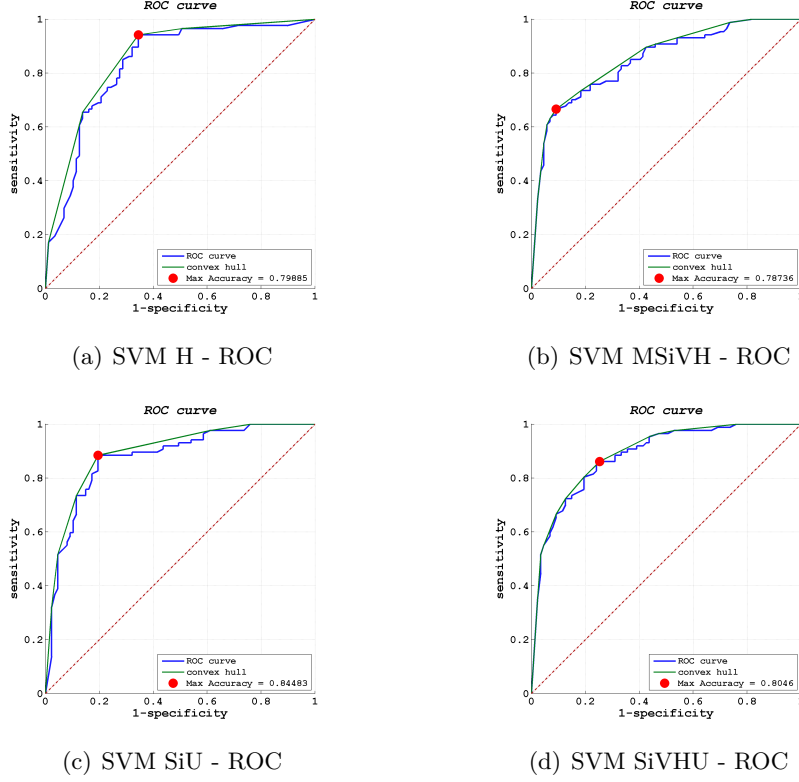


Figure 6.6: ROC curves for best feature-set - SVM classification

| Classifier | AUC | accuracy | precision | F ₁ -Score | sensitivity | specificity |
|-------------|------|----------|-----------|-----------------------|-------------|-------------|
| RF - iVHL | 0.90 | 83.91% | 79.80% | 0.85 | 77.01% | 90.80% |
| RF - MSHL | 0.89 | 81.03% | 89.71% | 0.79 | 91.95% | 70.11% |
| RF - MSiVHR | 0.91 | 83.91% | 81.05% | 0.85 | 79.31% | 88.51% |
| RF - SHL | 0.89 | 80.46% | 73.04% | 0.83 | 64.37% | 96.55% |

Table 6.11: Best RF results

| Classifier | TP | FN | TN | FP |
|-------------|----|----|----|----|
| RF - iVHL | 79 | 8 | 67 | 20 |
| RF - MSHL | 61 | 26 | 80 | 7 |
| RF - MSiVHR | 77 | 10 | 69 | 18 |
| RF - SHL | 84 | 3 | 56 | 31 |

Table 6.12: Best RF results - classified images

Comparison between classifiers

Having classified our evaluation set with a considerable number of different features, we could try to answer the question whether one of the two considered classifiers outperforms the other. We used, as a metric for our analysis, the *AUC* and the *accuracy*, and considered the three different complete feature sets: **MSiVHU**, **MSiVHR** and **MSiVHL**. Having tried all the possible

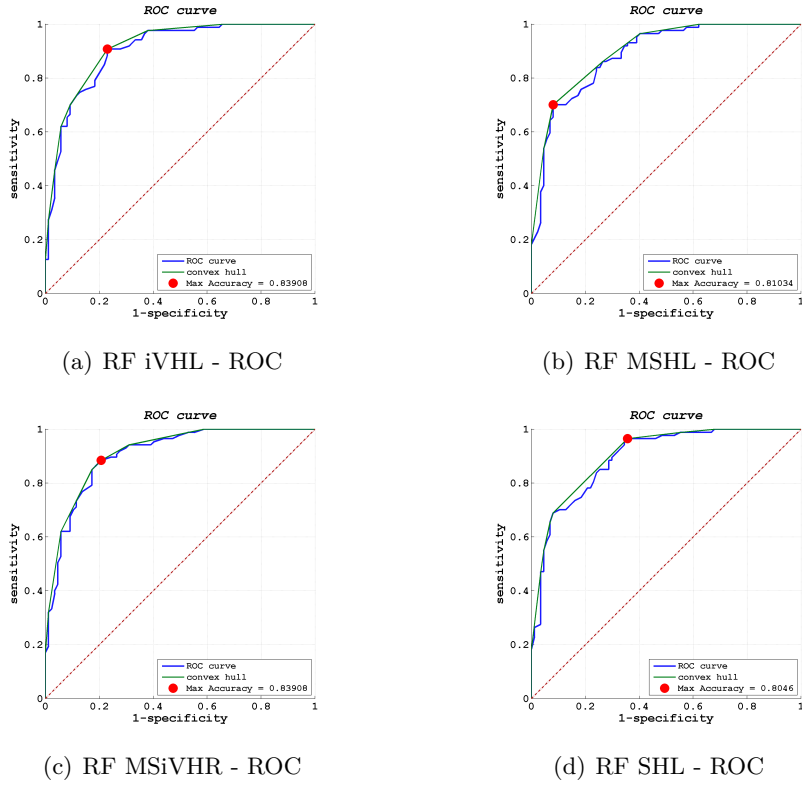


Figure 6.7: ROC curves for best feature-set - RF classification

combinations, the sorted the results obtained by the RF classifier in ascending order and plotted the results obtained by the SVM classifier in the same sequence.

The results are showed on Figures 6.8, 6.9 and 6.10.

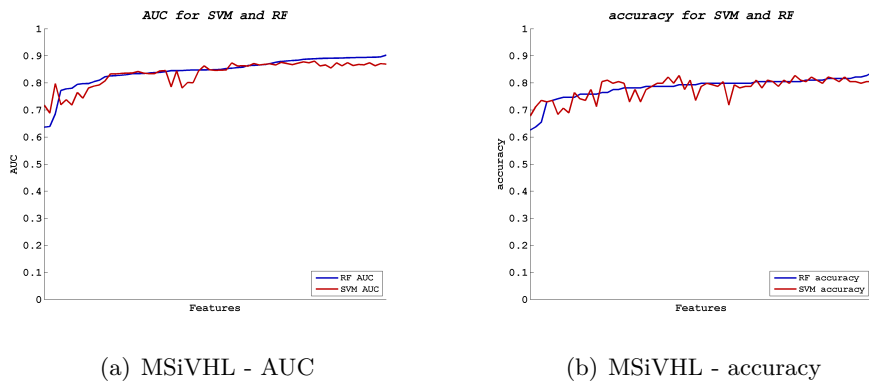


Figure 6.8: Features MSiVHL - overall performances

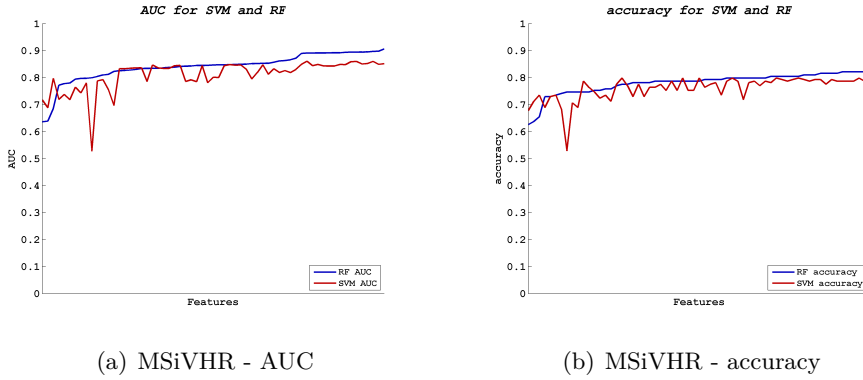


Figure 6.9: Features MSiVHR - overall performances

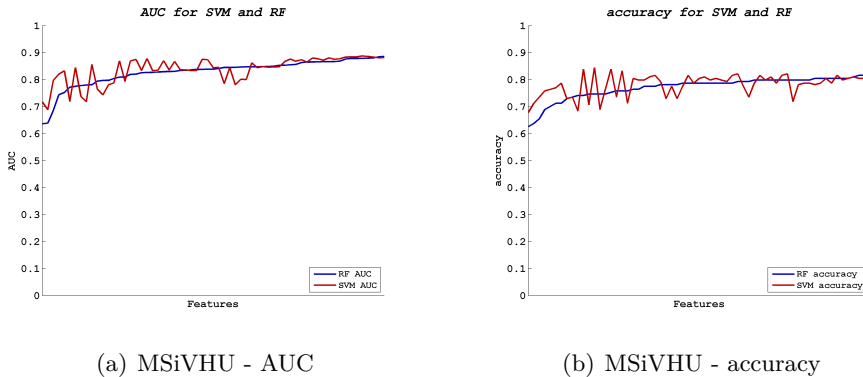


Figure 6.10: Features MSiVHU - overall performances

While it is generally true that the mean performance of the RF classifier is better (in terms of *AUC* and *accuracy*) than the one given by the SVM classifier, it is not possible to say that RF outperforms SVM. There are many cases in which the SVM performance turns out to be better, in particular when the LBP^{u2} feature is involved (see Figure 6.10). Nevertheless, the best RF performance is better than SVM's.

6.2.7 Dataset Dimension

In this experiment we analyzed the effect of the size of the training dataset on the classification performance, in term of selected instances. To achieve this goal, we repeatedly selected random subsets of the extended dataset and applied our classifier. To avoid the dependence on the specific selected subset, we run many different experiments with randomly chosen subsets

with the same size and then we averaged the results.

The Matlab code implemented to run *experiment 4* is listed in ??

6.2.8 Dataset Dimension: Experimental Results

Considering fractions of the *training* dataset ranging $1\% \rightarrow 100\%$, we performed the classification on the whole *evaluation* set having trained the classifier on a randomly selected subset. In order to reduce the risk of biases due to a specific subset, we made different trials, selecting at each time the training dataset. We used the following empirical rule to decide the number of trials in function of the subset size:

$$\frac{\text{subset-size}}{\text{trial}} \cdot (\# \text{ of trials}) \approx 3 \quad (6.4)$$

Equation 6.4 brings to the number of trials illustrated in Figure 6.11.

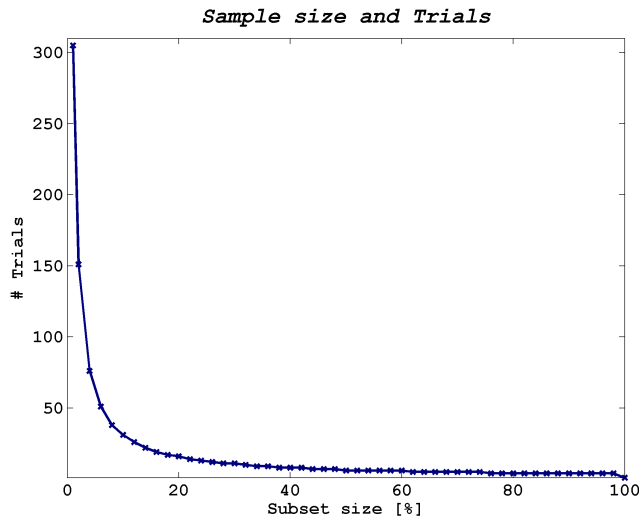


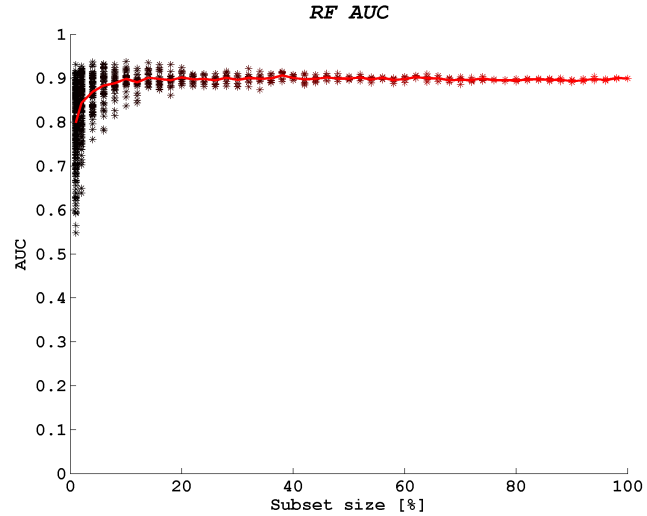
Figure 6.11: Subset size and number of trials

We run experiments on different sets of features that performed well in previous tests (not necessarily the best ones): iVHL, MiVHU and MSVHR. We initially used both of our classifiers. However, it emerged that, with some combination of instances, the SVM was unable to find a proper solution. For this reason we preferred to focus on the performances of the RF classifier, which contextually turned out to be more robust.

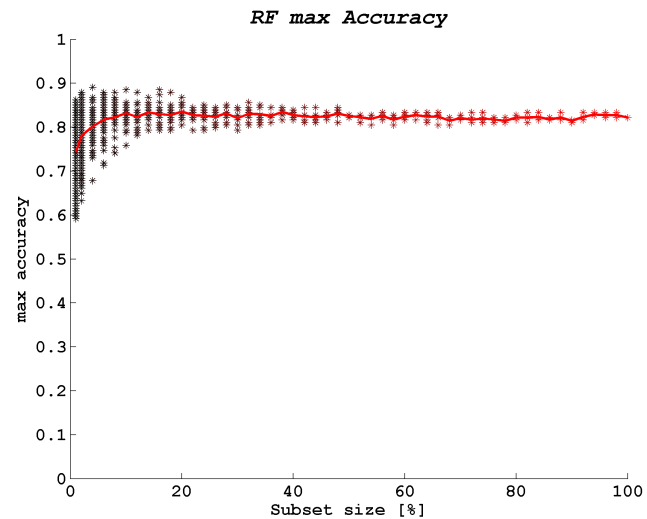
As usual we considered, as a metric of performance, *AUC* and *accuracy*.

Classifier: RF - Features iVHL

The results are shown in Figure 6.12, where the continuous line represents the average of the performance, and the *represent the single classification result.



(a) RF iVHL - AUC



(b) RF iVHL - accuracy

Figure 6.12: Features iVHL - sample size

It is apparent that, on one side, the performance grows with the subset size, and on the other side the variance of the performance reduces. Once

the 20% of the dataset size is reached, the average performance remains steady, but it is necessary to reach about the 50% of the dataset to have small variability of the data.

Classifier: RF - Features MiVHU

Figure 6.13, shows the results with MiVHU feature set.

The results are similar to the ones shown in Figure 6.13. In this case, at 20% of the dataset size a maximum of the *AUC* performance is reached, even if the negative slope of subsequent data is negligible (see Figure 6.13(a)).

Classifier: RF - Features MSVHR

Figure 6.14, shows the results with MSVHR feature set.

The results are similar to the previous ones: in this case the maximum *AUC* performance is reached even at lower subset dimension, and then a steady state is maintained, while a negligible variability is reached at about 40% of the dataset (see Figure 6.14(a)). In this experiment the variability of *accuracy* appears to be accentuated (see Figure 6.14(b)).

6.2.9 SVM parameters

In the experiments above we noted that SVMs are more sensible to the selected features and to the size of the dataset, meaning that, in some cases, SVM performs poorly on data. So we decided to analyze in a deeper way if some of the configuration options of the classifier (i.e. kernel type [Section 4.3.1], degree in kernel function, etc.) could improve the performance.

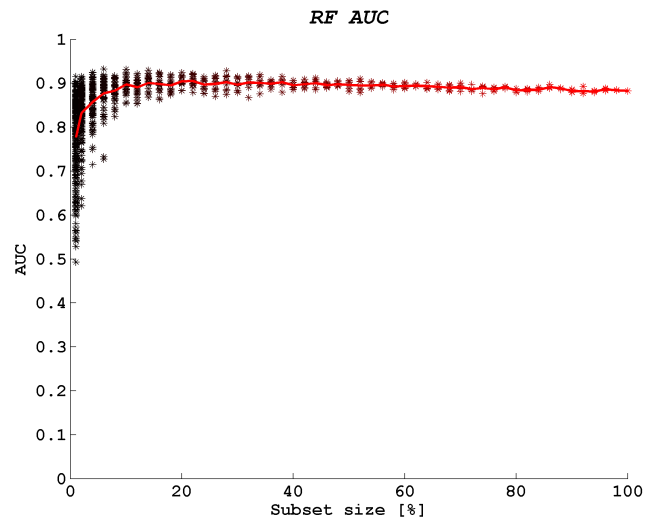
The Matlab code implemented to run *experiment 5* is listed in ??

6.2.10 SVM parameters: Experimental results

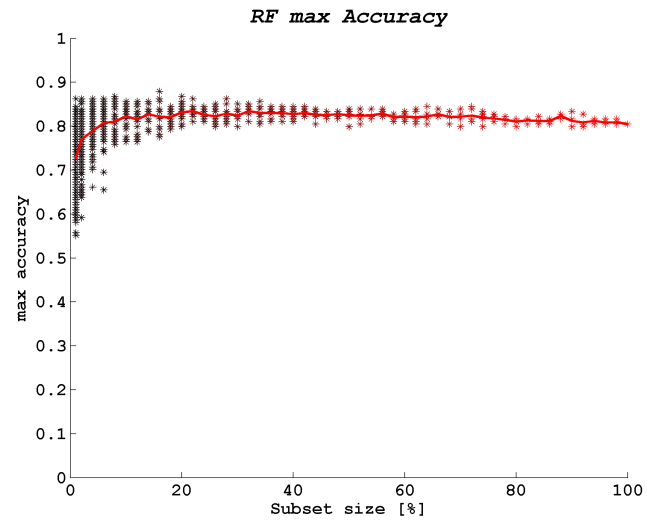
We tried different configuration parameters for the SVM classifier on the feature set **MSiHLV**, of which SVM performed poorly: $AUC = 0.531$ and $accuracy = 0.58$.

We changed the allowed parameters in the *libSVM* implementation that we used (see Section 4.3.1):

- *Kernel type*: RBFs (default) or sigmoidal,



(a) RF MiVHU - AUC

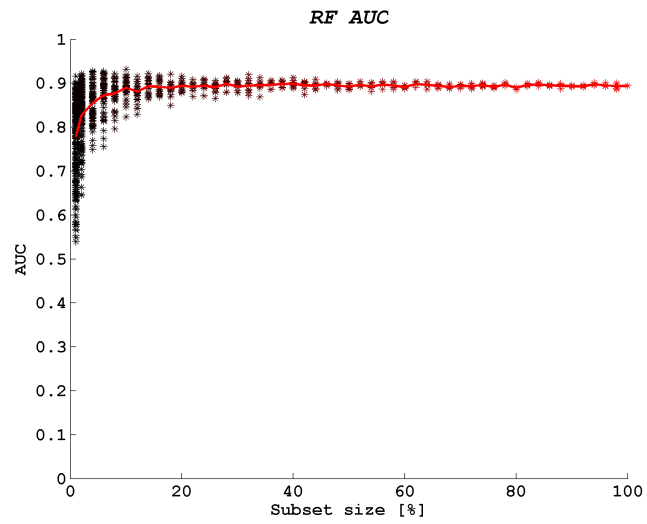


(b) RF MiVHU - accuracy

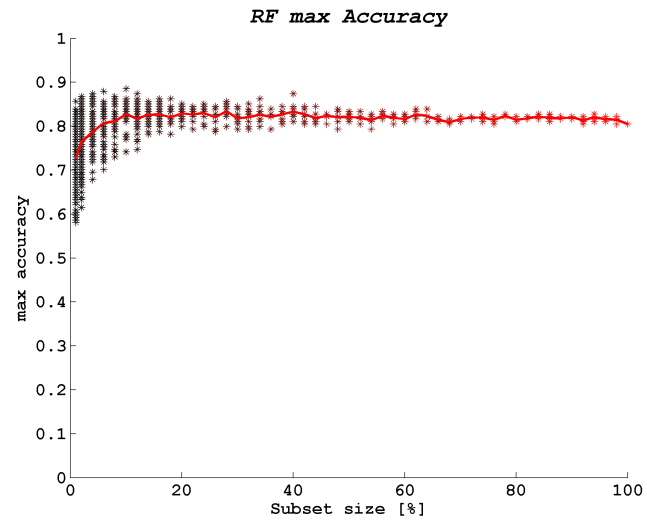
Figure 6.13: Features MiVHU - sample size

- *degree*: from 3 (default) up to 7.

As we didn't notice any particular benefit in modifying the parameters above (i.e. the performances remained identical), in the following experiments we continued using the default parameters. This experiments confirmed that, for our classification problem, RFs turned out to be more robust.



(a) RF MSVHR - AUC



(b) RF MSVHR - accuracy

Figure 6.14: Features MSVHR - sample size

6.2.11 Principal Component Analysis

Even when considering only simple features, the feature space can reach high dimensions (i.e. a lot of components). It is common experience, in many classification problems, that when the dimensionality increases, the volume of the space increases so fast that the meaningful data become sparse in a substrate of noise.

This situation is often referred to as the *curse of dimensionality* [7]. In ML problems that involve learning from a finite number of data samples in a high-dimensional feature space, with each feature having a number of possible values, an enormous amount of training data are required to ensure that there are several samples with each combination of values. With a fixed number of training samples, the predictive power reduces as the dimensionality increases, and this is known as the *Hughes effect* [70].

Principal Component Analysis (PCA) is a way to reduce the dimensionality of the dataset [49]. PCA is a mathematical procedure that uses an orthogonal transformation (SVD transformation) to convert a set of observations of possibly correlated variables into a set of values of linearly uncorrelated variables called *principal components*. This transformation is defined in such a way that the components are sorted in descending magnitude of *explained variance*: that is, the first principal component has the largest possible variance (accounts for as much of the variability in the data as possible), and each succeeding component, has the highest variance possible under the constraint that it is orthogonal to (i.e., uncorrelated with) the preceding components. PCA is sensitive to the relative scaling of the original variables, and so we applied it on normalized data [79]. In our experiments we selected some datasets with high dimension feature spaces, applied PCA and classified the resulting components adding one component at a time, with the aim to observe the classification performances in relation to the number of components and the percentage of explained variance.

The Matlab code implemented to run *experiment 6* is listed in ??

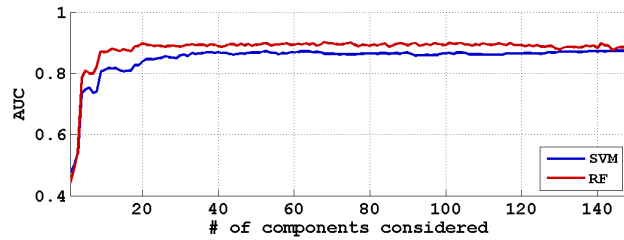
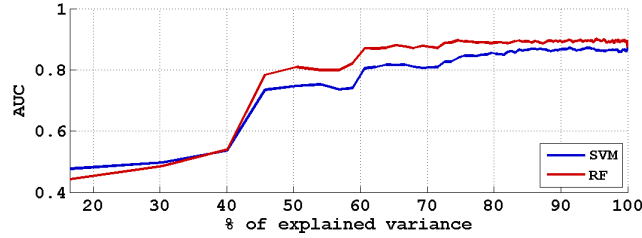
6.2.12 PCA: Experimental results

The Matlab function `pca` returns the principal component coefficients for a data matrix whose rows correspond to observations and columns correspond to variables (i.e. the training feature matrix). It returns a coefficient matrix. Each column of that matrix contains coefficients for one principal component, and the columns are in descending order of component variance. By default, `pca` uses the Singular Value Decomposition (SVD) algorithm. It also returns the percentage of the total variance explained by each principal component.

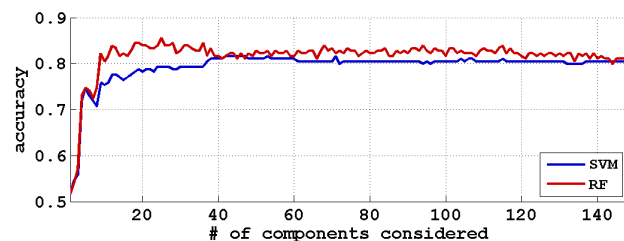
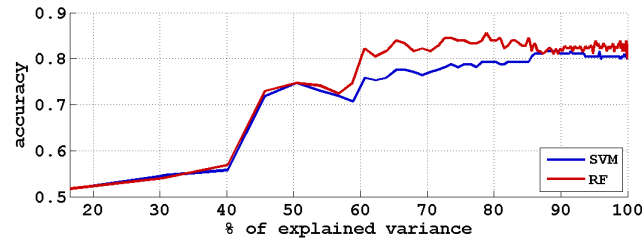
For our analysis we selected two sets of features with many components: `MSidHLV` (with 148 elements) and `MSidHUV` (with 292 elements). As in previous experiments, we used *AUC* and *accuracy* as measures of performance.

PCA: MSidHLV

Figure 6.15 shows the results of PCA applied to **MSidHLV** feature set. We plotted the results as function of percentage of explained variance and number of components considered.



(a) PCA MSidHLV - AUC



(b) PCA MSidHLV - accuracy

Figure 6.15: Features MSidHLV - Principal Component Analysis

The results show a generally better performance of RF than SVM. In terms of *AUC* (see Figure 6.15(a)), the RF classification reaches a maximum

at about 74% of explained variance (20 components), and then it remains almost stable with small fluctuations due to noise. The SVM classification shows similar behavior.

In terms of *accuracy* (see Figure 6.15(b)) the RF classification reaches a maximum at about 79% of explained variance (27 components) and then starts decreasing moderately. SVM shows a maximum at about 80% (43 components): the overall behavior appears to be steadier.

PCA: **MSidHUV**

Figure 6.16 shows the results of PCA applied to **MSidHUV** feature set. Also in this case, we plotted the results as function of percentage of explained variance and number of components considered.

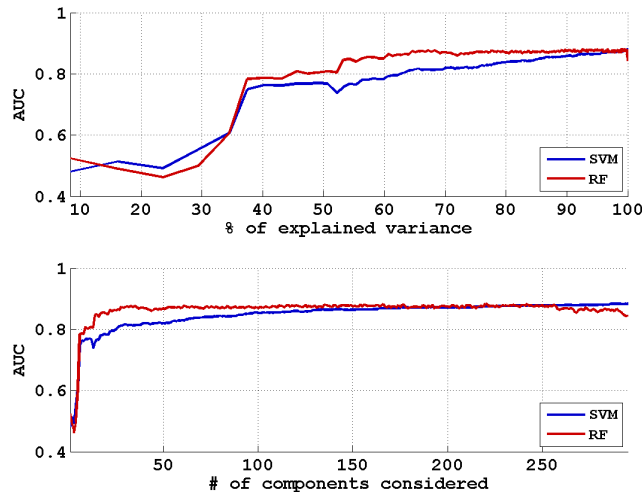
The results show a generally better performance of RF than SVM, even if, at high number of components (> 250), SVM still find information useful for classification and improves performance, while RF starts decreasing. It appears that, with a high number of components, RF becomes more sensible and the performance becomes more noisy. In terms of *AUC* (see Figure 6.16(a)), the RF classification reaches a maximum at about 69% of explained variance (33 components), and then it decreases with fluctuations due to noise induced by further components. The SVM classification appears more stable and continues increasing.

In terms of *accuracy* (see Figure 6.16(b)) the RF classification reaches a maximum at about 66% of explained variance (26 components) and then starts decreasing. SVM shows a local maximum at about 45% (just 12 components) and then has an important degradation of performance up to about 54% of explained variance. Then it starts increasing again up to the end.

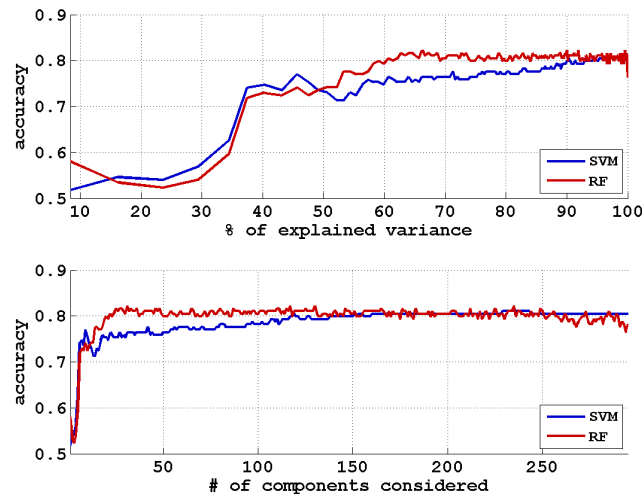
6.2.13 Size of the Image Patch

In all the experiments above, we considered the size of each image patch, on which to compute features, to be 100×100 pixels. We wanted to analyze if there is a smaller sub-image that includes all the meaningful information, while the boundary contains essentially background (i.e. noise for the purposes of classification), while an excessively small patch would not allow to classify data.

So we run experiments considering, from time to time, bigger portions of



(a) PCA MSidHUV - AUC



(b) PCA MSidULV - accuracy

Figure 6.16: Features MSidHUV - Principal Component Analysis

the images and analyzed the classification performances.

The Matlab code implemented to run *experiment 7* is listed in ??

6.2.14 Image Size: Experimental Results

We tried different image sizes, starting from 10px up to 100px, with a step of 10px. We calculated different feature sets on the images and finally we performed classifications. Even if it appeared to be quite hard to find a “best image size”, we could draw some considerations about the relation among image size and some of the features selected.

Here we report the most interesting ones, focusing in particular on the following features:

- Color Histograms (H),
- LBPr_i^{u2} (L),
- VAR (V).

In this case we used AUC as a measure of performance.

Image Size: SVM Classifier

By ordering the SVM classification results in ascending order for cumulate AUC along feature size, we could plot the behavior as reported in Figure 6.17 and in Figure 6.18

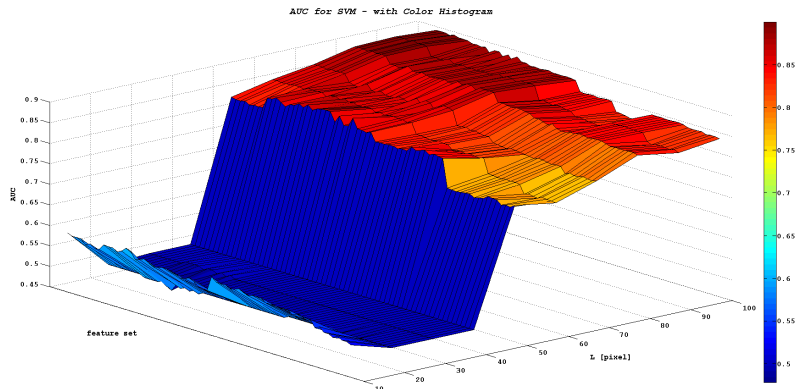


Figure 6.17: Image size and sets with ‘H’ feature - SVM classifier

Ordering the results we found that **all** the feature sets with the H elements have the same behavior. Figure 6.17 shows that SVM is unable to classify any dataset containing the H feature up to image size of 40px.

Please note that an *AUC* of 0.5 means “random classification”. After 50px the performance increases abruptly to high values.

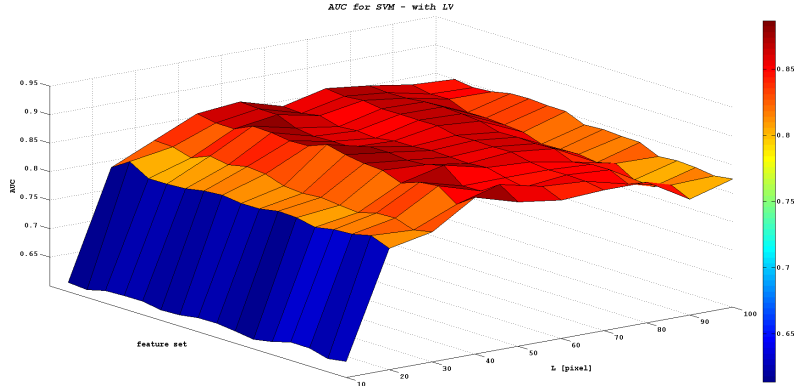


Figure 6.18: Image size and sets with 'LV' features - SVM classifier

Among the other feature set (i.e. the ones not containing H), it emerged that the ones containing the LV combination have the best performance. Figure 6.18 shows that those sets have a maximum generally at about 40px. With higher image size the performance slightly decreases.

Image Size: RF Classifier

We performed the same operations on the results coming from our RF classifier and found similar results. In this case, ordering in ascending order the result for mean performance over image size, we found that **all** the feature set containing the HLV components showed good results and also performed in the same way (see Figure 6.19).

Figure 6.19, similarly to Figure 6.18, shows a general maximum at about 40px.

6.3 Accuracy of Humans

In this section we illustrate the performances of the users of the website described in Chapter 5. We gathered data from a total of 45 test subjects, 8 of which have expertise in biology (i.e. may have some prior expectations or experience on a mitosis’ appearance), and none of which routinely works

with histology datasets. No subject was allowed to take the test twice. In total, subjects provided 3009 classifications (on average 67 per subjects), resulting in an average of 17.3 classifications for each of the 174 evaluation samples. Each subjects dedicated an average of 49 minutes to the test. Below, we compare the performance of such subjects to the 7 top-performing algorithms in the 2012 ICPR mitosis detection contest, all of which were learned on the training images of the MITOS dataset. For a given algorithm, a **C1** evaluation sample is considered a true positive if and only if, in the corresponding image of the MITOS dataset, the algorithm detected a mitosis whose centroid is within $8 \mu\text{m}$ (20 px) from the coordinates given by the algorithm; else, the sample is considered a false positive (this is the same criterion used for evaluation of the ICPR contest). A **C0** evaluation sample is a true negative if and only if the algorithm returned no detections in a range of $16 \mu\text{m}$ (40 px), else it is a false negative.

Note that the results reported below for algorithms do not directly map to the results of the ICPR contest (shown in Section 3.5). In fact, we are computing the algorithms' performance in a classification task on a balanced dataset, whereas the algorithms' parameters (such as thresholds) were optimized for solving a detection task where the prevalence of mitosis over non-mitosis was much lower. Therefore, we can expect that the reported performance for each algorithm is a lower bound of the performance it could obtain when properly tuned for this task. For this same reason, the results below should not be used to compare different algorithms with each other. We also compare the performances of the users with best classifications obtained in Chapter 4, which instead is designed on the same problem as the

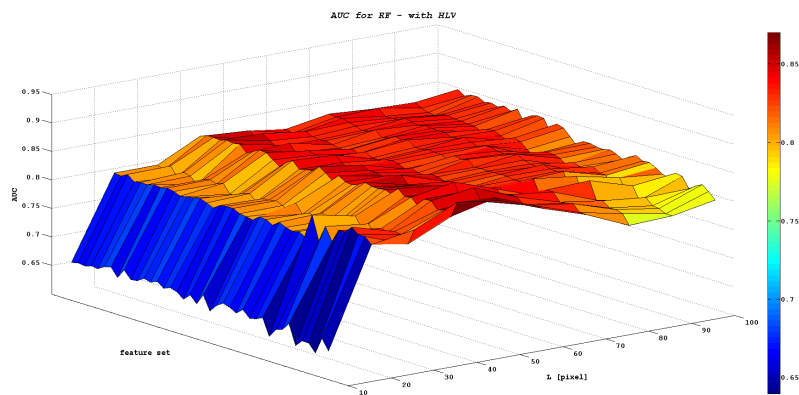


Figure 6.19: Image size and sets with 'HLV' features - RF classifier

one presented to the users.

6.3.1 Humans and ICPR Contest Algorithms

For a given set of N classifications produced by an human or algorithm, the accuracy is defined as the fraction of classifications which are correct¹. Because our evaluation set has the same prevalence of both classes, a random classifier has an expected accuracy = 0.5. Subjects could assign each sample to one of four probability values: for each user, we computed the accuracy when using all three meaningful thresholds ($p(C1) = 0.1, 0.5, 0.9$), and selected the maximum resulting accuracy value.

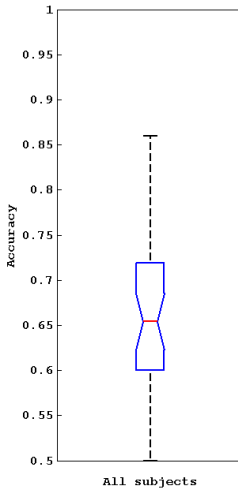


Figure 6.20: Accuracy distribution of humans

Figure 6.20 reports the accuracy distribution for all test subjects, while Figure 6.21 shows the performance of the 5 best test subjects (6.21(a)), compared with the performance of the 7 algorithms (6.21(a)). The average classification accuracy for users is 0.661, comparable with the accuracy of the worst of the considered algorithms; The best individual yielded an accuracy of 0.859 ± 0.012 , which is close to the accuracy of the second-scoring algorithm, and worse ($p < 0.01$) than the most accurate algorithm (accuracy = 0.873 ± 0.004).

All users with $N \geq 10$ performed better than chance; most achieved an accuracy between 0.60 and 0.75. Only three users (one of which with signif-

¹for all algorithms, $N = 174$ since we computed an output for each evaluation sample; instead, test subjects were not required to evaluate all samples

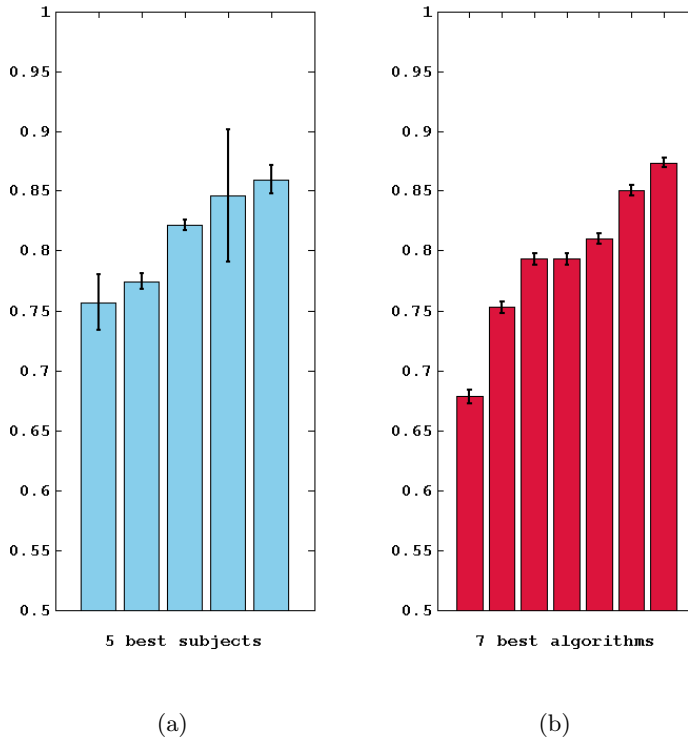


Figure 6.21: best Humans' performance vs. ICPR algorithms

icant experience in cytology but not in this specific problem) exceeded an accuracy of 0.80. Differences in human performance are partly explained by different amounts of motivation and effort put in the test; still, we observed that many users who dedicated a significant amount of time and effort to study the training set and complete the test obtained a performance close to the average. Most users described the problem as “very difficult”.

Some users gave indications about the evaluation criteria which they devised during classification. Most of them focused on the shape of the dark element in the middle. Mitotic samples where mostly the ones with blurry or bumpy edges, while non-mitotic samples were the ones with a smooth shape. Most of them ignored the surrounding area.

Figure 6.22 reports the performance of test subjects and algorithms in ROC space. IDSIA and Utrecht institutions provided confidence values for each classification, from which ROC curves were computed.

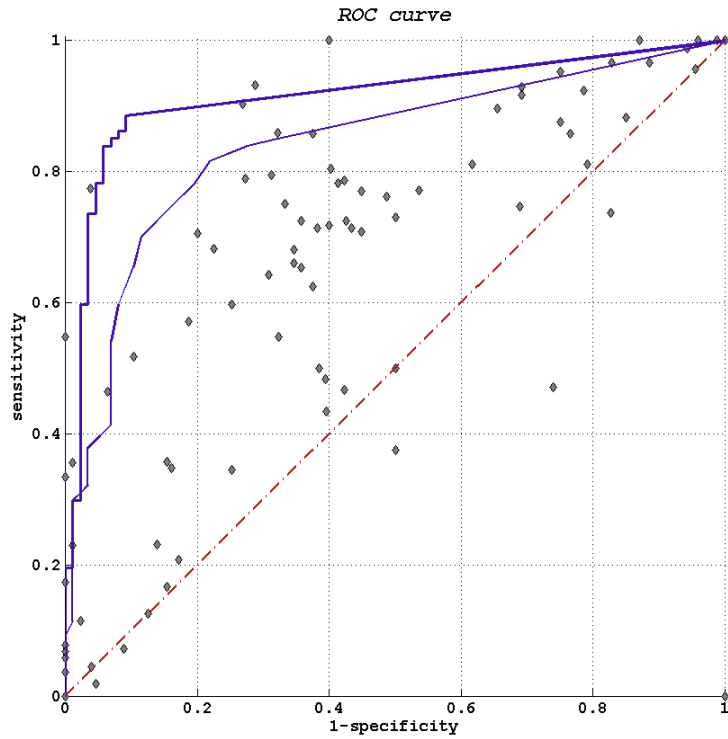


Figure 6.22: For each subject 3 points are reported, corresponding to the three possible thresholds. Full ROC curves could be plotted for IDSIA (thick blue) and Utrecht (thin blue), who provided soft confidence values for each detection.

6.3.2 Humans and ad hoc Classifiers

In this section we compare the performances of users with the classifiers that we trained on the same problem. In particular we selected two of the best performing classifiers with reference to Tables 6.9 and 6.11.

Figure 6.23 reports the ROC curves of the best performing SVM and RF classifiers and the user performances.

6.4 Difficulties

Even a superficial look at the dataset shows that some samples are easier to classify than others. Here we investigate whether samples that users find easy are also easier to classify for algorithms.

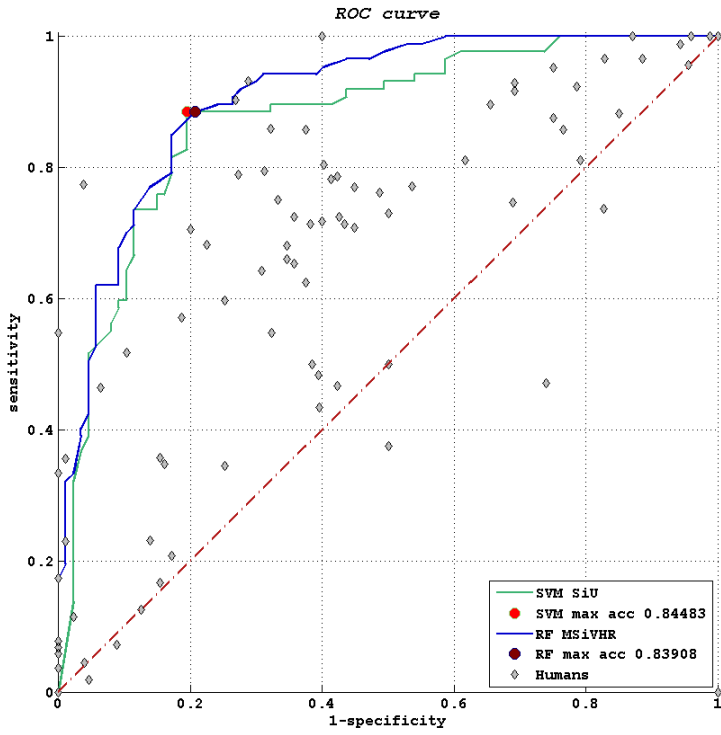


Figure 6.23: For each subject 3 points are reported, corresponding to the three possible thresholds. Full ROC curves are shown for two best feature-sets for SVM and RF

6.4.1 Humans vs. ICPR Algorithms

First, we define for each sample a score representing the classification difficulty for humans, defined as

$$D_h = \frac{1}{|S|} \cdot \sum_{s \in S} (|p_s(C1) - c|) \quad (6.5)$$

where:

- s represents a test subject,
- S is the set of test subjects who evaluated the considered sample, $|S|$ denotes its cardinality,
- $p_s(C1)$ is the probability assigned by the user to the **C1** class,
- c is a binary variable representing the true class of the sample.

Please note that D_h differs from accuracy because it also depends on the confidence that users expressed for each classification.

We divided the **C1** evaluation samples in three groups: E_{easy} , containing the 22 mitosis with the lowest D_h value (i.e. those which were identified most easily by humans), E_{hard} , containing the 22 mitosis with the highest D_h and E_{med} , containing the remaining 43 mitosis).

Appendix A, in particular Section A.2 shows the samples described in this section.

| Subset | humans | Algorithms | | | | | | |
|------------|--------|------------|-------|-------|-------|-------|---------|---------|
| | | IDSIA | IPAL | ISIK | Necla | NUS | Utrecht | Warwick |
| E_{easy} | 0.876 | 0.909 | 0.864 | 0.864 | 0.773 | 0.591 | 0.909 | 0.727 |
| E_{med} | 0.716 | 0.884 | 0.814 | 0.512 | 0.744 | 0.395 | 0.860 | 0.674 |
| E_{hard} | 0.496 | 0.545 | 0.545 | 0.318 | 0.364 | 0.136 | 0.500 | 0.409 |

Table 6.13: Accuracy of human and algorithms on easy, medium and difficult mitosis.

Table 6.13 reports the accuracy of algorithms on these samples. We observe that for each algorithm, the accuracy on E_{easy} is better than the accuracy on E_{med} , which in turn is better than the accuracy on E_{hard} ; this indicates that samples which are challenging for humans are also difficult for all considered algorithms.

6.4.2 Humans vs. ad hoc Classifiers

The same evaluations and comparisons made in previous Section can be carried out on the results obtained by our best classifiers.

Using the same division in E_{easy} , E_{med} and E_{hard} of the mitoses, we computed the average accuracy of each classifier for the samples of each subset. Tables 6.14 and 6.15 show the results, divided for SVM and RF best classifiers.

| Subset | humans | SVM classifiers | | | |
|------------|--------|-----------------|-------|-------|-------|
| | | H | MSiVH | SiU | SiVHU |
| E_{easy} | 0.876 | 0.954 | 0.818 | 1.000 | 1.000 |
| E_{med} | 0.716 | 0.853 | 0.721 | 0.861 | 0.791 |
| E_{hard} | 0.496 | 0.909 | 0.409 | 0.818 | 0.864 |

Table 6.14: Accuracy of human and SVM classifiers on sets of mitoses.

| Subset | humans | RF classifiers | | | |
|------------|--------|----------------|-------|--------|-------|
| | | iVHL | MSHL | MSiVHR | SHL |
| E_{easy} | 0.876 | 0.954 | 0.864 | 0.954 | 1.000 |
| E_{med} | 0.716 | 0.861 | 0.698 | 0.837 | 0.930 |
| E_{hard} | 0.496 | 0.954 | 0.545 | 0.909 | 1.000 |

Table 6.15: Accuracy of human and RF classifiers on sets of mitoses.

Tables 6.14 and 6.15 show that, most classifiers, even if trained on different features, have better performances on easy mitoses than on medium and hard, with a trend similar to human performance. This confirms that, in general, difficult mitoses for humans are generally more difficult also for classifiers.

On average, classifiers outperform humans on each set of mitoses, as shown in Table 6.16.

| Subset | humans | classifiers (avg.) |
|------------|--------|--------------------|
| E_{easy} | 0.876 | 0.943 |
| E_{med} | 0.716 | 0.831 |
| E_{hard} | 0.496 | 0.801 |

Table 6.16: Accuracy of human and average of classifiers on sets of mitoses.

The measure of the difficulty described in Equation 6.5 of an image sample can be used not only for **C1** samples, but also for **C0** samples. We divided the subset of negative samples of our evaluation dataset with the same criteria used for positive samples and performed the same comparison between humans and our classifiers. Tables 6.17 and 6.18 show the results, divided for SVM and RF best classifiers.

| Subset | humans | SVM classifiers | | | |
|------------|--------|-----------------|-------|-------|-------|
| | | H | MSiVH | SiU | SiVHU |
| E_{easy} | 0.801 | 0.750 | 0.917 | 0.958 | 0.875 |
| E_{med} | 0.626 | 0.683 | 0.951 | 0.732 | 0.732 |
| E_{hard} | 0.376 | 0.500 | 0.818 | 0.773 | 0.636 |

Table 6.17: Accuracy of human and SVM classifiers on sets of non-mitoses.

| Subset | humans | RF classifiers | | | |
|------------|--------|----------------|-------|--------|-------|
| | | iVHL | MSHL | MSIVHR | SHL |
| E_{easy} | 0.801 | 0.875 | 0.958 | 0.917 | 0.833 |
| E_{med} | 0.626 | 0.756 | 0.951 | 0.756 | 0.561 |
| E_{hard} | 0.376 | 0.682 | 0.818 | 0.727 | 0.591 |

Table 6.18: Accuracy of human and RF classifiers on sets of non-mitoses.

Tables 6.17 and 6.18 show that, most classifiers, even if trained on different features, have better performances on easy mitoses than on medium and hard, with a trend similar to human performance. This confirms that, in general, difficult non-mitoses for humans are generally more difficult also for classifiers.

On average, classifiers outperform humans on each set of non-mitoses, as shown in Table 6.19.

| Subset | humans | classifiers (avg.) |
|------------|--------|--------------------|
| E_{easy} | 0.801 | 0.885 |
| E_{med} | 0.626 | 0.765 |
| E_{hard} | 0.376 | 0.693 |

Table 6.19: Accuracy of human and average of classifiers on sets of non-mitoses.

Tables 6.16 and 6.19 also show that, for both humans and classifiers, on average mitoses are detected more easily than non-mitoses.

6.5 Difficulties among Classifiers

As a further analysis, we tried to find correlations among samples that appear to be difficult (i.e. are wrongly labeled) for several classifiers. for this analysis we used the same best classifiers determined in Section 6.2.5 and used also in Section 6.4.2. Among the 8 best classifiers (2 types of classifiers and 4 sets of features each), we considered if there exist samples that are not correctly classified by many classifiers.

In this analysis we intersected the FNs and FPs of all the classifiers and looked for frequencies. We considered only FNs and FPs with 5 or more occurrences, to be sure that they were misclassified by both SVM and RF. We started with FNs and found 6 samples: the results illustrated in Tables 6.20 and 6.21.

| Frequency | # of samples |
|---------------|--------------|
| 5 classifiers | 2 samples |
| 6 classifiers | 3 samples |
| 7 classifiers | 1 sample |
| 8 classifiers | no samples |

Table 6.20: Frequency of common misclassified mitoses.

| Subset | frequency |
|------------|------------|
| E_{easy} | no samples |
| E_{med} | 5 samples |
| E_{hard} | 1 sample |

Table 6.21: Correlation among frequency and human difficulty.

Among the 87 **C1** samples, 41 have been misclassified by at least one algorithm. Of 41 samples, only 6 have been wrongly labeled by 5 or more classifiers. Table 6.21 shows the distribution of the difficulty of the 6 samples. Most of them belong to E_{med} , with only one belonging to E_{hard} .

A similar analysis can be carried out on **C0** samples. Tables 6.22 and 6.23 show the results.

| Frequency | # of samples |
|---------------|--------------|
| 5 classifiers | 6 samples |
| 6 classifiers | 6 samples |
| 7 classifiers | 3 sample |
| 8 classifiers | 1 sample |

Table 6.22: Frequency of common misclassified non-mitoses.

| Subset | frequency |
|------------|-----------|
| E_{easy} | 2 samples |
| E_{med} | 8 samples |
| E_{hard} | 6 sample |

Table 6.23: Correlation among frequency and human difficulty.

Among the 87 **C0** samples, 46 have been misclassified by at least one algorithm. Of 46 samples, 16 have been wrongly labeled by 5 or more classifiers. Table 6.23 shows the distribution of the difficulty of the 16 samples. Most of them belong to E_{med} and E_{hard} , with only 2 belonging to E_{easy} .

Appendix A, in particular Section A.3 shows the samples described in this section.

Chapter 7

Conclusions

“διὸ οὐδέποτε νοεῖ ἀεν φαντάσματος ἢ ψυχῆ”

(The soul never thinks without a picture)

Αριστοτέλης (Aristotle, On the Soul 4.7.431a16)

7.1 Context and Results

Breast cancer is one of the most deadly cancers for women. According to the increasing incidence rate of breast cancer reported in many countries, early cancer detection and treatment play a major role in increasing the chances of recovery from the disease. Nottingham Grading System NGS is the standard grading procedures used in breast cancer assessment; it focuses on three criteria: Mitotic Count , Nuclear Pleomorphism , and Tubule Formation. Each criterion can be assigned with 3 scores, and the final equivalent NGS grade is the summation of all three criteria.

Breast tissue samples of patients are taken for grading by means of biopsy. The NGS grade of tissue samples are based on the deviation of the cell structures from normal tissues.

Pathologists need to assess lots of tissue samples under the microscope every day. Low agreement for medical cases is typical between pathologists because they exam breast tissue samples based on their experience and opinion. Hence, the evaluation of breast cancer grading is a subjective, manual, and time-consuming process.

Digital high resolution histo-pathological images are commonly used for extracting useful structural information from samples. With the rapid growth in computer technologies, many computer science researches have focused on computer aided diagnosis (CAD) systems to develop a standard and quantitative measurement for breast cancer assessment.

From the application point of view, the most important issue is whether such algorithms perform in such a way that can be compared to experts who routinely solve the same task. In our work, we considered the perspective of the machine learning algorithm designer. In this context, comparing an algorithm with an expert does not provide much useful information, because they are not competing fairly. In fact, during its formation and previous activity, the expert had access to an amount of training information (in form of criteria, guidelines and labeled examples) which is most probably much larger than the algorithm's training set. So if a detection algorithm underperforms, when compared to a pathologist, we can argue if it is due to its lack of detection ability (and then, effort should be focused on improving it), or because it has not enough data to learn (which implies that effort should be instead focused on gathering larger labeled datasets). We aimed to answer this question in the context of mitosis detection in breast cancer histological images using the public MITOS dataset. We built a balanced dataset (50% of mitoses and 50% of non-mitoses) using all the labeled samples provided with the MITOS dataset (216 mitoses in the training set and 87 mitoses in the evaluation set) and selected an equal number of negative samples which were not obviously non-mitoses.

We studied how top-performing algorithms in the recent ICPR2012 mitosis detection contest performed on the specific dataset. Furthermore we developed some detection algorithm using state of the art machine learning techniques.

We compared the results with the performance of humans which were new to the mitosis detection problem. In order to do so, we designed an user test that placed such humans in the same conditions as algorithms (i.e. they were provided with the same training data and tested on the same evaluation data).

In this context, human performance represents as a lower bound on the performance of the ideal algorithm.

If we had observed that the best performing among such humans significantly outperforms an algorithm, we could conclude that the algorithms lack either power or generalization ability, and can therefore be improved. Otherwise, the algorithm's performance may only be limited by the amount of available training data.

Our main contribution is an user study whose results provide strong evidence in favor of the second hypothesis : we found that the two top-scoring algorithms and the best ones that we developed perform comparably or better than the top-scoring human who took our test, which suggests that training set size may be limiting the performance of such algorithms.

7.2 Future Work

Our work focused on the comparison of the performance of humans and on algorithm from the classification point of view (i.e. the image candidates were previously selected). The whole process of mitotic count requires the detection of candidates and then classification. It would be interesting carry experiments on the detection phase, comparing human ability to detection algorithms' performance.

Our work could be extended by selecting some histologists and let them classify our dataset. The results would be interesting from different viewpoints: on one side their results can be compared to algorithms and other users, and gain some information on possible differences in the performances of the three sets. On the other side, as mitosis detection is widely recognized as a difficult problem, characterized by moderate agreement even among histologists, their results can be used to validate the quality of the dataset and in general to confirm the difficulty of the task.

A study similar to the one presented here could be carried out on a larger dataset, so that a comparison among algorithms and pathologists could give significant information: it could be possible to draw correlations among the errors of algorithms and humans and verify the accuracy of algorithms.

Finally, extending the test to histologist, could bring information on possible difference among different types of users. Non-expert users, being all trained in the same way, tend to present the same errors, without specific biases. Nevertheless, they tend to be less accurate. Histologists, being trained at different times, in different ways and maybe with different criteria, should reach great accuracy but could make different kind of errors, depending on their background.

Bibliography

- [1] National Comprehensive Cancer Network (NCCN) guidelines Breast Cancer Version 2.2011. http://www.nccn.org/professionals/physician_gls/pdf/breast.pdf, 2011.
- [2] The ICPR 2012 Mitosis Detection Challenge, and MITOS dataset. <http://ipal.cnrs.fr/ICPR2012/>, 2012.
- [3] Assessment of mitosis detection algorithms. <http://amida13.isi.edu.nl>, 2013.
- [4] ALBERTS, B., JOHNSON, A., AND LEWIS, J. E. A. *Molecular Biology of the Cell*. Garland Science, 2007.
- [5] AMIT, Y., AND GEMAN, D. Shape quantization and recognition with randomized trees. *Neural computation* 9, 7 (1997), 1545–1588.
- [6] BACHLE, M., AND KIRCHBERG, P. Ruby on rails. *Software, IEEE* 24, 6 (2007), 105–108.
- [7] BELLMAN, R. Dynamic programming. 2003.
- [8] BISHOP, C. M., ET AL. *Pattern recognition and machine learning*, vol. 1. springer New York, 2006.
- [9] BLOOM, H., AND RICHARDSON, W. Histological grading and prognosis in breast cancer: a study of 1409 cases of which 359 have been followed for 15 years. *British Journal of Cancer* 11, 3 (1957), 359.
- [10] BOSCH, A., ZISSERMAN, A., AND MUOZ, X. Image classification using random forests and ferns. In *Computer Vision, 2007. ICCV 2007. IEEE 11th International Conference on* (2007), pp. 1–8.
- [11] BRAY, F., McCARRON, P., AND PARKIN, D. M. The changing global patterns of female breast cancer incidence and mortality. *childhood* 4 (2004), 5.

- [12] BREIMAN, L. Random forests. *Machine Learning* 45, 1 (2001), 5–32.
- [13] BRO-NIELSEN, M. Rigid registration of CT, MR and cryosection images using a GLCM framework. In *CVRMed-MRCAS'97* (1997), Springer, pp. 171–180.
- [14] BROWN, C. D., AND DAVIS, H. T. Receiver operating characteristics curves and related decision measures: A tutorial. *Chemometrics and Intelligent Laboratory Systems* 80, 1 (2006), 24 – 38.
- [15] CANNY, J. A computational approach to edge detection. *Pattern Analysis and Machine Intelligence, IEEE Transactions on PAMI-8*, 6 (1986), 679–698.
- [16] CHAPELLE, O., HAFFNER, P., AND VAPNIK, V. Support vector machines for histogram-based image classification. *Neural Networks, IEEE Transactions on* 10, 5 (1999), 1055–1064.
- [17] CIRESAN, D., GIUSTI, A., GAMBARDELLA, L., AND SCHMIDHUBER, J. Mitosis detection in breast cancer histology images with deep neural networks. *Journal of Pathology Informatics special issue* (2013), to appear.
- [18] COHEN, J., ET AL. A coefficient of agreement for nominal scales. *Educational and psychological measurement* 20, 1 (1960), 37–46.
- [19] COLLINGBOURNE, H. *The book of Ruby*. No Starch Press, 2011.
- [20] DAMJANOV, I., AND FAN, F. *Cancer grading manual*. Springer Science+ Business Media, 2007, ch. 11, pp. 75 – 81.
- [21] DAVIS, J., AND GOADRICH, M. The relationship between Precision-Recall and ROC curves. In *Proceedings of the 23rd international conference on Machine learning* (New York, NY, USA, 2006), ICML '06, ACM, pp. 233–240.
- [22] DORFMAN, R. A formula for the gini coefficient. *The Review of Economics and Statistics* 61, 1 (1979), pp. 146–149.
- [23] DUNNE, B., AND GOING, J. Scoring nuclear pleomorphism in breast cancer. *Histopathology* 39, 3 (2001), 259–265.
- [24] ELICEIRI, K. W., BERTHOLD, M. R., GOLDBERG, I. G., IBÁÑEZ, L., MANJUNATH, B., MARTONE, M. E., MURPHY, R. F., PENG, H., PLANT, A. L., ROYSAM, B., ET AL. Biological imaging software tools. *Nature methods* 9, 7 (2012), 697–710.

- [25] ELSTON, C., AND ELLIS, I. Pathological prognostic factors in breast cancer. i. the value of histological grade in breast cancer: experience from a large study with long-term follow-up. *Histopathology* 19, 5 (1991), 403–410.
- [26] FORSYTH, D. A., AND PONCE, J. *Computer Vision: A Modern Approach*. Prentice Hall Professional Technical Reference, 2002, ch. 10.
- [27] FRANK, E., HALL, M., TRIGG, L., HOLMES, G., AND WITTEN, I. H. Data mining in bioinformatics using WEKA. *Bioinformatics* 20, 15 (2004), 2479–2481.
- [28] GANGULY, D., CHAKRABORTY, S., BALITANAS, M., AND KIM, T.-H. Medical imaging: A review. In *Security-Enriched Urban Computing and Smart Grid*, T.-h. Kim, A. Stoica, and R.-S. Chang, Eds., vol. 78 of *Communications in Computer and Information Science*. Springer Berlin Heidelberg, 2010, pp. 504–516.
- [29] GENESTIE, C. Mammary pathology. http://ipal.cnrs.fr/doc/projects/MammaryPathology_CatherineGenestie_2011.pdf, 2011.
- [30] GENESTIE, C., ZAFRANI, B., ASSELAIN, B., FOURQUET, A., ROZAN, S., VALIDIRE, P., VINCENT-SALOMON, A., SASTRE-GARAU, X., ET AL. Comparison of the prognostic value of scarff-bloom-richardson and nottingham histological grades in a series of 825 cases of breast cancer: major importance of the mitotic count as a component of both grading systems. *Anticancer research* 18, 1B (1998), 571.
- [31] GOUTTE, C., AND GAUSSIER, E. A probabilistic interpretation of Precision, Recall and F-Score, with implication for evaluation. In *Advances in Information Retrieval*, D. Losada and J. Fernández-Luna, Eds., vol. 3408 of *Lecture Notes in Computer Science*. Springer Berlin Heidelberg, 2005, pp. 345–359.
- [32] GUICAN, M., BOUCHERON, L., CAN, A., MADABHUSHI, A., RAJPOOT, N., AND YENER, B. Histopathological image analysis: A review. *Biomedical Engineering, IEEE Reviews in* 2 (2009), 147–171.
- [33] HALL, M., FRANK, E., HOLMES, G., PFAHRINGER, B., REUTEMANN, P., AND WITTEN, I. H. The WEKA data mining software: an update. *ACM SIGKDD Explorations Newsletter* 11, 1 (2009), 10–18.

- [34] HANLEY, J. A., MCNEIL, B. J., ET AL. A method of comparing the areas under receiver operating characteristic curves derived from the same cases. *Radiology* 148, 3 (1983), 839–843.
- [35] HANSSON, D. H., ET AL. Ruby on rails. *Website. Projektseite:* <http://www.rubyonrails.org> (2009).
- [36] HARALICK, R. M., SHANMUGAM, K., AND DINSTEIN, I. H. Textural features for image classification. *Systems, Man and Cybernetics, IEEE Transactions on*, 6 (1973), 610–621.
- [37] HARTLEY, R. I., AND ZISSELMAN, A. *Multiple View Geometry in Computer Vision*, second ed. Cambridge University Press, ISBN: 0521540518, 2004.
- [38] HO, T. K. Random decision forests. In *Document Analysis and Recognition, 1995., Proceedings of the Third International Conference on* (1995), vol. 1, pp. 278–282 vol.1.
- [39] HO, T. K. The random subspace method for constructing decision forests. *Pattern Analysis and Machine Intelligence, IEEE Transactions on* 20, 8 (1998), 832–844.
- [40] HONEYCUTT, C. E., AND PLOTNICK, R. Image analysis techniques and gray-level co-occurrence matrices (GLCM) for calculating bioturbation indices and characterizing biogenic sedimentary structures. *Computers & Geosciences* 34, 11 (2008), 1461–1472.
- [41] HORNIK, K., BUCHTA, C., AND ZEILEIS, A. Open-source machine learning: R meets WEKA. *Computational Statistics* 24, 2 (2009), 225–232.
- [42] HSU, C.-W., CHANG, C.-C., AND LIN, C.-J. A practical guide to support vector classification. Tech. rep., Department of Computer Science, National Taiwan University, Taipei 106, Taiwan, 2010.
- [43] HUANG, C.-H., AND LEE, H.-K. Automated mitosis detection based on exclusive independent component analysis. In *Pattern Recognition (ICPR), 2012 21st International Conference on* (2012), pp. 1856–1859.
- [44] HUANG, C.-H., VEILLARD, A., ROUX, L., LOMÉNIE, N., AND RACOCEANU, D. Time-efficient sparse analysis of histopathological whole slide images. *Computerized Medical Imaging and Graphics* 35, 7 - 8 (2011), 579 – 591. *jce:title;Whole Slide Image Process;jce:title;*

- [45] IRSHAD, H., GOUAILLARD, A., ROUX, L., AND RACOCEANU, D. Multispectral spatial characterization: Application to mitosis detection in breast cancer histopathology. *arXiv preprint arXiv:1304.4041* (2013).
- [46] IRSHAD, H., JALALI, S., ROUX, L., RACOCEANU, D., HWEE, L. J., LE NAOUR, G., AND CAPRON, F. Automated mitosis detection using texture, SIFT features and HMAX biologically inspired approach.
- [47] JÄHNE, B., AND HAUSSECKER, H. *Computer vision and applications: a guide for students and practitioners*. Academic Press, 2000.
- [48] JOACHIMS, T. *Text categorization with support vector machines: Learning with many relevant features*. Springer, 1998.
- [49] JOLLIFFE, I. *Principal component analysis*. Wiley Online Library, 2005.
- [50] JUSZCZAK, P., TAX, D., AND DUIN, R. Feature scaling in support vector data description. In *Proc. ASCI* (2002), Citeseer, pp. 95–102.
- [51] KHAN, A., EL-DALY, H., AND RAJPOOT, N. A gamma-gaussian mixture model for detection of mitotic cells in breast cancer histopathology images. In *Pattern Recognition (ICPR), 2012 21st International Conference on* (2012), pp. 149–152.
- [52] KHAN, A., SIMMONS, E., EL-DALY, H., AND RAJPOOT, N. HyMaP: A hybrid magnitude-phase approach to unsupervised segmentation of tumor areas in breast cancer histology images. *Journal of Pathology Informatics* 4, 2 (2013), 1.
- [53] LALKHEN, A. G., AND MCCLUSKEY, A. Clinical tests: sensitivity and specificity. *Continuing Education in Anaesthesia, Critical Care & Pain* 8, 6 (2008), 221–223.
- [54] LINDEBERG, T. *Scale-Space*. Wiley Online Library, 2008.
- [55] LIU, J., SUN, J., AND WANG, S. Pattern recognition: An overview. *IJCNS International Journal of Computer Science and Network Security* 6, 6 (2006), 57–61.
- [56] LJOSA, V., AND CARPENTER, A. E. Introduction to the quantitative analysis of two-dimensional fluorescence microscopy images for cell-based screening. *PLoS computational biology* 5, 12 (2009), e1000603.

- [57] LOWE, D. Object recognition from local scale-invariant features. In *Computer Vision, 1999. The Proceedings of the Seventh IEEE International Conference on* (1999), vol. 2, pp. 1150–1157 vol.2.
- [58] LU, D., AND WENG, Q. A survey of image classification methods and techniques for improving classification performance. *International journal of Remote sensing* 28, 5 (2007), 823–870.
- [59] MALON, C., BRACHTEL, E., COSATTO, E., GRAF, H. P., KURATA, A., KURODA, M., MEYER, J. S., SAITO, A., WU, S., AND YAGI, Y. Mitotic figure recognition: agreement among pathologists and computerized detector. *Analytical Cellular Pathology (Amst)* 35, 2 (2012), 97–100.
- [60] MANAVALAN, R., AND THANGAVEL, K. Evluation of textural feature extraction from GRLM for prostate cancer TRUS medical images. *International Journal of Computer Applications (0975-8887) Volume 36- No.12* (December 2011), pp.33 – 39.
- [61] MANN, H., AND WHITNEY, D. On a test of whether one of two random variables is stochastically larger than the other. *Ann. Math. Stat.* 18 (1947), 50–60.
- [62] MANNING, C. D., RAGHAVAN, P., AND SCHÜTZE, H. *Introduction to information retrieval*, vol. 1. Cambridge University Press Cambridge, 2008.
- [63] MEYER, J. S., ALVAREZ, C., MILIKOWSKI, C., OLSON, N., RUSSO, I., RUSSO, J., GLASS, A., ZEHNBAUER, B. A., LISTER, K., AND PARWARESCH, R. Breast carcinoma malignancy grading by bloom-richardson system vs proliferation index: reproducibility of grade and advantages of proliferation index. *Modern pathology* 18, 8 (2005), 1067–1078.
- [64] MITCHELL, T. *Machine Learning*. Mc Graw Hill, 1997.
- [65] MOELICH, M. Tracking objects with the chan-vese algorithm. *UCLA CAM Report* (2003), 03–14.
- [66] MOHRI, M., ROSTAMIZADEH, A., AND TALWALKAR, A. *Foundations of Machine Learning*. The MIT Press, 2012.
- [67] NIXON, M., AND AGUADO, A. S. *Feature extraction & image processing*. Academic Press, 2008.

- [68] OJALA, T., PIETIKÄINEN, M., AND MÄENPÄÄ, T. A generalized local binary pattern operator for multiresolution gray scale and rotation invariant texture classification. In *Advances in Pattern Recognition, ICAPR 2001 Proceedings* (2001).
- [69] OJALA, T., AND PIETIKÄINEN M & MÄENPÄÄ, T. Multiresolution gray-scale and rotation invariant texture classification with local binary patterns. *IEEE Transactions on Pattern Analysis and Machine Intelligence* 24(7) (2002), 971 – 987.
- [70] OOMMEN, T., MISRA, D., TWARAKAVI, N., PRAKASH, A., SAHOO, B., AND BANDOPADHYAY, S. An objective analysis of support vector machine based classification for remote sensing. *Mathematical Geosciences* 40, 4 (2008), 409–424.
- [71] PALIWAL, J., JAYAS, D., VISEN, N., AND WHITE, N. Quantification of variations in machine-vision-computed features of cereal grains. *Canadian Biosystems Engineering* 47 (2005), 7–1.
- [72] PAPAGEORGIOU, C. P., OREN, M., AND POGGIO, T. A general framework for object detection. In *Sixth International Conference on Computer Vision* (1998), IEEE, pp. 555–562.
- [73] RASMUSSEN, C. E. Gaussian processes in machine learning. In *Advanced Lectures on Machine Learning*. Springer, 2004, pp. 63–71.
- [74] RAVEN, P. H., AND JOHNSON, G. B. *Biology 9th edition*. Mc Graw Hill, 2010.
- [75] ROUX, L., TUTAC, A., LOMÉNIE, N., BALENSI, D., RACOCEANU, D., VEILLARD, A., LEOW, W.-K., KLOSSA, J., AND PUTTI, T. A cognitive virtual microscopic framework for knowlege-based exploration of large microscopic images in breast cancer histopathology. In *Engineering in Medicine and Biology Society, 2009. EMBC 2009. Annual International Conference of the IEEE* (2009), pp. 3697–3702.
- [76] RUBIN, C. M. The genetic basis of human cancer. *Annals of Internal Medicine* 129, 9 (1998), 759–759.
- [77] RUSSELL, S. J., AND NORVIG, P. *Artificial intelligence: a modern approach*, vol. 2. Prentice hall Englewood Cliffs, 2010.
- [78] SAEYS, Y., INZA, I., AND LARRAÑAGA, P. A review of feature selection techniques in bioinformatics. *Bioinformatics* 23, 19 (2007), 2507–2517.

- [79] SANGUANSAT, P., Ed. *Principal Component Analysis - Multidisciplinary Applications*. InTech, 2012.
- [80] SARIEGO, J. Breast cancer in the young patient. *The American Surgeon* 76, 12 (2010), 1397–1400.
- [81] SCHINDELIN, J., ARGANDA-CARRERAS, I., FRISE, E., KAYNIG, V., LONGAIR, M., PIETZSCH, T., PREIBISCH, S., RUEDEN, C., SAALFELD, S., SCHMID, B., ET AL. Fiji: an open-source platform for biological-image analysis. *Nature methods* 9, 7 (2012), 676–682.
- [82] SCHNEIDER, C. A., RASBAND, W. S., AND ELICEIRI, K. W. NIH Image to ImageJ: 25 years of image analysis. *Nat Methods* 9, 7 (2012), 671–675.
- [83] SCHÖLKOPF, B., AND SMOLA, A. J. *Learning with kernels: support vector machines, regularization, optimization and beyond*. the MIT Press, 2002.
- [84] SERTEL, O., KONG, J., SHIMADA, H., CATALYUREK, U., SALTZ, J. H., AND GURCAN, M. N. Computer-aided prognosis of neuroblastoma on whole-slide images: Classification of stromal development. *Pattern Recognition* 42, 6 (2009), 1093–1103.
- [85] SHAMIR, L., DELANEY, J. D., ORLOV, N., ECKLEY, D. M., AND GOLDBERG, I. G. Pattern recognition software and techniques for biological image analysis. *PLoS computational biology* 6, 11 (2010), e1000974.
- [86] SMITH, S. M., AND BRADY, J. M. SUSAN - a new approach to low level image processing. *International Journal of Computer Vision* 23, 1 (1997), 45–78.
- [87] SOMMER, C., FIASCHI, L., HAMPRECHT, F. A., AND GERLICH, D. W. Learning-based mitotic cell detection in histopathological images. In *Pattern Recognition (ICPR), 2012 21st International Conference on* (2012), IEEE, pp. 2306–2309.
- [88] STALLKAMP, J., SCHLIPSING, M., SALMEN, J., AND IGEL, C. Man vs. computer: Benchmarking machine learning algorithms for traffic sign recognition. *Neural Networks* 32, 0 (2012), 323 – 332.
- [89] STEHMAN, S. V. Selecting and interpreting measures of thematic classification accuracy. *Remote sensing of Environment* 62, 1 (1997), 77–89.

- [90] STRICKER, M., AND SWAIN, M. The capacity of color histogram indexing. In *Computer Vision and Pattern Recognition, 1994. Proceedings CVPR '94., 1994 IEEE Computer Society Conference on* (1994), pp. 704–708.
- [91] SUYKENS, J. A. K., AND VANDEWALLE, J. Least squares support vector machine classifiers. *Neural Process. Lett.* 9, 3 (June 1999), 293–300.
- [92] SWEDLOW, J. R., GOLDBERG, I. G., ELICEIRI, K. W., ET AL. Bioimage informatics for experimental biology. *Annual review of biophysics* 38 (2009), 327.
- [93] TARCA, A. L., CAREY, V. J., CHEN, X.-W., ROMERO, R., AND DRĂGHICI, S. Machine learning and its applications to biology. *PLoS computational biology* 3, 6 (2007), e116.
- [94] TAY, C. *Algorithms for Tissue Image Analysis using Multifractal Techniques*. University of Canterbury. Computer Science and Software Engineering, 2012.
- [95] THEODORIDIS, S., AND KOUTROUMBAS, K. *Pattern recognition*. Academic Press, Boston MA, USA (2008).
- [96] UNSER, M., AND ALDROUBI, A. A review of wavelets in biomedical applications. *Proceedings of the IEEE* 84, 4 (April 1996), 626–638.
- [97] UNSER, M., AND BLU, T. Wavelet theory demystified. *IEEE Transactions on Signal Processing* 51, 2 (February 2003), 470–483.
- [98] VETA, M., VAN DIEST, P. J., AND PLUIM, J. P. W. Detecting mitotic figures in breast cancer histopathology images. *Proc. SPIE 8676, Medical Imaging: Digital Pathology*, 867607 (2013).
- [99] VIOLA, P., AND JONES, M. Rapid object detection using a boosted cascade of simple features. pp. 511–518.
- [100] VIOLA, P., AND JONES, M. Robust real-time object detection. In *International Journal of Computer Vision* (2001).
- [101] WANG, B.-H., WANG, H.-J., AND QI, H.-N. Wood recognition based on grey-level co-occurrence matrix. In *Computer Application and System Modeling (ICCASM), 2010 International Conference on* (2010), vol. 1, IEEE, pp. V1–269.

- [102] WITTEN, I. H., FRANK, E., AND HALL, M. A. *Data Mining: Practical Machine Learning Tools and Techniques*, 3 ed. Morgan Kaufmann, Amsterdam, 2011.
- [103] WRIGHT, J., YANG, A. Y., GANESH, A., SASTRY, S. S., AND MA, Y. Robust face recognition via sparse representation. *Pattern Analysis and Machine Intelligence, IEEE Transactions on* 31, 2 (2009), 210–227.
- [104] YIN, Z., BISE, R., CHEN, M., AND KANADE, T. Cell segmentation in microscopy imagery using a bag of local bayesian classifiers. In *Biomedical Imaging: From Nano to Macro, 2010 IEEE International Symposium on* (2010), pp. 125–128.
- [105] YOGESAN, K., JØRGENSEN, T., ALBREGTSEN, F., TVETER, K., AND DANIELSEN, H. Entropy-based texture analysis of chromatin structure in advanced prostate cancer. *Cytometry* 24, 3 (1996), 268–276.
- [106] ZWEIG, M. H., AND CAMPBELL, G. Receiver-operating characteristic (ROC) plots: a fundamental evaluation tool in clinical medicine. *Clinical chemistry* 39, 4 (1993), 561–577.

Appendix A

Samples

Sample images

A.1 C1 and C0 samples

A.2 Human Difficulties

A.3 Classifier Difficulties